Massive MIMO for Dependable Communication

Willhammar, Sara

2022

Document Version:
Publisher's PDF, also known as Version of record

Massive MIMO for Dependable Communication

Sara Willhammar

Lund 2022

Series of licentiate and doctoral theses
No. 151
ISSN 1654-790X
ISBN 978-91-8039-459-8 (print)
ISBN 978-91-8039-460-4 (pdf)

This thesis is produced by using the LaTeX Documentation System
Printed in Sweden by *Tryckeriet i E-huset*, Lund.

Department of Electrical and Information Technology
Lund University, Box 118, SE-221 00 Lund, Sweden

If you have ever doubted yourself, this one is for you

Popular science summary

Wireless communication is constantly evolving, more connectivity is needed in more areas of society and the era of digitalisation has only begun. In the beginning, wireless communication was mostly about connecting mobile phones and hence, about connecting *people*. Nowadays it is about digitalising the whole society and more about connecting *things*. In this work, two applications of wireless systems are investigated: industrial automation and Internet-of-Things.

To support these new applications, with their new requirements, new technologies are needed. Massive multiple-input multiple-output (MIMO) is one technology, which has shown to improve the communication by using how radio signals propagate in a physical room. In massive MIMO, the number of antennas at the base station side is increased. With this comes a number of benefits such as an array gain, which can be used to increase the coverage, favourable propagation, making it easier to separate different users, and channel hardening, which means that the system becomes more stable and reliable.

This thesis focuses on the question of how massive MIMO systems can be used to make the communication more *dependable*, meaning that the communication needs to be reliable, available, and with sufficient coverage. The system performance is influenced by the antenna array deployed, which in the next step interacts with the channels. The channels, i.e., the medium between transmitter and receiver, sets the limit of what performance that can be achieved by a system. For the two applications, the channels are here investigated in several environments, in different frequency bands, and with various antenna arrays. These channels are measured, characterized, and models are provided.

Channel characteristics are different in different environments and therefore targeted studies in the considered environments are needed to develop accurate models that can be used to test and develop systems. The applications considered here are:

- **Industrial automation:** Industrial environments usually have tall machinery and walls, which can be blocking the signals but are also causing a lot of reflections. The environment is dynamic as robots and humans

are moving around in the factory and there is a risk of interference with the manufacturing process itself if the wireless communication is blocked.

- **Internet-of-Things:** Here outdoor environments with networks deployed to support remote monitoring services are considered. The users are usually static but things in the environment can change as e.g. people and cars pass by. The users are placed over a wide area and are battery-powered with the goal to remain autonomous for a long time.

To conclude, the main findings are that it has been experimentally validated that there is a prominent channel hardening effect in all investigated frequency bands that makes the channel more stable, and distributed antenna arrays can be deployed to reduce large-scale power variations, hence, further improving reliability. Finally, massive MIMO is indeed an enabler of dependable communication and can improve industrial automation and Internet-of-Things networks.

Populärvetenskaplig sammanfattning

Trådlös kommunikation utvecklas ständigt, mer uppkoppling behövs inom fler områden i samhället och digitaliseringens era har bara börjat. I början handlade trådlös kommunikation mest om att ansluta mobiltelefoner och därmed om att koppla ihop *människor*. Numera handlar det om att digitalisera hela samhället och mer om att koppla ihop *saker*. I detta arbete undersöks två tillämpningar av trådlösa system: industriell automation och Internet-of-Things, eller sakernas internet.

För att stödja dessa nya applikationer, med deras nya krav, behövs ny teknik. Massive multiple-input multiple-output (MIMO) är en teknik som har visat sig förbättra kommunikationen genom att utnyttja hur radiosignaler sprids i ett fysiskt rum. I massive MIMO ökar antalet antenner på basstationssidan. Med detta följer en rad fördelar som till exempel en arrayförstärkning, som kan användas för att förbättra täckningen, det är mer gynnsam vågutbredning, vilket gör det lättare att separera olika användare, och kanalhärdning, som gör systemet mer stabilt och pålitligt.

Denna avhandling fokuserar på frågan hur massive MIMO-system kan användas för att göra kommunikationen mer *pålitlig*, vilket innebär att kommunikationen måste vara tillförlitlig, tillgänglig och med tillräcklig täckning. Systemets prestanda påverkas av antennuppsättningen, som i nästa steg interagerar med kanalerna. Kanalerna, det vill säga mediet mellan sändare och mottagare, sätter gränsen för vilken prestanda som kan uppnås av ett system. För de två applikationerna, undersöks här kanalerna i flera miljöer, i olika frekvensband och med olika antennuppsättningar. Dessa kanaler mäts, karakteriseras och modeller presenteras.

Kanalegenskaper är olika i olika miljöer och därför behövs riktade studier i relevanta miljöer för att kunna utveckla lämpliga modeller som kan användas för att testa och utveckla system. De applikationer som behandlas här är:

- **Industriell automation:** Industriella miljöer har vanligtvis höga maskiner och väggar, vilket kan blockera signalerna men som också or-

sakar många reflektioner. Miljön är dynamisk då robotar och människor rör sig i fabriken och det finns risk för störningar i själva tillverkningsprocessen om den trådlösa kommunikationen blockeras.

- **Internet-of-Things:** Här undersöks utomhusmiljöer med nätverk utplacerade för att stödja fjärrövervakningstjänster. Användarna är oftast statiska men saker i miljön kan förändras, som till exempel att människor och bilar passerar. Användarna är placerade över ett stort område och är batteridrivna med målet att förbli autonoma under lång tid.

Sammanfattningsvis är de huvudsakliga resultaten att det har experimentellt visats att det finns en framträdande kanalhärdande effekt i alla undersökta frekvensband som gör kanalen mer stabil, och distribuerade antennuppsättningar kan användas för att minska storskaliga effektvariationer, därmed förbättras tillförlitligheten ytterligare. Slutligen är massive MIMO en lösning för pålitlig kommunikation och kan förbättra industriell automation och Internet-of-Things-nätverk.

Populair-wetenschappelijke samenvatting

Draadloze communicatie evolueert voortdurend, er is meer connectiviteit nodig voor diverse toepassingen van de samenleving: het tijdperk van digitalisering is nog maar net begonnen. In het begin focuste draadloze communicatie vooral op het verbinden van mobiele telefoons en dus over het verbinden van *mensen*. Tegenwoordig is de ambities het om het digitaliseren van de hele samenleving te ondersteunen en meer om het verbinden van *dingen*. In dit werk worden twee toepassingen van draadloze systemen onderzocht: industriële automatisering en Internet-of-Things.

Om deze nieuwe toepassingen, met hun nieuwe eisen, te ondersteunen, zijn nieuwe technologieën nodig. Massive multiple-input multiple-output (MIMO) is een technologie waarvan is aangetoond dat deze de communicatie verbetert door in te spelen op hoe radiosignalen zich voortplanten in een fysieke ruimte. Bij massive MIMO rust men het basisstation uit met een groot aantal antennes. Dit brengt verschillende voordelen met zich mee, zoals een winst, waardoor het bereik kan worden vergroot, gunstige propagatie, waardoor het makkelijker wordt om verschillende gebruikers te onderscheiden, en kanaalverharding waardoor het systeem stabieler en betrouwbaarder wordt.

Dit proefschrift richt zich op de vraag hoe massive MIMO-systemen kunnen worden gebruikt om de communicatie *betrouwbaar* te maken, wat inhoudt dat de communicatie robuust en beschikbaar moet zijn. De systeemprestaties worden beïnvloed door het gebruik van een antenne-array, die in de volgende stap samenwerkt met de kanalen. De kanalen, d.w.z. het medium tussen zender en ontvanger, bepalen de grens van de prestatie die een systeem kan bereiken. Voor de twee toepassingen worden de kanalen hier onderzocht in verschillende omgevingen, in verschillende frequentiebanden en met verschillende antennearrays. Deze kanalen worden hier gemeten, gekarakteriseerd en er worden modellen ontwikkeld.

Kanaalkenmerken zijn verschillend in verschillende omgevingen en daarom zijn gerichte studies in de beschouwde omgevingen nodig om nauwkeurige mod-

ellen te ontwikkelen die kunnen worden gebruikt om systemen te testen en te ontwikkelen. De hier beschouwde toepassingen zijn:

- **Industriële automatisering:** Industriële omgevingen hebben meestal hoge machines en muren, die de signalen kunnen blokkeren maar ook veel reflecties veroorzaken. De omgeving is dynamisch omdat robots en mensen zich in de fabriek bewegen en er is een risico op interferentie met het productieproces zelf als de draadloze communicatie is geblokkeerd.
- **Internet-of-Things:** Hier wordt gekeken naar buitenomgevingen met netwerken om remote monitoring services te ondersteunen. De geconnecteerde toestellen zijn meestal statisch, maar omstandigheden in de omgeving kunnen veranderen, zoals b.v. mensen en auto's passeren. De toestellen kunnen op grote afstand geïnstalleerd worden, werken op batterijen, en dienen lange tijd autonoom te kunnen werken.

Concluderend, zijn de belangrijkste bevindingen dat experimenteel gevalideerd werd dat er een prominent kanaalverhardend effect is in alle onderzochte frequentiebanden dat het kanaal stabieler maakt, en dat gedistribueerde antenne-arrays kunnen worden ingezet om grootschalige vermogensvariaties te verminderen, waardoor de betrouwbaarheid verder wordt verbeterd. Ten slotte is massive MIMO inderdaad een technologie die betrouwbare communicatie mogelijk maakt en industriële automatisering en Internet-of-Things-netwerken kan verbeteren.

Abstract

Cellular communication is constantly evolving; currently 5G systems are being deployed and research towards 6G is ongoing. Three use cases have been discussed as enhanced mobile broadband (eMBB), massive machine-type communication (mMTC), and ultra-reliable low-latency communication (URLLC). To fulfill the requirements of these use cases, new technologies are needed and one enabler is massive multiple-input multiple-output (MIMO). By increasing the number of antennas at the base station side, data rates can be increased, more users can be served simultaneously, and there is a potential to improve reliability. In addition, it is possible to achieve better coverage, improved energy efficiency, and low-complex user devices. The performance of any wireless system is limited by the underlying channels. Massive MIMO channels have shown several beneficial properties: the array gain stemming from the combining of the signals from the many antennas, improved user separation due to favourable propagation – where the user channels become pair-wise orthogonal – and the channel hardening effect, where the variations of channel gain decreases as the number of antennas increases. Previous theoretical works have commonly assumed independent and identically distributed (i.i.d.) complex Gaussian channels. However, in the first studies on massive MIMO channels, it was shown that common outdoor and indoor environments are not that rich in scattering, but that the channels are rather spatially correlated. To enable the above use cases, investigations are needed for the targeted environments. This thesis focuses on the benefits of deploying massive MIMO systems to achieve dependable communication in a number of scenarios related to the use cases. The first main area is the study of an industrial environment and aims at characterizing and modeling massive MIMO channels to assess the possibility of achieving the requirements of URLLC in a factory context. For example, a unique fully distributed array is deployed with the aim to further exploit spatial diversity. The other main area concerns massive MIMO at sub-GHz, a previously unexplored area. The channel characteristics when deploying a physically very large array for IoT networks are explored. To conclude, massive MIMO can indeed bring great advantages when trying to achieve dependable communication. Although channels in regular indoor environments are not i.i.d. complex Gaussian, the model can be justified in rich scattering industrial en-

vironments. Due to massive MIMO, the small-scale fading effects are reduced and when deploying a distributed array also the large-scale fading effects are reduced. In the Internet-of-Things (IoT) scenario, the channel is not as rich scattering. In this use case one can benefit from the array gain to extend coverage and improved energy efficiency, and diversity is gained due to the physically large array.

Sammanfattning

Cellulär kommunikation utvecklas ständigt; för närvarande installeras 5G-system och forskning kring 6G pågår. Tre användningsfall som diskuteras är enhanced mobile broadband (eMBB), massive machine-type communication (mMTC) och ultra-reliable low-latency communication (URLLC). För att uppfylla kraven i dessa användningsfall behövs ny teknik och en kandidat är massive multiple-input multiple-output (MIMO). Genom att öka antalet antenner på basstationens sida kan datahastigheterna ökas, fler användare kan betjänas samtidigt och det finns en potential att förbättra tillförlitligheten. Dessutom är det möjligt att uppnå bättre täckning, förbättrad energieffektivitet och lågkomplexa användarenheter. Prestandan för alla trådlösa system begränsas av de underliggande kanalerna. Massive MIMO-kanaler har visat flera fördelaktiga egenskaper: arrayförstärkning som kommer från kombinationen av signalerna från de många antennerna, förbättrad användarseparation på grund av gynnsam vågutbredning – där användarkanalerna blir parvis ortogonala – och kanalhärdningseffekten, där variationerna av kanalstyrkan minskar när antalet antenner ökar. Tidigare teoretiska arbeten har vanligtvis antagit oberoende och identiskt distribuerade komplexa Gaussiska kanaler. I de första studierna på massive MIMO-kanaler visades det dock att vanliga utomhus- och inomhusmiljöer inte är så rika på spridare, utan att kanalerna är rumsligt korrelerade. För att möjliggöra ovanstående användningsfall behövs undersökningar i relevanta miljöer. Denna avhandling fokuserar på fördelarna med massive MIMO-system för att uppnå pålitlig kommunikation i ett antal scenarier relaterade till användningsfallen. Det första huvudområdet är en studie av en industriell miljö som syftar till att karakterisera och modellera massive MIMO-kanaler för att bedöma möjligheten att uppnå kraven för URLLC i en fabrikskontext. Till exempel används en unik fullt utspridd array i syfte att ytterligare utnyttja rumslig diversitet. Det andra huvudområdet gäller massive MIMO vid sub-GHz-frekvenser, ett tidigare outforskat område. Kanalegenskaperna när en använder en fysiskt mycket stor array för IoT-nätverk utforskas. Sammanfattningsvis kan massive MIMO ge stora fördelar när en försöker uppnå pålitlig kommunikation. Även om kanaler i vanliga inomhusmiljöer inte är oberoende och identiskt distribuerade komplexa Gaussiska kanaler, så kan modellen motiveras i industriella miljöer med rik spridning. Tack vare massive MIMO re-

duceras de småskaliga fädningseffekterna, och med en utspridd array reduceras även de storskaliga fädningseffekterna. I scenariot Internet-of-Things (IoT) är kanalen inte lika rik på spridning. I detta användningsfall kan en dra nytta av arrayförstärkningen för att utöka täckningen och förbättra energieffektiviteten, samt diversitet fås på grund av den fysiskt stora arrayen.

Beknopte samenvatting

Mobiele communicatie evolueert voortdurend; momenteel worden 5G systemen geïnstalleerd en is er onderzoek naar 6G aan de gang. 5G-systemen beogen drie categorieën van toepassingen: enhanced mobile broadband (eMBB), massive machine-type communication (mMTC) en ultra-reliable low-latency Communications (URLLC). Massive multiple-input multiple-output (MIMO) wordt aanzien als een essentiële technologie om aan de vereisten van deze gebruiksscenario's te kunnen voldoen. Door een zeerg groot aantal antennes aan de basisstations te voorzien, kunnen de datasnelheden worden verhoogd, kunnen meer gebruikers tegelijkertijd worden bediend, en is er een potentieel om de betrouwbaarheid te verbeteren. Daarnaast zijn een groter bereik, verbeterde energie-efficiëntie, en eenvoudige gebruikersapparaten mogelijk. De prestaties van elk draadloos systeem worden bepaald door de onderliggende kanalen. Massive MIMO-kanalen vertonen verschillende gunstige eigenschappen: array-versterking die voortkomt uit het combineren van de signalen van de vele antennes, verbeterde mogelijkheden om gebruikers te onderscheiden door gunstige propagatie – waarbij de gebruikerskanalen paarsgewijs orthogonaal worden – en het effect waarbij het kanaal 'verhardt', waarbij de variaties in kanaalwinst afnemen naarmate het aantal antennes toeneemt. Eerdere theoretische werken gingen uit van onafhankelijke en identiek verdeelde complexe Gaussische kanalen. In de eerste onderzoeken naar massive MIMO-kanalen werd echter aangetoond dat typische buiten- en binnenomgevingen niet zo rijk zijn aan verstrooiing, maar dat de kanalen eerder ruimtelijk gecorreleerd zijn. Om de bovenstaande gebruiksscenario's mogelijk te maken, is onderzoek nodig naar de performantie van massive MIMO in de beoogde omgevingen. Dit doctoraat focust zich op de voordelen van het inzetten van massive MIMO-systemen om betrouwbare communicatie op te zetten voor toepassingen binnen de bovenstaande gebruiksscenario's. De eerste focus is de studie van een industriële omgeving die gericht is op het karakteriseren en modelleren van massive MIMO-kanalen om de mogelijkheid te beoordelen om aan de vereisten van URLLC in een fabriekscontext te kunnen voldoen. Zo wordt een volledig gedistribueerde array ingezet met als doel de ruimtelijke

diversiteit beter te benutten. Het tweede gebied van het onderzoek betreft massive MIMO voor sub-GHz frequenties, een voorheen onontgonnen gebied, waarin de kanaalkenmerken bij het inzetten van een fysiek grote array voor IoT-netwerken worden bestudeerd. Er kan geconcludeerd worden dat massive MIMO inderdaad grote voordelen kan bieden bij het streven naar betrouwbare communicatie. Hoewel kanalen in reguliere binnenomgevingen geen onafhankelijke en identiek verdeelde complexe Gaussische kanalen zijn, kan het model worden gerechtvaardigd in rijke verstrooiende industriële omgevingen. Door massive MIMO worden de kleinschalige fading-effecten sterk gemilderd, en bij het inzetten van een gedistribueerde array ondervindt men ook minder grootschalige fading-effecten. In het Internet-of-Things (IoT)-scenario is er minder rijke verstrooing in het kanaal. Dankzij de fysiek grote array, kan men in dit geval nog altijd profiteren van de array-versterking en diversiteit om het bereik uit te breiden, de energie-efficiëntie te verbeteren, en de betrouwbaarheid te verhogen.

Preface

This doctoral thesis consists of two parts. Part I gives an overview of the research field and serves as an introduction to the main scientific work, which is composed of six papers and presented in Part II. The papers are published under my former last name and may be updated in (some) online resources in the future. The following papers are included:

Paper I **Sara Gunnarsson**, Liesbet Van der Perre and Fredrik Tufvesson, "Massive MIMO channels", in *Wiley 5G Ref*, pp. 1–21, May 2020.

Personal contributions: I was leading the work on this overview paper. I did the literature review and wrote the content.

Paper II **Sara Gunnarsson**, José Flordelis, Liesbet Van der Perre and Fredrik Tufvesson, "Channel hardening in massive MIMO: Model parameters and experimental assessment", in *IEEE Open Journal of the Communications Society*, vol. 1, pp. 501-512, Apr. 2020.

Personal contributions: I took the lead with the work on this paper. I was planning and measuring with the LuMaMi testbed and performed the simulations with the COST2100 channel model. To be able to measure the channel with the LuMaMi testbed, I was involved in implementing a real-time channel logging. I processed the data and made most of the analysis as well as wrote the paper.

Paper III **Sara Gunnarsson**, Liesbet Van der Perre and Fredrik Tufvesson, "Fading in reflective and heavily shadowed industrial environments with large arrays", submitted to *IEEE Journal on Selected Areas in Communications 2022*.

Personal contributions: I took the lead with the work on this paper. I was planning and measuring with the LuMaMi testbed. I processed the data, made the analysis and wrote the content of the paper.

Paper IV Gilles Callebaut, **Sara Gunnarsson**, Andrea P Guevara, Fredrik Tufvesson, Liesbet Van der Perre and Anders J Johansson, "Massive MIMO goes Sub-GHz: Implementation and experimental exploration for LPWANs", in *Proc. 54th Asilomar Conference on Signals, Systems, and Computers (ASILOMAR)*, Pacific Grove, California, U.S., Nov. 2020.

Personal contributions: I made the implementation of the required changes on the KulMaMi testbed. I contributed to the system design and planning of the measurements. I contributed to the measurement campaign in Belgium but did most of it as remote support due to the corona pandemic and provided instead detailed manuals of how to operate the testbed. I contributed to the ideas and wrote parts of the paper.

Paper V Gilles Callebaut, **Sara Gunnarsson**, Andrea P Guevara, Anders J Johansson, Liesbet Van der Perre and Fredrik Tufvesson, "Experimental exploration of unlicensed sub-GHz massive MIMO for massive Internet-of-Things", in *IEEE Open Journal of the Communications Society*, vol. 2, pp. 2195-2204, Sep. 2021.

Personal contributions: I made the implementation of the required changes on the KulMaMi testbed. I contributed to the system design and planning of the measurements. I contributed to to the measurement campaign in Belgium but did most of it as remote support due to the corona pandemic aand provided instead detailed manuals of how to operate the testbed. I contributed to the ideas and wrote some of the sections in the paper.

Paper VI **Sara Gunnarsson**, MinKeun Chung, Andreas Johansson, Liang Liu, Fredrik Tufvesson, Ove Edfors, Olof Zander, Zhinong Ying, Kamal Samanta and Chris Clifton, "mmWave massive MIMO in real propagation environment: Performance evaluation using LuMaMi28GHz", in *Proc. 55th Asilomar Conference on Signals, Systems, and Computers (ASILOMAR)*, Pacific Grove, California, U.S., Nov. 2021.

Personal contributions: I took the lead with the work on this paper. I planned and conducted the measurements. I also did the data processing, analysis and wrote the paper.

During my PhD studies, I have also contributed to the following papers, which are not included in the thesis:

- **Sara Gunnarsson**, Micaela Bortas, Yanxiang Huang, Cheng-Ming Chen Liesbet Van der Perre and Ove Edfors, "Lousy processing increases energy efficiency

in massive MIMO systems", in *Proc. European Conference on Networks and Communications (EuCNC)*, Oulu, Finland, June 2017.

- Laura Monteyne, Andrea P Guevara, Gilles Callebaut, **Sara Gunnarsson**, Liesbet Van der Perre and Sofie Pollin, "Matrix pencil method: Angle of arrival and channel estimation for a massive MIMO system", in *Proc. IEEE International Conference on Communications (ICC)*, Dublin, Ireland, June 2020.
- Michiel Sandra, **Sara Gunnarsson**, and Anders J Johansson, "Internet of Buoys: An Internet of Things implementation at sea", in *Proc. 54th Asilomar Conference on Signals, Systems, and Computers (ASILOMAR)*, Pacific Grove, California, U.S., Nov. 2020.
- BR Manoj, Guoda Tian, **Sara Gunnarsson**, Fredrik Tufvesson and Erik G Larsson, "Moving object classification with a sub-6 GHz massive MIMO array using real data", in *Proc. IEEE International Conference on Acoustics, Speech and Signal Processing (ICASSP)*, Toronto, Canada, June 2021.
- BR Manoj, Guoda Tian, **Sara Gunnarsson**, Fredrik Tufvesson and Erik G Larsson, "Sensing and classification using massive MIMO: A tensor decomposition-based approach", in *IEEE Wireless Communications Letters*, vol. 10, no. 12, pp. 2649-2653, Sep. 2021.
- MinKeun Chung, Liang Liu, Andreas Johansson, **Sara Gunnarsson**, Martin Nilsson, Zhinong Ying, Olof Zander, Kamal Samanta, Chris Clifton, Toshiyuki Koimori, Shinya Morita, Satoshi Taniguchi, Fredrik Tufvesson and Ove Edfors, "LuMaMi28: Real-time millimeter-wave multi-user MIMO systems with antenna selection", submitted to *IEEE Transactions on Wireless Communications*.
- Emma Fitzgerald, Michał Pióro, Harsh Tataria, Gilles Callebaut, **Sara Gunnarsson** and Liesbet Van der Perre, "A light signalling approach to node grouping for massive MIMO IoT networks", in *Computers*, vol. 11, no. 6, 98, June 2022.

Besides the above, I have also contributed to the following temporary documents within the European Cooperation in Science and Technology (COST) Action.

- **Sara Gunnarsson**, José Flordelis, Liesbet Van der Perre and Fredrik Tufvesson, "Channel hardening in massive MIMO: Model parameters and experimental assessment", TD(18)08048 in *COST IC1004*, Podgorica, Montenegro, Oct. 2018.
- **Sara Gunnarsson**, Liesbet Van der Perre and Fredrik Tufvesson, "Fading in reflective and heavily shadowed industrial environments with large arrays", TD(22)03029 in *COST CA20120*, Valencia, Spain, Sept. 2022.

Furthermore, I have also contributed to the following deliverables for the EU project 5G-SMART – 5G for smart manufacturing (http://5gsmart.eu/).

- "Impact and dissemination plan for academic research, development of industry, standardisation and regulation synergies", Technical Report, 5G-SMART D6.1 V1.0, Aug. 2019.
- "Report on 5G radio deployability in the factory", Technical Report, 5G-SMART D4.2 V2.0, May 2022.

Acknowledgements

First I would like to thank my supervisors Fredrik Tufvesson and Liesbet Van der Perre. Thank you for the discussions and guidance during these years. Thank you Fredrik for paying attention to the details of my work and placing me in contexts where I am encouraged to take responsibility and given opportunities to develop. Thank you Liesbet for always giving feedback at exactly the level I need, for the feeling that everything is possible after a meeting with you, and for always being able to see synergies and enabling collaborations. Thanks to both of you for handling my tendency to doubt myself and encouraging me in those moments. Thanks to my supervisory committee for valuable discussions and input over the years. Thanks to my examination committee for the great questions and feedback during my preliminary defence.

Thanks to Ove Edfors I ended up doing my master's thesis in massive MIMO, otherwise, maybe I would not have ended up on this PhD journey. Thank you, Anders J Johansson, for our collaborations, continuous support, and all the discussions during the years regarding everything from the theory of science, research ethics, time and stress management, academic writing, and all those other topics that are essential when becoming an independent researcher. A big thanks to José Flordelis for helping me get started on this journey. Thanks, Harsh Tataria and Steffen Malkowsky for the collaboration when measuring in an operating semiconductor factory. Thank you Gilles Callebaut and Andrea P Guevara for the fruitful collaboration regarding sub-GHz massive MIMO and the DRAMCO group for assistance with the measurement campaign when a pandemic came in the way for my Belgium trips. Thanks, Andreas Johansson and MinKeun Chung for the assistance with the mmWave setup and measurements.

Thanks to all my fellow teachers who I learned from during my teaching experiences. Thank you to the students for your valuable feedback and for showing me that you can make a difference as a teacher. Thank you to all the TA personnel for their continuous support and for making everything in the department work.

During this journey, I have not only had the benefit of having only one

home research group, but rather three groups who have always made me feel welcome. Thank you for all the fun times we have had. Thanks to all my current and previous colleagues in the division of communications engineering (Lund University) for all the fikas and nice discussions. Thanks to the DRAMCO group (KU Leuven, Ghent) for the good times and for including me in the group even though I was not always physically present. Thanks to the networked systems group (KU Leuven, Leuven) for always welcoming me during my visits and for many fun rounds of card games over lunch during the years. To all the people I have gotten to know during my stays in Belgium, it is thanks to you that I have gained one more country that feels like home to me.

Being involved in student organizations and politics has been a big part of me during this PhD, all the way from faculty representation, to national matters, to the European level. A big thanks to everybody involved and who I have had an opportunity to collaborate with, you made this journey a lot more fun. Your enthusiasm and will to improve make me believe in an even better future.

Thanks to my family for always encouraging me and believing in me, I could not have done this without you. Thanks to my friends for all your support and fun times during the years, I can not describe how valuable you are to me. Finally, thank you Emil for being by my side during this journey. Thank you for all the support and for always believing in me. Thank you, Julian, who came to us at the end of this journey, for encouraging me with your smile to write the last parts. Thank you to the little one for keeping me company when finalizing this thesis, and we are looking forward to meeting you.

Sara

Lund, November 2022

List of acronyms and abbreviations

3D	3-Dimensional
4G	Fourth Generation of mobile telecommunications technology
5G	Fifth Generation of mobile telecommunications technology
6G	Sixth Generation of mobile telecommunications technology
AI	Artificial Intelligence
AWGN	Additive White Gaussian Noise
BER	Bit Error Rate
BS	Base Station
CDF	Cumulative Distribution Function
COST	Co-Operation in Science and Technology
CSI	Channel State Information
DRAM	Dynamic Random Access Memory
eMBB	enhanced Mobile Broadband
EGC	Equal Gain Combining
EVM	Error-Vector-Magnitude
FDD	Frequency-Division Duplex
FFT	Fast Fourier Transform
FPGA	Field-Programmable Gate Array
GSCM	Geometry-based Stochastic Channel Model
IF	Intermediate Frequency
i.i.d.	independent and identically distributed
IoT	Internet-of-Things
KulMaMi	KU Leuven Massive MIMO
LIS	Large Intelligent Surface
LoRa	Long Range
LoS	Line-of-Sight
LPWAN	Low-Power Wide-Area Network
LS	Large-Scale

LTE	Long Term Evolution
LuMaMi	Lund University Massive MIMO
MIMO	Multiple-Input Multiple-Output
MMSE	Minimum Mean-Squared Error
mMTC	massive Machine Type Communication
MPC	Multipath Component
MR	Maximum Ratio
MRC	Maximum Ratio Combining
MRT	Maximum Ratio Transmission
MU-MIMO	Multi-User Multiple-Input Multiple-Output
NB-IoT	Narrow-band Internet-of-Things
NLoS	Non Line-of-Sight
OFDM	Orthogonal Frequency Division Multiplexing
OOB	Out-of-Band
OTA	Over-the-Air
PDF	Probability Density Function
PL	Path-loss
QoS	Quality of Service
RF	Radio Frequency
RX	Receiver
RZF	Regularized Zero-Forcing
SDMA	Space-Division Multiple-Access
SDR	Software-Defined Radio
SNR	Signal-to-Noise Ratio
SS	Small-Scale
SU-MIMO	Single-User Multiple-Input Multiple-Output
TDD	Time Division Duplex
TX	Transmitter
UCA	Uniform Cylindrical Array
UE	User Equipment
ULA	Uniform Linear Array
URA	Uniform Rectangular Array
URLLC	Ultra-Reliable Low-Latency Communication
USRP	Universal Software Radio Platform
ZF	Zero-Forcing

Contents

Part I

Overview of the research field

Chapter 1

Introduction

This introduction starts with presenting the context and motivation of the research conducted. Then the picture is narrowed down to the scope of this thesis followed by the research questions investigated. Finally, the outline of the thesis is presented.

1.1 Context and motivation

Since the first generation of mobile cellular networks introduced in the 1980s, there has been a new generation released approximately every ten years. At the moment, the standardization of the first releases of the fifth generation (5G) [2] is completed and 5G systems are currently being deployed. In the research community, efforts are in the direction towards the sixth generation (6G) [3]. With every generation, the requirements on data rates, reliability, latencies, and number of connected devices are increasing.

To specify the stringent requirements, three main use cases for 5G have been defined: enhanced mobile broadband (eMBB), ultra-reliable low-latency communication (URLLC) [4], and massive machine-type communication (mMTC) [5]. Although much research efforts have been invested to realize these use cases, many requirements remain unfulfilled and will hence continue to be relevant when aiming towards the next generation of wireless cellular technologies.

With 6G, new use cases are not as clearly defined yet but envisioned use cases are holographic communication and applications requiring even higher data rates, tactile and haptic applications (as a continuation of the URLLC use case), connectivity for everything in society (as an evolution of mMTC), and even internet of bio- or nanothings [3][6]. Considered technologies to realize

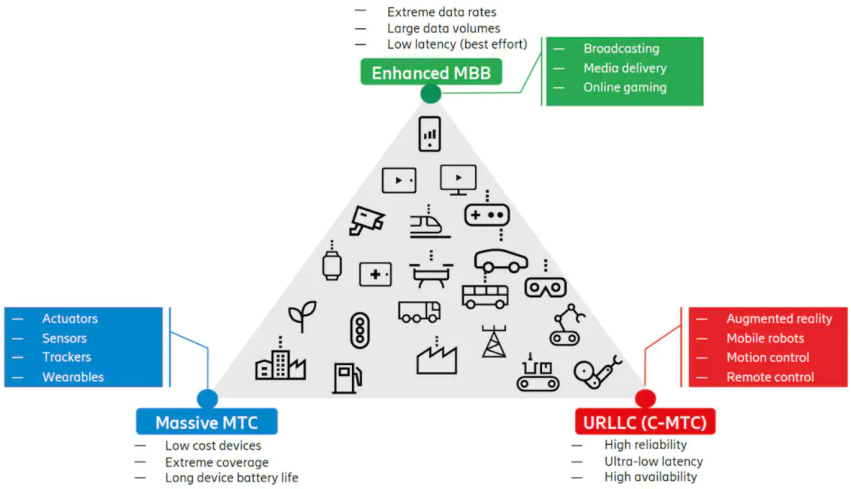

Figure 1.1: The 5G use cases with applications, from [1].

6G networks are terahertz (THz) communications, ultra-massive MIMO, large intelligent surfaces (LIS), artificial intelligence (AI), among others [6][7].

The first industrial revolution started due to mechanical production enabled by e.g. steam-power. With the second industrial revolution mass production started, powered by electricity and supported by assembly lines. The third industrial revolution began with the automation of production supported by computers and electronics, i.e., digitalization. The current ongoing industrial revolution, Industry 4.0, is about robotics and cyber-physical systems, where 5G systems and beyond plays an important role [8][9][10]. Many of the requirements for Industry 4.0 are expressed in the URLLC use case [11], including industrial Internet-of-Things (IoT) networks [12].

Two trends for smart manufacturing are more flexible production and more autonomous operations with monitoring in order to improve productivity and quality [13]. To increase the flexibility in the production, wireless solutions are needed. A factory is often a very complex environment for wireless communication. With high machinery blocking the signals, shadowing becomes a prominent problem, and with robots and humans working together and moving around, it is also a very dynamic environment. Often there is a time-critical process to be executed and hence high reliability in combination with low latency is a necessity. Industrial IoT networks also exhibit similar challenges, where the sensors/devices could be located in difficult places with the task to monitor the status of the machinery to provide information for maintenance or asset tracking. There needs to be communication between robots, between robots and sensors as well as between robots and the human factory operators [3].

IoT networks are also to be deployed in other parts of the society and their requirements often relates to the mMTC use case. The current trend of cellular systems is that it is less about connecting people and more about connecting things, in e.g. IoT networks. The devices in these networks need to be of low-complexity and energy-efficient such that they can remain in operation without human interaction for many years. They are also usually spread out over large areas, in e.g. low-power wide-area networks (LPWANs), and hence coverage is essential in order to monitor these remote devices. By deploying wireless systems to enable the operation of these devices, a diverse set of applications is possible.

To enable these networks and use cases, new technologies are needed. With 5G, the concept of massive multiple-input multiple-output (MIMO) became an essential part of the standard. In massive MIMO systems, the number of antennas is increased, which has proven to improve performance. Data rates can be increased, reliability improved and more devices can be served in the same time-frequency resource with limited interference. With more antennas and signal processing at the base station side, the complexity requirements of the user devices can be kept low, enabling low-power devices.

When increasing the number of antennas and coherently combining the many antennas in massive MIMO systems, an array gain is achieved. This array gain can be used to either extend the coverage or decrease the transmit power. Furthermore, as the number of antennas increases, the experienced channel variations decreases and the channel hardening effect appears, making the system more reliable [14]. Another effect of increasing the number of antennas is the increase in favourable propagation conditions, thus the user separation is improved [15]. Hence massive MIMO has an essential role in future cellular systems to fulfill the requirements of eMBB, URLLC, and mMTC, and enabling industrial automation and IoT networks.

1.2 Scope

The scope of this thesis is about how to achieve reliable and efficient communication with massive MIMO, with focus on the channels. The targeted use cases are primarily on the scale between URLLC and mMTC, in order to enable applications such as industrial automation and IoT networks. The question is how reliable communication can be achieved by exploiting the many antennas in a massive MIMO system. Since this thesis focuses on the channels, investigations include channel measurements, channel characterization, and channel modeling.

The characteristics of massive MIMO channels are studied and an overview of them are presented in Paper I. The focus of the paper is on the interaction between the channel and the system. Throughout the work the influence of

the number of antennas and how they are distributed is investigated. Channel measurements have been designed and conducted in environments relevant for the URLLC and mMTC use cases. To perform channel measurements, testbeds have been extended so that the channels are stored for offline analysis and such that sub-GHz channel measurements could be performed according to regulations.

Much attention has been given to the channel hardening effect, which is the main focus of Paper II. Specifically, investigations concerning how a rich scattering environment is different from a typical outdoor scenario and how the system is interacting with this rich scattering environment are performed. Investigations of channel hardening are also included in the more scenario-specific papers.

The industrial environment is quite complex from a propagation perspective and needs to be explored. The mid-band channel characteristics in such an environment are studied in Paper III. Shadowing can be severe as there is usually many walls and tall machinery. This, however, also results in a very rich scattering environment, being beneficial in terms of channel hardening. A fully distributed array is also deployed and compared to a co-located array. Indoor mmWave channel characteristics are studied in Paper VI.

For the IoT scenario, the effect of using a lower frequency is investigated in Paper IV and Paper V. The influence of a (physically) large array is investigated and sub-GHz massive MIMO channel characteristics are explored.

1.3 Research questions

Massive MIMO has been shown to bring great potential in earlier work for typical indoor and outdoor environments. With future wireless systems, the requirements are even more stringent in terms of reliability, latency, and massive connectivity. Through channel measurements, characterization, and modeling, this thesis aims to answer the following questions:

- How rich in scattering are different environments and how do the system interact with these environments?
- What are the underlying propagation processes that affect channel hardening in practical massive MIMO systems?
- How pronounced are massive MIMO channel characteristics in different frequency bands and how can dependable communication be realized in these bands?
- How are practical antenna arrays interacting with the channel and influence the system performance? Can more diversity be achieved by deploy-

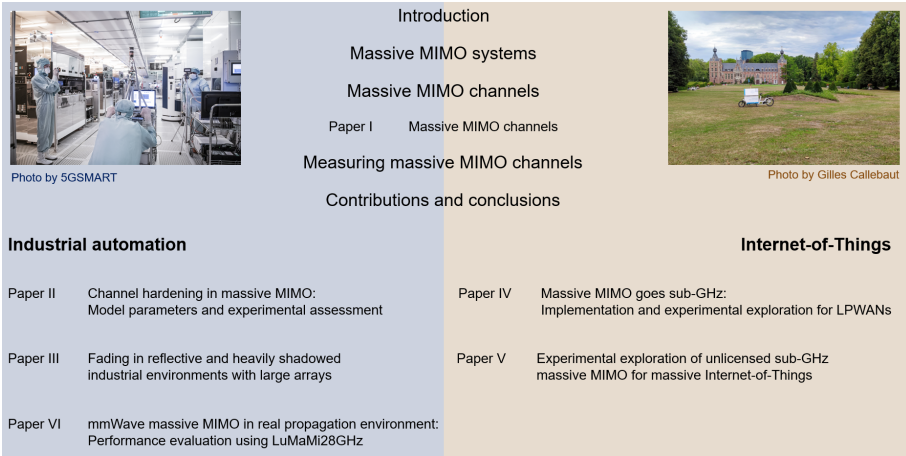

Figure 1.2: An overview of the thesis structure, including overview chapters and paper collection.

ing a distributed array and how does that influence the overall system in comparison to a co-located array?

- Is URLLC realizable in industrial environments? How is the system interacting with a rich scattering and heavily shadowed environment?
- Can massive MIMO systems efficiently provide reliable communication for LPWANs and IoT networks?

1.4 Thesis outline

This thesis consists of two parts. Part I presents an overview of the research field and gives a context to the main research contributions. These contributions are detailed in the collection of articles in Part II, which are in different ways targeting industrial automation and IoT scenarios. Fig. 1.2 presents the outline of the thesis with the chapters in Part I in the middle, where also Paper I is included, serving as the introduction to the rest of the included papers in Part II.

In the overview, Chapter I, Introduction, presents the context and motivation, outlines the scope, and presents the research questions, and the structure of this thesis. Chapter 2, on Massive MIMO systems, elaborates on the emergence of massive MIMO and preceding wireless systems. It describes key concepts of massive MIMO systems and what assumptions that are made about the system in this work. This is followed by a discussion about the importance of channel knowledge for system design. Moving on from the system perspective,

Chapter 3 presents key concepts of Massive MIMO channels. Although much of the content of this chapter is presented in the included paper "Massive MIMO channels", this chapter presents some more fundamentals on propagation and channel characterization. Scenario-specific channels are outlined as well as on the role of measurements for channel modeling.

To characterize and model massive MIMO channels, measuring them first is required. Chapter 4 elaborates on Measuring massive MIMO channels. Starting with an introduction of wireless channel measurements and testbeds in general, it continues with explaining the equipment developed and used in the included papers. Finally, the scenarios investigated in the included papers are outlined.

Chapter 5, Contributions and conclusions, presents the research contributions and the general conclusions of this work before providing an outlook on research directions to be pursued where this thesis ends.

Chapter 2

Massive MIMO systems

This chapter starts with an introduction to wireless systems in general. It continues with a more thorough description of massive MIMO systems and related concepts. Lastly, the importance of channel knowledge for system design is discussed.

2.1 Wireless systems

Wireless systems can be deployed as cellular networks where the area is divided into cells, each having a base station serving near-by users. Currently the technology 5G is being deployed, which, as its predecessors, is a cellular network. IoT networks could also be cellular networks as e.g. narrow-band (NB)-IoT [16].

IoT devices usually need to communicate efficiently over long ranges with limited energy budgets. LoRa [16] and Sigfox [17] have been developed for this purpose in unlicensed bands. These technologies operate in the unlicensed sub-GHz band where devices are allowed to transmit provided that regulations, concerning e.g. transmit power, bandwidth, and duty cycle, are respected. The sub-GHz band offers better propagation conditions for long-range communication whereas the mid-band often used in mobile networks suffers from more shadowing while having the benefit of being a licensed band and able to support larger bandwidths to achieve higher throughput.

Higher throughput and higher capacity have always been desired for future wireless systems. To increase the data rates and network capacity, mainly three things are to be considered 1) cell densification 2) more frequency spectrum or 3) improved spectral efficiency [18]. In 5G, as in previous generations, cells are made small where the traffic demands are high. 5G networks are also using the mmWave band, i.e., using even higher carrier frequencies, where

larger bandwidth is available, although with less favourable propagation conditions. Furthermore, spectral efficiency is radically increased by e.g. deploying multiple-antenna techniques, such as massive MIMO.

The received signal power varies with time, frequency, and space due to so called small-scale fading caused by constructive and destructive superpositioning of signals. These fluctuations in signal level are harmful for the performance of the wireless system but can be combated by applying diversity techniques in different domains. This under the assumption that different channels fade more or less independently, and hence that the different transmitted signals can be combined in such a way that the received signal strength is sufficient. In the time domain this can be done by e.g. adding redundancy by coding, transmitting multiple copies in time and by interleaving the bits to be sent. However, if low-latency is a requirement, then these alternatives might not be viable options. Frequency diversity could also be exploited under the assumption that different channels in frequency fade independently. Techniques to this are, e.g., frequency hopping and orthogonal frequency-division multiplexing (OFDM). Polarization diversity can also be exploited by using the different polarization modes. The main focus of this thesis however, is to exploit spatial diversity by deploying multiple antennas.

By using multiple antennas at both transmit and receive side in so called MIMO systems, spatial diversity can be exploited and system performance can be improved. MIMO technology is essential in many wireless systems and are used in e.g. Wi-Fi and long term evolution (LTE) [19]. With multiple antennas, diversity techniques can be exploited to combat fading assumed that fairly independent fading can be experienced on the different antenna elements, and then the variations of signal strength can be reduced. Depending on the availability of channel state information (CSI), different diversity techniques can be applied. Diversity techniques that can be used are selection diversity, maximum ratio combining (MRC), and equal-gain-combining (EGC) [20]. In case of full CSI, MRC can be utilized and the signal-to-noise ratio (SNR) is with proper weights maximized as the signals from different antenna elements are added up coherently in a desired direction [18]. The average signal strength can also be improved by applying beamforming techniques, and hence getting an array gain. Lastly, more data can be transmitted by dividing it into substreams and sending multiple streams at the same time, each stream travelling through different channels and can therefore be separated at the receiver side. This is called spatial multiplexing.

MIMO systems have originally been deployed as single-user (SU)-MIMO or multiple-user (MU)-MIMO. In SU-MIMO sytems, also called point-to-point MIMO systems, one user at the time is served and multiple antennas are used at both sides, requiring more complex user devices. In these systems, benefits such as improved coverage due to the array gain, more reliable links due to the decreased variations of signal strength, and higher data rates due to simultan-

eously transmitting several streams with the techniques outlined above can be achieved.

In MU-MIMO systems, an antenna array serves several user devices in the same time-frequency resource using spatial multiplexing. The same benefits as mentioned for SU-MIMO systems can be obtained and further improvements can be achieved in terms of system capacity. The challenge that needs to be handled is interference between users, which requires channel knowledge [21]. To summarize, multiple antenna systems can bring great improvements in terms of capacity, coverage, angular information and most important in this work: reliability.

Taking the idea of MU-MIMO one step further, massive MIMO was introduced by Thomas Marzetta in 2010 [22]. He proposed a cellular system where a base station (BS) is simultaneously serving many single-antenna terminals in the same time-frequency resource. When going to massive MIMO, the number of base station antennas is increased even further, possibly even into the hundreds [23]–[26]. The BSs with these large arrays are to serve even more (although typically smaller than the number of antennas) low-complex users simultaneously and the throughput and spectral efficiency can be radically improved. Furthermore, with the large arrays, small-scale fading effects and uncorrelated noise average out and inter-user interference asymptotically vanishes, if the user channels become orthogonal when the number of antennas grows large. This makes linear processing in both uplink and downlink almost optimal and is relaxing hardware requirements. The system in [22] was time-division duplex (TDD)-based and assumed the channel to be reciprocal. The channel was estimated in uplink by pilot signaling, with the number of pilots only scaling with the number of users, and its conjugate transpose used as linear precoding in the downlink. The main difference in comparison to MU-MIMO being that only the BS needs to estimate the channel and concluding that these systems would leave only inter-cellular interference due to pilot contamination [27] as the main drawback [22]. In the next section, massive MIMO systems are further described, including the assumptions made in this thesis.

2.2 System description

Since Marzettas seminal paper [22], massive MIMO has evolved and a number of definitions and variants of it have been proposed. The definition used here goes back to the one used by Marzetta in his original paper. An overview of a massive MIMO system is depicted in Fig. 2.1 where a BS with M antennas is serving K single-antenna users in the same time-frequency resource with spatial multiplexing. The channel H is the downlink channel and due to reciprocity, the uplink channel is H^T. In general, M is larger than K, multi-

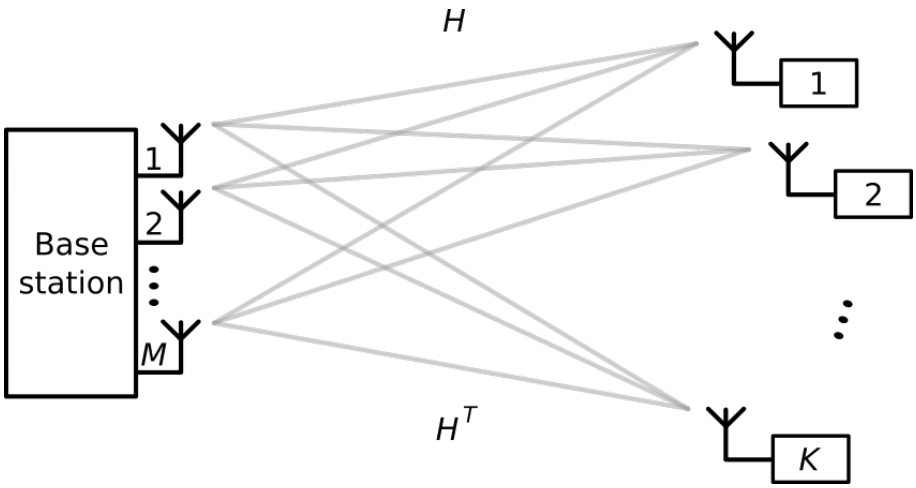

Figure 2.1: An overview of a massive MIMO system, from Paper 1. H is the downlink channel and due to reciprocity, the uplink channel is H^T.

carrier transmission is assumed and a TDD scheme is applied to limit the overhead stemming from CSI acquisition [18]. Those are the most commonly used assumptions although researchers have also investigated the feasibility of e.g. multiple antenna user terminals [28], single-carrier transmission, and FDD operation [29].

2.2.1 Spectral efficiency and capacity

Fundamentally, the maximum spectral efficiency is the average number of bits of information that can be reliably transmitted over the channel under consideration in the unit bit/s/Hz [18] and is determined by the channel capacity, introduced by Shannon [30]. The capacity of a single additive white Gaussian noise (AWGN) channel depends on the SNR. To improve the spectral efficiency one can 1) increase the transmit power, 2) deploy multiple antennas, 3) serve more users in the same time/frequency resource using space-division multiple-access (SDMA), and 5) acquire and utilize CSI [18]. It should however be noted that increased transmit power also increases the interference, and might not even be possible due to, e.g., regulations and design restrictions. To serve more users, more BS antennas may be needed to deal with the increased interference. More antennas implies increased complexity. Challenges with CSI acquisition are discussed later on.

2.2.2 Spatial multiplexing

One key challenge for earlier cellular systems has been to provide enough network capacity and fulfill the traffic demands by the customer. This is also the situation in the 5G use case eMBB, and many of the envisioned use cases for 6G networks. Massive MIMO contributes to an increased capacity due to spatial multiplexing. Many early studies on massive MIMO focused on the capacity increase while here the main attention is to the reliability aspect as an important motivation for deploying massive MIMO systems in general.

2.2.3 Duplexing schemes

Although many earlier systems are using frequency division duplex (FDD), massive MIMO systems are typically serving users in a TDD-manner [31]. FDD has in general been considered as infeasible as much resources are needed for the uplink and downlink pilot signaling and feedback of CSI. The benefit of a TDD-based system is that due to channel reciprocity [32], only orthogonal pilots in the uplink are needed and therefore the overhead needed for channel acquisition only increases with the K users and not the M antennas as in FDD [18]. Studies have investigated the feasibility of using FDD in massive MIMO systems e.g. [33]. A measurement-based study compared the TDD-scheme and four different FDD beamforming strategies, concluding that reciprocity-based TDD beamforming is the best alternative to handle many different propagation conditions [29].

2.2.4 Channel reciprocity

Being a fully digital system using TDD, the system can rely on channel reciprocity, i.e., that the channel response is the same in both directions. The channel coefficients for each antenna pair in the downlink channel matrix H, can be acquired by using the uplink channel matrix acquired by the K uplink pilots. While the channel is reciprocal [32], the radio frequency (RF)-chains are in general not, and hence reciprocity calibration is needed to in some way estimate calibration coefficients that can be applied to compensate the channel estimates from the uplink pilot signaling [34]. For a thorough discussion on channel reciprocity and calibration strategies, see [35].

2.2.5 Channel estimation

The channel matrix is estimated based on uplink pilots and affects how the channel is experienced by the BS. A challenge associated with channel acquisition is the update rate, which can be challenging in high mobility scenarios when the channel is changing rapidly [36]. Then a large overhead is needed due

to increased uplink pilot signaling. Another challenge associated with channel estimation is the influence of pilot contamination, as acknowledged in [22]. Although later studies have shown that in theory, the capacity can continue to grow unbounded as the number of BS antennas increases, even in presence of pilot contamination from neighbouring cells [37].

2.2.6 Precoding techniques

At the BS side, the CSI is used for precoding and this will affect how the channel is experienced by the user. With precoding, signals can be transmitted from all BS antennas such that they add up constructively at the intended user and out of phase, or with random phase, at other users. The simplest technique is maximum ratio (MR) and other commonly used precoding techniques are zero-forcing (ZF) and MMSE/regularized-ZF (RZF). MR maximizes the SNR and is optimal in noise limited scenarios [38]. In high SNR scenarios, ZF is better, as MR will be limited by interference. MMSE/RZF is a good trade-off between signal strength and interference suppression for the full SNR range. Compared to ZF and RZF, with MR each user can benefit from the full array gain and the technique has the lowest computational complexity as no matrix operation is involved and it can be done in parallel for each user and antenna [18].

2.2.7 Array gain

When coherently combining the signals from all BS antennas, an array gain can be achieved, which improves the SNR without increasing the transmit power. The array can hence be used to reduce the transmit power without reducing the coverage, or increasing the coverage without increasing the transmit power. It can also be essential when going up in frequency to maintain the required coverage. In reality, the power transmitted from BSs is limited due to regulations and consequently the most suitable option might be to scale down the transmitted power with the array gain, relaxing the hardware requirements, and making the system more energy efficient. When using MRC, or maximum ratio transmission (MRT), an array gain of M can be achieved in both uplink and downlink. In the uplink due to that the BS can coherently combine the signals from the M antennas, while the noise is added incoherently; in the downlink due to that the signals from the M transmit antennas can be added coherently at the user side [18].

2.3 Hardware and antenna aspects

In the following, hardware aspects related to both the BS and user equipment (UE) is outlined, including antenna aspects.

2.3.1 Base station hardware

With a fully digital beamforming architecture, each antenna is connected to one RF-chain each and therefore much more hardware is needed. Fortunately, similar to other noise sources, the effect of distortion due to hardware impairments asymptotically vanishes as the number of antennas increases since it is non-coherently combined. The problem is rather with the user equipment since self-distortion is coherently combined and hence, capacity will be mainly limited by the quality of the UE [39][40]. Furthermore, the extra degrees of freedom coming from the multiple antennas can be used, as previously stated, to reduce the transmit power, or they can be used to better tolerate hardware impairments [18]. A drawback of reducing the hardware quality is out-of-band (OOB) radiation. Antenna selection could be used to to reduce the number of RF chains, or other hybrid architectures. This could be especially beneficial for higher frequency as more antennas might be needed to combat the increased path-loss.

2.3.2 Antenna arrays

A system design will naturally include the design of antennas and the array configuration. An antenna can be characterized by its directionality, efficiency, mean-effective gain, polarization, and bandwidth [19]. When organizing the antennas in an array configuration, they can interact with each other due to mutual coupling which can degrade the performance [23][34]. The design and the size of an antenna will depend on the wavelength and therefore the carrier frequency; the longer the wavelength, the larger the antenna. Antennas in an array should be placed with at least half a wavelength apart to reduce the mutual coupling. Naturally, an array for a lower frequency will be physically very large as M grows while an antenna array at e.g. mmWave will be much more compact.

There are many possible antenna configurations that can be considered, examples being a uniform linear array (ULA), uniform rectangular array (URA), uniform cylindrical array (UCA) or a distributed array. The choice of antenna configuration will depend on the deployment scenario and its interaction with the environment will affect the system performance. Depending on the configuration, the near- and far-field will change, and that will also affect how the system is experiencing the channel and how prominent different massive MIMO channel characteristics will be. Furthermore, traditionally BS antennas have been installed to avoid interaction with objects in the near vicinity of the array, with a massive amount of antennas and in indoor scenarios, this might not be possible.

2.3.3 User equipment

As previously mentioned, even though user hardware can be less complex in a massive MIMO system, its hardware is also the main limitation for the achievable capacity. In addition, the interaction with the UE itself and the users will cause effects such as shadowing and the loading of the antenna will make the system less efficient. One way to counteract these effects is to exploit diversity also at the user side [28].

2.4 Channel-dependent aspects

Massive MIMO channel characteristics and channel-dependent characteristics can be further read about in Paper I. Here only the channel-dependent characteristics are mentioned, as a part of the system overview as they affect the system design and reliability. The two characteristics are user separation, which improves as an effect of favourable propagation conditions and channel hardening, which improves the link reliability. These two characteristics are related and makes the system performance almost independent of small-scale fading and hence mainly dependent on large-scale fading. They are, however, different properties and it is not necessarily that both improve for a certain channel [18]. For example, the keyhole channel provides favourable propagation but not channel hardening. On the other hand, two line-of-sight (LoS) channels with signals from the same direction can provide channel hardening while not experiencing favourable propagation conditions [41]. Another difference is that spatial correlation in the channel will reduce the level of channel hardening but can improve the favourable propagation, if the users have different spatial signatures [18].

2.4.1 Favourable propagation

The favourable propagation condition implies that user channels asymptotically become orthogonal with the number of antennas, and as a result the inter-user interference decreases, therefore contributing to a more reliable system. Due to the user channel orthogonality, linear processing becomes nearly optimal [31][42], and therefore the previously discussed precoding/detection schemes are suitable for massive MIMO systems.

2.4.2 Channel hardening

As mentioned before, the channel hardening effect means that the relative variation of the channel gain decreases as the number of antennas increases. The effect of small-scale fading asymptotically disappears as M grows large [14]. This results in more stable channels as the effective channel to each user,

i.e., the channel after combining/precoding, becomes more deterministic. The combining scheme used has shown to not have a significant impact although schemes with interference suppression comes with a small loss of experienced channel hardening. It is rather the effect of imperfect CSI that matters for these schemes, while it for MRC is not as important [18]. Advantages of channel hardening is that power allocation can be done more infrequent, only considering the large-scale effects. The same is true for the channel estimation which results in more stable precoders and detectors. It also reduces the required fading margins, making it a more energy efficient system.

2.5 Assumptions

To summarize, the assumed massive MIMO systems in this thesis are specified as following:

- Cellular single-cell system
- M is larger than K
- A TDD-based system relying on channel reciprocity
- MRC is utilised due to its simplicity
- Multi-carrier transmission is used for both channel sounding and in the testbeds

The frequency bands considered are the unlicensed 868 MHz band, licensed mid-band with center frequency 3.7 GHz and licensed mmWave band with center frequency 28 GHz. Channel bandwidths considered are both narrowband in the IoT scenario and more wideband for the other scenarios. For the two lower bands, a fully digital system is assumed while in the higher band, a hybrid architecture with antenna selection on the user side is deployed. Furthermore, a wide range of antenna arrays are deployed: ULA, URA, UCA, and also a fully random distributed array. User terminals are single-antenna, in the industrial automation scenario there is moderate movement while in the IoT scenario they are assumed static.

2.6 On the role of channels for system design

The performance and behaviour of any wireless system will depend on the propagation channel, i.e., the medium between the transmitter and receiver antennas. Therefore, it is essential to have an understanding of the propagation channel to be able to use this information when designing the system.

Especially in the URLLC use case, where the challenge is to achieve high reliability while having a low latency. Previously, high reliability has been achieved by, e.g., adding redundancy, using long codes, and re-transmissions; this is not applicable here as this increases the latency. Hence, the question is how to use other techniques and/or system designs to achieve dependable communication channels. Exploiting diversity in different domains is one part of it.

With knowledge about how the channel behaves, relevant parameters can be extracted to create models. These channel models are needed to design, plan, and simulate systems. It is important that these models accurately captures the aspects of the channel that influence performance in order to be useful. Deterministic channel models, that use location-specific information, are useful for network planning and system deployment. Stochastic channel models are an important tool that can be used for system design and to compare different systems [19].

$$\text{Received power} = \text{Transmittet power} + \text{Gains} - \text{Losses} \tag{2.1}$$

Ultimately, reliability is about successfully transmitting data within a certain time. In order to achieve successful transmission, the received power needs to be above a threshold in order to decode the message. In any system, there will be gains and losses which will be added and removed from the transmitted power, when expressed in dB, as seen in (2.1). From a system perspective, the gains can be associated with the gains of the antennas and the losses can occur in different parts of the system. The aspects stemming from the channels, which need to be accounted for in the system design, will be discussed in the next chapter.

Chapter 3

Massive MIMO channels

Paper I gives an overview of massive MIMO channel characteristics, channel-dependent characteristics, and channel modeling approaches. Here this paper is complemented with a general background on wireless channels and scenario-specific channels. The suggested reading order is first Section 3.1, then Paper I, and then continue with Section 3.2 and onwards where an overview of scenario-specific channels are presented, i.e., industrial and IoT channels, followed by a note on measurements for channel modeling to link to the next chapter.

3.1 Wireless channels

The fundamental limit of a wireless system is the channel, the medium over which wireless signals are sent between transmitter and receiver. Hence, an understanding of the underlying channels is essential for system design. The processes that the electromagnetic wave undergoes in the propagation channel is governed by Maxwell's equations. The term radio channel is used when the effect of the antennas is also included, as these effects can be hard to separate. In the case of isotropic antennas, the propagation channel and radio channel would be equal. The definition of propagation channel and radio channel is visualized in Fig. 3.1. The radio channel can be seen as a linear time-invariant or time-varying filter [19][43].

As a signal propagates through the propagation channel, the amplitude gets attenuated, the phase rotated, and noise is added at the receiver. The signal will interact with objects, so called scatterers, in the environment in different ways. If it is a smooth surface, then the wave is reflected upon and transmitted through the surface. If the surface is a rough (in terms of wavelengths), then the waves are scattered. Waves can also be diffracted at the edges of scatterers

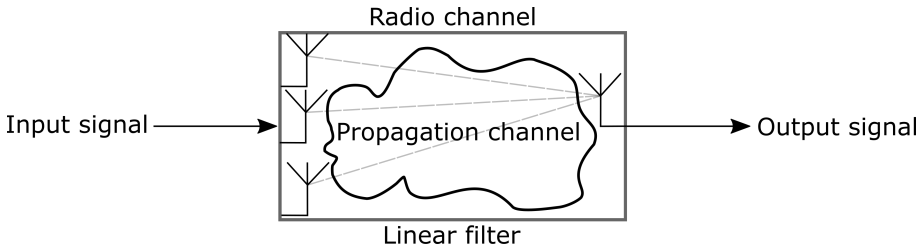

Figure 3.1: The propagation channel and the radio channel.

and undergo waveguiding in e.g. corridors and tunnels [19]. Waves usually interact with one or several scatterers before reaching the receiver.

These mechanisms are dependent on carrier frequency, and hence wavelength, and therefore the channel will be different depending on the band in which the system is operating. Diffraction for different frequencies is analysed in [44] and the roughness of surfaces causing scattering is analysed in [45][46]. Also the weather, such as fog and rain, will influence differently at different frequencies [47].

As a signal is transmitted and travels through a medium to the receiver, there may or may not be a LoS connection. As the wave travels through the medium it experiences the effects as mentioned above when interacting with scatterers in the environment. In indoor environments, the scatterers can be e.g. walls and furniture whereas in outdoor environments it can be buildings, cars and trees. The interaction with scatterers in the environment results in multipath components (MPCs). These MPCs can all be effects of the previously mentioned propagation phenomena. These MPCs eventually superposition, adding up constructively or destructively, at the receiver, yielding the channel response. All these processes can be calculated exactly using Maxwell's equations, although in complex environments this is not feasible. The superposition of MPCs can lead to fading dips, which harm the performance. Hence small-scale fading is important to consider in system design and deployment, but it is hard to predict the behaviour for all locations.

It is a very cumbersome process to describe all these processes that the MPCs go through and hence it is convenient to describe them stochastically. An alternative approach is to perform measurements, extract parameters and create simplified models which can be used to accurately reproduce certain behaviours. Relevant parameters, such as received power and its statistics can be analysed and probabilities for the relevant parameters can be extracted. For system development it may be enough to estimate the mean and the variance. On average, the signal power decreases with distance. Channel gain is one parameter that is very important since it is directly related to the received power or field strength [19].

In a wireless communication system, transmitter, receiver and/or scatterers

can move, which will make the channel change over time, since the different path lengths of the MPCs change and potentially also the interactions with the scatterers. This converts the spatially varying fading to time varying fading, with a rate depending on the speed of the movement. This movement also leads to a shift in frequency, called the Doppler shift, and can be computed as, $\upsilon = -\frac{v}{\lambda} = -\frac{f_c v}{c_0}$ under the assumption that the movement is in the direction of the wave propagation. λ is the wavelength, v the speed of the movement, c_0 the speed of light, and f_c is the carrier frequency. Different MPCs will experience different shifts and the sum of these shifted MPCs will lead to fading dips with a rate of change of the channel that depends on the Doppler frequency [19].

3.1.1 Link budget

A link budget can be a tool when analysing power levels in the systems. This constitutes a clear way of computing the required transmit power, considering the potential gains and losses. An equation of the received power in logarithmic scale, including propagation channel related aspects, can be expressed as

$$P_{RX}(d) = P_{TX} - PL(d) - LS - SS, \tag{3.1}$$

where P_{TX} is the transmit power, $PL(d)$ is the distance-dependent path-loss, LS is the large-scale fading and SS is the small-scale fading. In this chapter, antenna related aspects and system losses are not included and the focus is on the propagation channel aspects. As seen, different channel-related aspects can reduce the received power. These are usually characterised with a distribution having a mean and some variation. The values in these equations are usually the means and therefore a fading margin needs to be added to compensate for these variations and to avoid outage [19].

3.1.2 Path-loss

There is distance dependent attenuation called the path-loss, which is described as the ratio of the transmit power to the mean received power [19]. It is common to characterize it as a log-distance power law according to

$$PL(d) = PL_0 + 10n \log_{10}\left(\frac{d}{d_0}\right), \tag{3.2}$$

where PL_0 is the power at the reference distance d_0, d is the distance between transmitter and receiver and n is the path-loss exponent, which depends on the considered environment.

3.1.3 Large-scale fading

The large-scale fading (in terms of wavelength), is caused by shadowing and attenuation due to blockage by obstacles. This means that the amplitude of the signal, of one or several MPCs, will change with time and location, leading to shadowing and a non LoS (NLoS) scenario if the LoS component is shadowed. The large-scale fading is usually described as a log-normal distribution, i.e., normal distribution on a log-scale, with mean $\mu = 0$ and a standard deviation σ_{LS}, which is scenario-dependent.

3.1.4 Small-scale fading

The previously mentioned propagation phenomena cause small-scale fading, which results in fluctuations in the received signal due to the super-positioning of MPCs as these add up constructively or destructively depending on their phase. As users and scatterers move, this will change the amplitude of the received signal. Small-scale means that it varies over short distances, as compared to the wavelength. This is usually described stochastically by a mean and the variations around this mean.

If there is a large number of scatterers, it is not efficient to deterministically compute each MPC and then one must rely on stochastic solutions. The independent identically distributed (i.i.d.) complex Gaussian, or Rayleigh fading, channel model has historically been shown to offer a good approximation in many practical scenarios. As it has no dominant component, it can be used as a worst case approximation. However, in massive MIMO systems this case is actually beneficial. The model has the advantage that it is simple to describe and for mathematical convenience as it can often lead to closed-form solutions [19]. Having i.i.d. complex Gaussian channel coefficients requires that MPCs come from all directions. This can occur if the environment is rich in scattering. It has been commonly used for theoretical analysis of massive MIMO channels due to its convenience and that the model can provide closed-form expressions. In LoS scenarios there is a dominant specular component which is usually described by a Ricean distribution. The Rayleigh distribution, which is commonly assumed in NLoS scenarios, is the amplitude of the i.i.d. complex Gaussian channel coefficients and is captured in the following probability density function

$$p(r) = \frac{r}{\sigma_{SS}^2} e^{-\frac{r^2}{2\sigma_{SS}^2}}, \tag{3.3}$$

where r is the amplitude and σ_{SS} is the variance. One should note however that an i.i.d. model has its limitations and is not an accurate model for all cases such as in, e.g., LoS scenarios and environments that are not rich in scattering.

3.2 Scenario-specific channels

In different types of environments/scenarios, different channel characteristics will be differently pronounced due to different underlying propagation conditions. This means that the scattering and other propagation phenomena will differ, which affects what the resulting channel will be. In this thesis, two scenarios with different characteristics have been investigated.

3.2.1 Industrial channels

As production processes continue to evolve, more and more factory units will be connected. Because of difficult placements of e.g. sensors and moving robots, it is not always possible to have cabled connections. Furthermore, if there is a need to change something in the production, being dependent on cables makes this change a very cumbersome process. The purpose of the sensors may be to monitor the status of the machinery or tracking assets in the factory. Placing sensors inside of a machinery may be complicated in terms of coverage and the sensors may then also interact with the machinery, the process, or the asset it is supposed to track. Hence, it is preferred to use wireless technologies and a need to study the industrial wireless channel.

A factory environment is in general complex, and each factory is unique and different from other types of buildings, and hence industry-specific parameters are needed [48]. There is usually many walls, which separate different parts of the factory or create aisles. In addition, there may be tall machinery and other equipment that can block the signals. There are often also robots and humans moving around, creating a dynamic environment leading to that Doppler shifts need to be considered.

The complex factory environment creates complex propagation processes with reflections, diffractions, and scattering from e.g. metallic machinery, causing a lot of multipath. Typical propagation processes in industrial environments can be summarized as 1) noise and interference from machinery, 2) many MPCs from a wide range of different reflective structures and 3) path-loss parameters that are substantially varying with the environment, frequency, link configuration [49]. Naturally, lower frequencies will have a better possibility to combat the large-scale fading while higher frequencies will suffer from severe shadowing. This can, however, be counteracted by using beamforming, large arrays, and densification. Then even mmWave systems can fulfil the requirements of URLLC with higher capacity than mid-band [50].

Noise in factory environments is discussed in, e.g. [51][52]. The many MPCs create a rich scattering environment as confirmed in [53], where relevant parameters were extracted. Although being a very rich scattering environment, signals are found to not coming from all directions in previous MIMO-based studies. They do instead tend to come in clusters. Although there is dense

multipath scattering and in one study, more than 100 components were needed to capture 50% of the energy. The channel was measured as almost i.i.d complex Gaussian, except for the LoS component [54][55]. Similar behaviour was reported in [56], where the dense multipaths were 23-70% of the total channel power.

3.2.2 Outdoor Internet-of-Things channels

IoT channels are in many ways different from industrial channels. Here, the focus is on outdoor IoT networks to be deployed for e.g. remote reliable monitoring applications. They require long-range communication and the users need to be energy-efficient to ensure long-term battery-driven operation. In these outdoor scenarios the users will in general be static but potentially with scatterers that are moving. There is infrequent, narrow-band communication and it could be in an unlicensed band with unpredictable interference from other users.

From a propagation point of view there is not much scattering and the channel response will likely be dominated by the LoS component or a few strong MPCs. The channel will therefore have dominant component(s). Since long-range is required, lower frequency bands will be beneficial. For lower frequency bands, the antenna arrays will grow even (physically) larger and consequently the far-field will be further away and the massive MIMO channel characteristics, as elaborated on in Paper I, will likely be even more prominent.

3.3 On the role of measurements for channel modeling

Different channel modeling approaches with their corresponding benefits and drawbacks are discussed in Paper I. For both deterministic and stochastic channel models, channel measurements are vital since the models are based on data. Deterministic models need to be validated with measured data to ensure relevance whereas stochastic models require extensive measurement campaigns to have enough data to extract parameters from.

With many scatterers, the work of describing the propagation phenomena that each MPC is affected by deterministically becomes very challenging and hence a more feasible option is to create stochastic models that can statistically describe the relevant channel characteristics. To get these characteristics, measurement campaigns need to be planned and performed. To plan fir measurement campaigns to be used for general system simulations is hard and requires careful experiment design. Insights can be acquired, but there will be limitations due to, e.g., how much data that is collected, and the scenarios and

experiments that have been measured. Examples of aspects that are important to consider are the equipment used and how that influences the channel measurements, antenna configurations, bandwidth and how to plan the experiments. This in order to make sure that one is measuring what is intended to be measured. As systems and scenarios become more complex, so do also measurement equipment, measurement campaign design, and planning. Channel characteristics in different environments are different and therefore targeted measurement campaigns need to performed. The measurement equipment used for the experiments in this thesis and a brief overview of the performed measurement campaigns are presented in the next chapter.

Chapter 4

Measuring massive MIMO channels

To characterise and model massive MIMO channels in a realistic way, the channels need first to be measured. Consequently, equipment is needed and careful planning of the measurement campaign has to be performed. In this chapter, the foundations of measuring wireless channels is first described and the role of testbeds for wireless communication research is briefly discussed. After that, the equipment used in this thesis work is described: The RUSK Lund channel sounder, the Lund University massive MIMO (LuMaMi) testbed and the KU Leuven massive MIMO (KulMaMi) testbed. Lastly, the considered measurement scenarios are outlined.

4.1 Wireless channel measurements and testbeds

When sounding channels, a transmitter sends a known sounding signal and the receiver records the corresponding received signal transmitted over the channel. By comparing the received signal with the known sounding signal, the channel response can be estimated. Depending on if the result of the channel sounding is stored in time or frequency domain, the resulting output is an impulse response $h(t, \tau)$, as a function over time and delay, or a transfer function $H(t, f)$, as a function over time and frequency. Information-wise they are equivalent as one can obtain one from the other using the (inverse) Fourier transform.

With massive MIMO, the number of channels that need to be measured drastically increases in comparison to more conventional MIMO systems, and hence also the complexity of the equipment. There are a number of ways to

perform massive MIMO channel sounding, where each solution is associated with different opportunities and challenges. A trade-off between complexity and accuracy needs to be made and the targeted scenario needs to considered, such as whether static or dynamic channels are to be measured.

Virtual arrays provide the lowest complexity solution to measure massive MIMO channels, meaning that the large array is enabled by moving one antenna element and for each position measuring the channel between transmitter and receiver. The drawback is that it only allows for static measurements and does not capture effects between antenna elements such as mutual coupling, which has been shown to affect the performance [57]. Depending on the purpose of the measurements, this could be an issue.

A slightly more complex solution is to use a switched-array architecture. In this case only one RF-chain is required, but all antennas need to be deployed. This technique is faster compared to virtual arrays as no mechanical movement of antennas is involved. During the measurements, a switched channel sounder measures each transmit-receive antenna pair by sweeping through all combinations and for each combination, a sounding signal is transmitted, which is then recorded at the receiver side. With this solution, the individual channels are not measured simultaneously, which needs to be taken into account when designing the measurement campaign.

The most complex solution is to have a real-time system, where each antenna element is connected to its own RF-chain. In such a system, the channels between all transmit-receive pairs can be measured simultaneously and therefore time-variant channels can be accurately measured, without concerns of channel variations between individual channel measurements. An issue with these systems can be that calibration of the system might be needed.

Measuring time-variant channels one needs to take the coherence time of the channel (the time for which a channel can be considered static) into account. Thus the repetition rate f_{rep} has to be at least twice the maximum Doppler frequency f^D_{max}, i.e., $f_{rep} \geq 2f^D_{max}$. For a given repetition rate, the maximum speed that can be supported v_{max} can be computed as

$$v_{max} = \frac{cf_{rep}}{2f_c} \tag{4.1}$$

where c is the speed of light and f_c is the carrier frequency. It also needs to be ensured that the repetition period of the sounding signal is longer than the pulse duration, and that it is longer than the delay dispersion of the channel [19].

Both the antennas in the massive MIMO array and the UEs used for the measurement equipment are important as they are considered a part of the radio channel. Depending on the antennas deployed, the experienced channel will be different. Depending on the purpose of the measurement and what is to be investigated, different choices can be made. For example in the UE

case, with omni-directional antennas, signals from all directions can be received while directional antennas receive from a certain span of angles. The array configuration of the massive MIMO array is also important to consider and is selected depending on the scenario.

With new technologies and trends emerging, there is a need for testing theoretical assumptions. Then prototypes need to be built and realized in order to see if the technology is practically feasible. Designing and building testbeds is essential in order to bridge the gap between theory and reality. Since massive MIMO emerged, testbeds for these purposes have been developed and a summary of these is provided in Paper IV.

There are a number of reasons for designing and building testbeds. First of all, as previously mentioned, there is a need to verify theoretical results and concepts with real equipment. Furthermore, testbeds can provide insights into system design challenges. These insights can be used for further development. The requirements for a testbed are usually quite different in comparison to commercial products as the focus is rather on the flexibility of the testbed, to have an opportunity to validate new architectures and algorithms rather than factors such as power consumption and physical dimensions [35][58].

4.2 RUSK Lund channel sounder

The RUSK Lund channel sounder is a switched-array channel sounder, which uses a switched-array architecture at both the transmit and receive side [59]. The transfer functions of each transmit-receive antenna pair are measured rapidly after each other, creating a snapshot of the double-directional channel [60]. An OFDM-like multi-tone sounding signal is used to sound the channel in the frequency domain. The channel sounder is able to operate in the 300 MHz, 2 GHz, and 5 GHz band, with a bandwidth up to 240 MHz.

The channel sounder is for our purposes equipped with a cylindrical antenna array with a center frequency of 2.6 GHz and designed for 200 MHz of bandwidth. The cylindrical array consists of 64 dual-polarized patch antennas, which are arranged in four circles with 16 antennas each. Each patch antenna has two ports, one for the vertical polarization and one for the horizontal polarization, and hence the array adds up to 128 antenna ports in total. The antenna at the UE sida was a vertically polarized SkyCross SMT-2TO6MB-A. This channel sounder has been used to acquire the results in Paper II.

4.3 Lund University massive MIMO testbed

LuMaMi, which was the first real-time massive MIMO testbed in the world [61][62][58], is a software-defined radio (SDR)-based real-time testbed

Figure 4.1: The Lund University massive MIMO testbed with the T-shaped array deployed.

operating at 3.7 GHz with 20 MHz of bandwidth. It can be seen in Fig. 4 and consists of 50 universal software radio peripheral (USRPs), with two RF-chains each, adding up to a total of 100 RF-chains. LuMaMi operates in a TDD-mode and can serve up to twelve users simultaneously in the same time-frequency resource. It uses LTE-like parameters and OFDM signaling. The UEs use similar USRPs, with two RF-chains per SDR that are independently processed and can therefore be considered as two single-antenna users.

The frame schedule is LTE-based where one frame is 10 ms, consisting of ten subframes, each including two timeslots and each timeslot containing seven OFDM symbols. The first timeslot is used for the synchronization signal sent from the BS. The symbols following consist of uplink and downlink pilots and data. Being a reciprocity-based system, the channel estimates obtained from the orthogonal uplink pilots are used for precoding the downlink signals.

The BS and UE can be synchronised both over-the-air (OTA) and externally with either cables between the two units or atomic clocks. Using OTA synchronization allows for more flexible measurements while synchronization through cables or atomic clocks is more reliable.

Originally, a T-shaped array with 160 $\lambda/2$-spaced dual-polarized patch an-

tennas with a center-frequency of 3.7 GHz was developed for the testbed, i.e., in total 320 antenna ports. This array allows for experiments with antenna configurations of different shapes as well as polarizations. As the testbed is equipped with 100 RF-chains, a selection out of the 320 antenna ports needs to be made for the real-time measurements. In most of the measurements in this thesis, the four upper rows with 25 antennas each has been connected with alternating polarizations, starting with the vertically polarized antenna port connected in the upper left corner (as seen from the front). The LuMaMi testbed has been used to measure channels in Paper II, Paper III, and Paper VI.

4.3.1 Channel logging

As the testbed is originally not built to be a channel sounding equipment but rather a real-time communication system, a real-time channel logging facility has been developed as a contribution of this thesis, in collaboration with a former PhD student [28]. To characterise and model channels, the measurement equipment needs to store the channels. The implemented channel logging can capture the channel in real-time, with the UE being the transmitter and the LuMaMi testbed being the receiver that stores the channel responses. The received uplink pilots are used to estimate the channel and then recorded for analysis later on.

Due to the flexible implementation, everything from one sample per frame up to 20 samples per frame for all twelve users can be recorded. To be able to store the channel estimates in real-time at the given repetition rate, this process needed to be implemented in the field-programmable gate arrays (FPGAs), in order to access the dynamic random-access memories (DRAMs). Up to approximately 13 000 snapshots can be stored in the DRAMs. After the measurement has finished, these samples are sent to a hard drive, via the host, and can then be used for post-processing and analysis. A snapshot is of dimensions $F \times M$, for the M antennas and F frequency points, and for K users and N snapshots. The transfer function H will be 4-dimensional with parameters $H = [N \times F \times M \times K]$. Depending on the chosen repetition rate and the number of users K, the channel can be recorded for some seconds up to a few minutes.

4.3.2 Distributed array

Unique for the work in this thesis, a fully distributed array (within practical constraints) has also been deployed when measuring in the industrial scenario. Here 100 dipole antennas were deployed at random places with random orientations, connected with 3 and 5 meters cables to the testbed. The deployment can be seen in Fig. 4.2 and the results are analysed in Paper III.

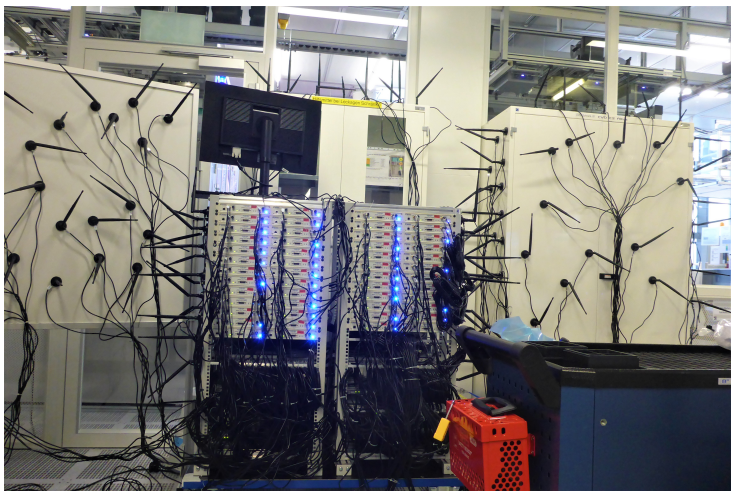

Figure 4.2: The Lund University massive MIMO testbed with a distributed antenna array deployed in a Bosch semiconductor factory, from Paper III.

4.3.3 Hybrid mmWave extension

The LuMaMi testbed has been extended with a hybrid mmWave setup, which is used in Paper VI. The digital subsystems are the same as for the LuMaMi testbed and an analog subsystem has been developed in [63][64]. The analog subsystem converts the 2.5 GHz intermediate frequency (IF) to an RF frequency of 28 GHz, which is then connected to the antenna array. For the experiments in Paper VI, at the base station side, 16 transceiver chains were used for transmitting and receiving, as this is what was the available hardware at the time of the experiments. The testbed can also be extended to include front-end modules at the BS side to be able to switch through beams at both sides, as described in [63][64].

4.4 KU Leuven massive MIMO testbed

The KulMaMi testbed is based on the same architecture as the LuMaMI testbed but with SDRs designed for another frequency range, and it is possible to operate this testbed at sub-GHz frequencies. In total it has 32 USRPs, i.e., 64 RF-chains, although in this work half of them were used. It is usually equipped with a vertically polarized patch antenna array designed for a carrier frequency of 2.6 GHz [65]. The array can easily be re-configured to the shape of a 32-element ULA or a 4x8 URA. This testbed has been used to obtain the results presented in Paper IV and Paper V.

4.4.1 Sub-GHz antenna array

To perform the sub-GHz measurements, a new modular antenna array was developed, as described in Paper IV. Patch antennas were designed for transmission in the unlicensed 868 MHz band. To create a wide variety of array configurations, antenna holders were developed. Each antenna holder could host two elements each, such that arrays of $\lambda/2$-spaced antenna elements could easily be assembled. For the work in this thesis a 32-element ULA and a 4x8 URA were deployed, same as for the mid-band.

4.4.2 Modifications to comply with the regulations

The testbed also needed to be compliant with the unlicensed sub-GHz band regulations and hence the framework had to be adapted to support narrowband transmission and a new frame schedule. The implementation was therefore changed such that only the two subcarriers in the middle of the resource blocks were used. The frame schedule was adapted to only transmit in the first timeslot of each frame in order to comply with restrictions regarding duty cycle. Modifications were also made to be able to have external synchronization through rubidium clocks instead. The last thing to take into account was the transmit power, which was easily changed for compliance in the user interface. As a quality measure, an error-vector-magnitude (EVM) logging was implemented too.

4.5 Measurement scenarios

The previously described channel sounder and testbeds have been used for measurements in different scenarios. In Table 4.1, an overview of the measured scenarios included in this thesis can be found. Measurements have been done in both indoor and outdoor environments as well as in an indoor factory environment and an outdoor environment in the context of massive MIMO for IoT. The measurements in these environments are related to both the URLLC and the mMTC use case, aiming for increased reliability and massive connectivity.

Measurements have been performed in three different bands: the unlicensed sub-GHz band, the sub-6 GHz band, and a mmWave band. Investigations include propagation conditions and massive MIMO channel characteristics in different scenarios where four BS array configurations have been deployed: ULA, URA, UCA, and a fully distributed array. Even though the environment remains the same, how the channel is experienced by the system depends on a wide range of parameters and consequently targeted measurements are needed.

Performing a measurement campaign requires careful planning and preparations. It is hard (and sometimes impossible) to control the surroundings making repeatability of measurements difficult. The purpose in most of the

measurements has been to have a realistic environment for the considered use case, and in that way get realistic results for the system performance that one could expect in a real-world scenario. In reality, one does not control the environment and that has to be taken into account in the system design. The measurement scenarios are chosen to fill gaps and to investigate the research questions outlined in Chapter I. The identified gaps and questions for each scenario is further described in the following.

Table 4.1: Summary of measured scenarios, frequency bands and array configurations.

		Low-band		Mid-band				High-band
		ULA	URA	ULA	URA	UCA	Dist	URA
Indoor	Indoor				x	x		x
	Industry				x		x	
Outdoor	Semi-urban					x		
	IoT	x	x	x	x			

4.5.1 Mid-band indoor auditorium with cylindrical and planar arrays

These measurements were the start of investigating the interaction between a rich scattering environment and the massive MIMO system in a typical indoor environment. The questions addressed by the measurements were

- Does a typical indoor environment provide as rich scattering as the theoretically assumed i.i.d. complex Gaussian channel model?
- How much channel hardening can be experienced in this environment?
- What is the influence of the BS array configuration?

The first set of measurements that has been analysed was conducted before thesis work started [66] with the RUSK Lund channel sounder at 2.6 GHz with 40 MHz of bandwidth. A UCA was deployed. During the measurements nine closely-spaced users were sitting, while moving a tilted antenna, in an indoor auditorium at Lund University. The second set of measurements aimed at repeating parts of the previous measurements but now with the LuMaMi testbed. A planar array was used to investigate and make comparisons of the performance when different antenna arrays are deployed. All these measurements were analysed in Paper II.

4.5.2 Mid-band semi-urban outdoor with a cylindrical array

Related to the previous measurements, the outdoor measurements aimed at providing further insights what is the difference between an outdoor and indoor scenario in terms of scattering and how much channel hardening can be achieved in this environment. The measurements, as analysed in this thesis, also originates from a measurement campaign conducted before this thesis work started [66] with the RUSK Lund channel sounder at 2.6 GHz with 40 MHz of bandwidth and the UCA deployed. The UCA was deployed on the roof-top of one of the campus buildings at Lund University and serving nine closely-spaced users moving within a confined circle in both LoS and NLoS. The results from these measurements are presented in Paper II.

4.5.3 Mid-band industrial indoor with planar and distributed arrays

For an industrial environment, even richer scattering is expected due to metallic parts, a lot of machinery, etc. It is a dynamic environment with robots and humans moving around. The questions to be answered with this measurement campaign were

- How rich can scattering be in a typical industrial environment in comparison to a more typical indoor environment?
- How much channel hardening can be harvested and how is the heavy shadowing experienced by the system?
- By deploying a fully distributed array, can more diversity be extracted and how does this compare to the co-located array?
- Can URLLC be achieved in this type of environment?

These measurements were conducted within the European project 5G-SMART [67] in an operating semiconductor factory in Reutlingen, Germany. There were many practical difficulties when preparing the LuMaMi testbed for experiments in a clean room. The regular planar array was deployed as well as a fully distributed array of dipole antennas. These measurements are analysed in Paper III.

4.5.4 Low-band and mid-band Internet-of-Things outdoor with linear and planar arrays

The scenario described here focuses on exploring sub-GHz massive MIMO to be used for LPWANs and IoT applications. Although most studies have targeted

mid-band massive MIMO, these measurements aimed at characterising sub-GHz massive MIMO channels with a (physically) very large array. Te goal was to study the reliability and massive connectivity in an IoT network.

These measurements were conducted at the KU Leuven campus in Leuven, with the KulMaMi testbed operating at 2.6 GHz and 870 MHz with 195 kHz bandwidth, i.e., narrow-band transmission. Both a ULA and a URA were deployed. The measurements were done with a UE at static points along different paths in the outdoor environment. These measurements have been analysed in Paper IV and V.

4.5.5 High-band lab indoor with a planar array

For higher frequencies, massive MIMO can be the key component to achieve the coverage needed thanks to the array gain. Higher frequencies suffer from increased shadowing effects and hence diversity techniques at the UE side might be essential. How does the shadowing behave at these frequencies? Can antenna switching contribute to increased reliability?

The measurements in the scenario here have been performed in an indoor lab at Lund University, using the LuMaMi testbed with the hybrid mmWave extension. A planar antenna array was deployed at the BS side and the UE was using either a patch or a yagi antenna. Static and continuous measurements were performed in both LoS and NLoS conditions. These measurements have been analysed in Paper VI.

Chapter 5

Contributions and conclusions

In this chapter, the research contributions are outlined, as per included paper, and the content is summarized. Some general conclusions from this work are summarized before presenting an outlook of future research directions.

5.1 Research contributions

5.1.1 Paper I: Massive MIMO channels

This paper is a comprehensive overview paper of massive MIMO channels and can be seen as a part of the overview of the research field and as a research contribution as entailed by the included papers in Part II. After outlining the fundamentals for massive MIMO channels, we present state-of-the-art of channel characterization and modeling methods. We also make an outlook on where the topic of massive MIMO channel characterization and modeling is going, unsolved matters and research directions that are of interest.

5.1.2 Paper II: Channel hardening in massive MIMO: Model parameters and experimental assessment

Theoretical work of massive MIMO channels typically assumes that the channel would be i.i.d. complex Gaussian, and hence that the channel hardening effect would be very prominent. Here we show that this is not necessarily the case, and that the i.i.d. complex Gaussian channel model is overestimating the experienced channel hardening, at least in some relevant indoor and outdoor scenarios, where the channels in general are spatially correlated. The paper

includes a comparison of channel hardening in theory, simulation, and measured channels, and performance evaluations of two different co-located arrays: A cylindrical and planar array. This work was one of the earlier studies to extensively validate channel hardening by conducting experiments in a number of different real environments to assess how rich scattering they actually provide and to investigate how these different environments are interacting with the system. Relevant parameters related to propagation and antenna characteristics are extracted, aiming at identifying propagation processes that affects channel hardening in practical massive MIMO systems. General conclusions from the work are that for the channel hardening effect: (i) the power distribution over the array is essential and (ii) the antenna pattern has a significant influence as it creates power variations in time that are hard to predict, since UE movements are in general unknown.

5.1.3 Paper III: Fading in very reflective and heavily shadowed industrial environments with large arrays

For massive MIMO systems in a factory environment, we showed that the rich scattering needed to get an almost i.i.d. complex Gaussian channel can be found in real industrial environments. Furthermore, we have deployed a unique randomly distributed antenna array (within practical constraints) aiming at further exploiting diversity against large-scale variations in the spatial domain. We investigate propagation conditions based on channel measurements from a reflective and heavily shadowed real-operating factory. With the many antennas, a very prominent channel hardening effect is experienced both for the co-located and the distributed array. With the distributed array configuration, the large-scale power variations can also be reduced, even with unknown UE movement in heavily shadowed environments. Due to this and the vanishing small-scale fading, fading margins can be significantly reduced, achieving a more energy efficient system. The fact that we are here approaching an i.i.d. complex Gaussian channel suggests that one should rethink the system design in such an environment. Channel coding can be done with shorter block-lengths, shorter packets are feasible and re-transmissions could potentially be eliminated. The results in this work show that achieving URLLC in such an environment could be possible, with both the array configurations.

5.1.4 Paper IV: Massive MIMO goes sub-GHz: Implementation and experimental exploration for LP-WANs

Experimental investigations of massive MIMO systems operating at sub-GHz frequencies was until this work lacking. To be able to do experimental re-

search on this topic, a testbed had to be developed and hence we extended the KulMaMi testbed to operate in the unlicensed sub-GHz band and equipped it with a newly designed modular antenna array, yielding the first massive MIMO measurements in this frequency band. Channels were collected with a ULA and a URA in different outdoor scenarios, showing the potential to deploy sub-GHz massive MIMO systems to reliably serve energy-constrained devices in LPWANs.

5.1.5 Paper V: Experimental exploration of unlicensed sub-GHz massive MIMO for massive Internet-of-Things

Continuing where the previous paper finished, this paper further explores the potential of deploying sub-GHz massive MIMO systems to support IoT networks where the focus is on reliable narrow-band communication to a massive number of energy-constrained devices distributed in a wide area. For the first time, sub-GHz massive MIMO channel conditions were investigated and assessed in terms of reliability, coverage and energy efficiency. We compare measured results from outdoor measurements with a ULA and a URA to a theoretical framework. Here, again, the assumption of i.i.d. complex Gaussian channels in massive MIMO does not hold as measurements show that there are dominant directions, which can be used for scheduling devices. The channel orthogonality of different devices, as an effect of favourable propagation conditions, is investigated, showing that a ULA is better at decorrelating devices, even perpendicular to the array. The array gain can be used to extend the coverage or to reduce transmit power. The experienced channel hardening is quantified, with the result being slightly more channel hardening with the ULA.

5.1.6 Paper VI: mmWave massive MIMO in real propagation environment: Performance evaluation using LuMaMi28GHz

In the last part of this thesis work, massive MIMO channels in the mmWave band was explored. In the mmWave band, the array gain can be an absolute necessity to achieve a reliable link. Moreover, hybrid architectures might be useful as a good trade-off between complexity and reliability, also at the UE side. This study presents a performance evaluation of antenna selection at the UE side in hybrid mmWave systems, based on both LoS/NLoS measurements with patch and yagi UE antennas.

5.2 General conclusions

Massive MIMO has gone from a theoretical concept to a key component of the standard for 5G systems. It will most likely evolve in different directions in the future. Massive MIMO brings capacity improvements, more reliable systems, enables long-range communication, and can support user terminals with stringent energy requirements. With 5G, the use cases eMBB, URLLC and mMTC were envisioned, each with its own set of applications and requirements. Although much research effort has been spent in the field, some visions might not yet be entirely realizable but will continue to evolve with new releases and many envisioned applications for 6G are about taking the next step from the applications envisioned for 5G.

To assess the performance of a wireless system, one needs to consider the underlying channels as their interaction with the system will set boundaries of what is achievable, and, hence, the underlying channels need to be accounted for in the system design to optimize performance. The first studies concerning massive MIMO channels were conducted at mid-band and a fundamental understanding and exploration of how these channels behave and affect system performance had been done already before the start of this thesis. Since then, much research has been in the direction of higher frequencies, a track which is also partially explored in this work. Prior to this thesis, not much work had been done for lower frequencies. Furthermore, studies investigating how to realize the envisioned use case have been needed, with this work some more insights are obtained regarding URLLC and mMTC. Following these very general conclusions, an elaborated answer to each of the research questions as presented in Chapter I is outlined.

How rich in scattering are different environments and how do the system interact with these environments?

The first theoretical work regarding massive MIMO assumed that the environment would be so rich in scattering that the channels could be assumed to be i.i.d. complex Gaussian. Early experimental studies showed, however, that massive MIMO channels in general are spatially correlated. In this thesis, the richness of scattering is investigated in terms of channel hardening. It was shown that channels in a typical indoor scenario are spatially correlated. Consequently, the channel hardening effect was not as prominent as predicted by the theoretical assumption. Hence, a typical auditorium can not be expected to offer that rich scattering, such that this theoretical assumption of massive MIMO channels is fulfilled. Note that the channel hardening effect was much more prominent indoors than in typical outdoor scenarios. There the channels are even more spatially correlated, i.e., even less rich scattering, and the signal has very dominant directions.

Even though the theoretical assumption of i.i.d. complex Gaussian channels in indoor environments could not be met, there is still a significant channel hardening effect that will contribute to a more reliable communication system. Further exploring the channel hardening effect in more scenario-specific contexts, the effect can still improve the reliability even in outdoor IoT scenarios, even though these environments are not very rich scattering. Therefore the channel is not i.i.d. complex Gaussian but rather has dominant directions, leading to some channel hardening due to the many antennas, but not that close to the theoretical assumption. However, in very rich scattering indoor industrial environments, the theoretical prediction was reasonably accurate and a huge portion of the expected channel hardening could be obtained.

With richer scattering, more channel hardening can be obtained, i.e., the experienced channel becomes more stable with less fading, and, hence, making it a more reliable system. Furthermore, when accounting for this in the system design, smaller fading margins are required to counteract fading, which reduces the need of retransmissions to achieve reliability, therefore improving the latency. The channel hardening effect also affects suitable channel coding schemes and could allow for reliable transmission of short packets. In environments that are not as rich in scattering, some channel hardening can still be obtained. Knowledge of dominant directions, as e.g. found in outdoor scenarios, is also important and can be used for e.g. grouping and scheduling users.

What are the underlying propagation processes that affects channel hardening in practical massive MIMO systems?

Continuing further elaborating on the channel hardening effect and factors that affect how much channel hardening can be achieved, it all depends on the characteristics of the environment. An environment with a lot of scatterers will lead to low spatial correlation thus more channel hardening and an environment with open spaces will lead to higher spatial correlation thus less channel hardening. The power distribution over the array is essential, and with massive MIMO, there are usually nonstationarities over the array, which is also related to the physical size of the array as well as the environment and deployment. Moreover, exploiting different polarization modes can improve the channel hardening effects as more independent channels can be utilized. The channel hardening is also, as expected, more prominent in NLoS scenarios than in LoS scenarios, since in NLoS there are usually more reflections contributing to the received power. This does not make LoS channels unreliable in any way since it can already be a reliable channel and in some way it is already "pre-hardened" with steep cumulative distribution functions (CDFs) of channel gain. Lastly, especially in not as rich scattering environments, the antenna pattern and the movement of the user terminals affect the experienced channel hardening.

How pronounced are massive MIMO channel characteristics in different frequency bands and how can dependable communication be realized in these bands?

In this thesis, the word dependable is used in the sense that both reliability and availability are addressed. Fundamentally, reliability in wireless communication is about diversity and this can be exploited in many different ways. In massive MIMO, spatial diversity is exploited with the many antennas. Frequency diversity can be exploited with multi-carrier transmission schemes, such as OFDM, but also with the digital precoding. Both of these are applied in all the measurements performed in this work. Adding to these two, spatial diversity can be further exploited with distributed arrays and combined with e.g. switched diversity at the user side. Time diversity is in general not an option in the URLLC use case, since it increases the latency. Diversity becomes even more important for higher frequencies, which inherently are suffering from severe shadowing. This challenge needs to be addressed when aiming for high reliability and availability. In general, different diversity techniques in the various domains can be combined to achieve more dependable communication.

Typical massive MIMO channel characteristics, i.e., experiencing spherical wavefronts, nonstationarity over the array, and increase in 3-dimensional (3D) propagation and polarization effects, stems from having a physically large array due to the many antennas. Hence, these characteristics become even more prominent for lower frequencies as the array becomes physically larger due to the longer wavelength. These characteristics are usually also more prominent in NLoS than in LoS, especially if the entire array can see the LoS component. For lower frequencies, it is easier to realize reliable communication due to lower path-loss. However, there might be practical reasons regarding deployment that makes these array less tractable. For higher frequencies, achieving reliability can be more difficult, complex and costly if each antenna element is supposed to have a RF-chain. Instead a hybrid architecture could be a solution. It could also be more important to exploit other diversity techniques, such as e.g. switched diversity, at the user side.

All bands experience channel hardening, i.e., reduced small-scale fading effects, which contributes to reliable communication. With the small-scale fading effects significantly reduced, reliability is to a larger extent determined by large-scale fading effects, which will create power variations over time. These effects can be reduced by deploying a distributed antenna configuration, potentially at the cost of reduced channel hardening and then a trade-off has to be made.

How are practical antenna arrays interacting with the channel and influence the system performance? Can more diversity be achieved by deploying a distributed array and how does that influence the overall system in comparison to a co-located array?

The experiments in this thesis have shown that in the considered environments, larger performance improvements can be achieved by deploying a physically large array, e.g. extending the array in the horizontal domain or by distributing the antennas, than extending in the vertical domain. Although this depends on the angular power spectrum and hence the specific environment and locations of users, and the choice of antenna configuration naturally needs to be made with the targeted environment and placement of users in mind.

For the measurements in the industrial scenario, the comparison between the distributed array and the co-located array showed that the small-scale fading statistics were similar for the two deployments. However, the large-scale fading was reduced with the distributed array since this array was better suited to account for unknown user movement. This due to that it is more likely that some antennas in the distributed array will have a strong channel to the user, while some will have a very weak channel. However, on average the received signal strength can be sufficient and large-scale fading effects can to some extent be combated when the contributions from all antenna elements are coherently combined.

Is URLLC realizable in industrial environments? How is the system interacting with a rich scattering and heavily shadowed environment?

The experiments in this study showed that an industrial environment with many interacting objects and metallic equipment can indeed provide enough scattering such that it results in an almost i.i.d. complex Gaussian fading channel. The CDFs of channel gain get steeper with more antennas and the experienced channel hardening is very prominent. The small-scale fading effects are significantly reduced as the number of antennas increases. This environment was also one with very heavy shadowing, with lots of machinery creating large-scale fading effects. By distributing the antennas, the large-scale power variations could be reduced. The experiments were performed at mid-band and the result is very promising for achieving URLLC in industrial environments. To do so, the entire system needs to be designed with the channel behaviour in mind to optimize e.g. channel coding, packet structures and potentially eliminating re-transmissions to further reduce latency while still achieving high reliability.

Can massive MIMO systems efficiently provide reliable communication for IoT networks?

Massive MIMO systems could indeed be a part of the solution to provide reliable communication for IoT networks. In outdoor environments, the channel will likely have dominant directions, while still obtaining some of the channel hardening effect associated with massive MIMO. These dominant directions can, however, be exploited in e.g. grouping and scheduling of IoT nodes. With the array gain, the coverage can be extended to serve nodes over a larger area, or it could be used to reduce the transmit power for energy efficiency. There are possibilities to deploy these networks at both unlicensed band at lower frequencies, benefiting from the lower path-loss, or in the licensed mid-band. There is also a potential to switch between the bands in case of too heavy interference or if higher throughput would be needed. In IoT networks, the number of nodes in general grows large, and here the potential to efficiently serve many nodes simultaneously has been shown.

5.3 Outlook

When starting this work, the massive MIMO concept was relatively new and during this work much other research work has been going on simultaneously, including theoretical, simulation-based, and experimental/measurement-based studies. The topic has matured and here are some directions in which the aspects presented in this work could continue to evolve:

- **More antennas:** The initial idea of massive MIMO was that the number of antennas was going towards infinity [22]. This is of course not practical and current systems saturate around at most a few hundreds antennas. The number of antennas in future systems may still increase even further. With more antennas, and hence physically larger arrays, the massive MIMO channel characteristics will likely be even more prominent. Nonstationarity over the array will likely be more pronounced and that can cause problems if it is ignored, but helpful if it is accounted for [68]. Depending on the environment, if there are more scatterers to be exploited, then even more channel hardening could be obtained. With more antennas, more RF-chains or hybrid architectures are needed. In most cases, all antennas are not contributing equally at a certain moment, and therefore there is a potential to reduce the number of RF-chains while still increasing the number of antennas.

- **Distributed antennas:** With many antennas, there is also a possibility for more innovative array configurations, and a potential to distribute the antenna elements over a larger area. With many antennas, the small-scale

fading effects can potentially be averaged out and by distributing the antennas, the large-scale fading effects can be reduced. With a distributed setup, the probability that one or several antennas have LoS conditions increases, which contributes to a more reliable link. However, the power imbalances over the array will likely also increase, which could reduce the experienced channel hardening and therefore there could be a need of a trade-off between these two. A fully random distribution of the antennas also opens up the opportunity to further exploit spatial and polarization diversity while also creating uncertainty of how the antennas are affecting each other and interacting with the surrounding environment. Especially in scenarios like an indoor factory with a lot of equipment in the surroundings. Another advantage of distributing the antennas is that it accounts for more diverse and unexpected user movements, being beneficial when this movement is unknown. A challenge is how to actually make the practical setup, as it will require a lot of cabling to connect the elements to a central processing unit. To reduce this, ways of performing distributed processing should be considered.

- **Cell-free systems:** Another trend that is being investigated is to move away from the long used cellular architecture and instead go towards cell-free systems where many distributed access points are spread over a large area and co-operatively are serving all users. This will likely, similar to using distributed arrays, reduce the large-scale fading and increase the probability that at least one, or a few, access points have a reliable link to the user while this comes as a trade-off of decreased channel hardening depending on the environment and how many antennas each access point has; this is in line with the more theoretical study in [69] but should also be investigated in practise.

- **Higher frequencies:** As higher data rates and more users are to be connected, more bandwidth is needed and this can be found in even higher frequency bands. Currently mmWave systems, also explored in this work, are becoming more mature. Meanwhile research is targeting even higher frequencies, such as the sub-THz and THz bands. With even higher frequencies, reliability will become even more of a challenge as the shadowing is more severe and more antennas are needed in order to achieve the array gain to counteract this. Also here, hybrid architectures might be needed as a trade-off between getting the massive MIMO benefits and complexity and cost.

- **Combined diversity techniques:** Fundamentally, reliability in wireless systems is about diversity and hence, in order to achieve reliable communication, diversity in all possible domains should be exploited.

- **New and more evolved use cases:** The requirements on wireless communication will likely continue to increase in terms of data rates, reliability, number of users, etc. The visions are aiming higher, but some requirements as envisioned for 5G might still remain unfulfilled. There have been a lot of investigations in the area of URLLC and Industry 4.0, showing promising results similar to those in this thesis, but the question of how to actually bring these systems into factories and commercialise this remain open. Also, each factory is unique and hence site-specific investigations and deployments are needed in order to fulfill the often stringent requirements in the considered factory.

- **System design:** As the channel affects the system performance, it needs to be considered in the system design. To fulfill the requirements of the URLLC use case, which could be possible with a massive MIMO system under favourable conditions, the system design needs to be thought through carefully as this affects how e.g. coding and re-transmission strategies should be applied. Hence a cross-layer approach would be beneficial. The same applies for IoT networks. Massive MIMO could improve the performance but it requires a system approach where physical layer techniques are integrated with the protocol design [70].

References

[1] A. Osseiran, S. Parkvall, P. Persson, A. Zaidi, S. Magnusson and K. Balachandran, *5G wireless access: An overview*, version 1/28423-FGB1010937, Apr. 2020.

[2] M. Shafi, A. F. Molisch, P. J. Smith *et al.*, "5G: A tutorial overview of standards, trials, challenges, deployment, and practice," *IEEE Journal on Selected Areas in Communications*, vol. 35, no. 6, pp. 1201–1221, 2017.

[3] H. Tataria, M. Shafi, A. F. Molisch, M. Dohler, H. Sjöland and F. Tufvesson, "6G wireless systems: Vision, requirements, challenges, insights, and opportunities," *Proceedings of the IEEE*, vol. 109, no. 7, pp. 1166–1199, 2021.

[4] Z. Li, M. A. Uusitalo, H. Shariatmadari and B. Singh, "5G URLLC: Design challenges and system concepts," in *2018 15th International Symposium on Wireless Communication Systems (ISWCS)*, 2018, pp. 1–6.

[5] C. Bockelmann, N. K. Pratas, G. Wunder *et al.*, "Towards massive connectivity support for scalable mMTC communications in 5G networks," *IEEE Access*, vol. 6, pp. 28 969–28 992, 2018.

[6] Z. Zhang, Y. Xiao, Z. Ma *et al.*, "6G wireless networks: Vision, requirements, architecture, and key technologies," *IEEE Vehicular Technology Magazine*, vol. 14, no. 3, pp. 28–41, 2019.

[7] K. B. Letaief, W. Chen, Y. Shi, J. Zhang and Y.-J. A. Zhang, "The roadmap to 6G: AI empowered wireless networks," *IEEE Communications Magazine*, vol. 57, no. 8, pp. 84–90, 2019.

[8] H. Lasi, P. Fettke, H.-G. Kemper, T. Feld and M. Hoffmann, "Industry 4.0," *Business & Information Systems Engineering*, vol. 6, no. 4, pp. 239–242, 2014.

[9] A. Varghese and D. Tandur, "Wireless requirements and challenges in Industry 4.0," in *2014 International Conference on Contemporary Computing and Informatics (IC3I)*, 2014, pp. 634–638.

[10] H. Ji, S. Park, J. Yeo, Y. Kim, J. Lee and B. Shim, "Ultra-reliable and low-latency communications in 5G downlink: Physical layer aspects," *IEEE Wireless Communications*, vol. 25, no. 3, pp. 124–130, 2018.

[11] P. Popovski, u. Stefanović, J. J. Nielsen *et al.*, "Wireless access in ultra-reliable low-latency communication (URLLC)," *IEEE Transactions on Communications*, vol. 67, no. 8, pp. 5783–5801, 2019.

[12] J. Cheng, W. Chen, F. Tao and C.-L. Lin, "Industrial IoT in 5G environment towards smart manufacturing," *Journal of Industrial Information Integration*, vol. 10, pp. 10–19, 2018.

[13] J. Sachs and K. Landernäs, "Review of 5G capabilities for smart manufacturing," in *2021 17th International Symposium on Wireless Communication Systems (ISWCS)*, 2021, pp. 1–6.

[14] B. Hochwald, T. Marzetta and V. Tarokh, "Multiple-antenna channel hardening and its implications for rate feedback and scheduling," *IEEE Transactions on Information Theory*, vol. 50, no. 9, pp. 1893–1909, 2004.

[15] H. Q. Ngo, E. G. Larsson and T. L. Marzetta, "Aspects of favorable propagation in massive MIMO," in *2014 22nd European Signal Processing Conference (EUSIPCO)*, 2014, pp. 76–80.

[16] R. S. Sinha, Y. Wei and S.-H. Hwang, "A survey on LPWA technology: LoRa and NB-IoT," *ICT Express*, vol. 3, no. 1, pp. 14–21, 2017.

[17] A. Lavric, A. I. Petrariu and V. Popa, "Sigfox communication protocol: The new era of IoT?" In *2019 International Conference on Sensing and Instrumentation in IoT Era (ISSI)*, 2019, pp. 1–4.

[18] E. Björnson, J. Hoydis and L. Sanguinetti, "Massive MIMO networks: Spectral, energy, and hardware efficiency," *Foundations and Trends® in Signal Processing*, vol. 11, no. 3-4, pp. 154–655, 2017.

[19] A. Molisch, *Wireless Communications*, English. United States: John Wiley & Sons Inc., 2005.

[20] D. Brennan, "Linear diversity combining techniques," *Proceedings of the IEEE*, vol. 91, no. 2, pp. 331–356, 2003.

[21] T. L. Marzetta, E. G. Larsson, H. Yang and H. Q. Ngo, *Fundamentals of Massive MIMO*. Cambridge University Press, 2016.

[22] T. L. Marzetta, "Noncooperative cellular wireless with unlimited numbers of base station antennas," *IEEE Trans. Wireless Commun.*, vol. 9, pp. 3590–3600, 11 Nov. 2010.

[23] F. Rusek, D. Persson, B. K. Lau *et al.*, "Scaling up MIMO: Opportunities and challenges with very large arrays," *IEEE Signal Process. Mag.*, vol. 30, no. 1, pp. 40–60, 2013.

[24] E. Björnson, J. Hoydis and L. Sanguinetti, *Massive MIMO Networks: Spectral, Energy, and Hardware Efficiency (Foundations and Trends in Signal Processing)*. Now Publishers Inc, 2018.

[25] E. G. Larsson, O. Edfors, F. Tufvesson and T. L. Marzetta, "Massive MIMO for next generation wireless systems," *IEEE Communications Magazine*, vol. 52, no. 2, pp. 186–195, 2014.

[26] L. Sanguinetti, E. Björnson and J. Hoydis, "Toward massive MIMO 2.0: Understanding spatial correlation, interference suppression, and pilot contamination," *IEEE Transactions on Communications*, vol. 68, no. 1, pp. 232–257, 2020.

[27] J. Jose, A. Ashikhmin, T. L. Marzetta and S. Vishwanath, "Pilot contamination and precoding in multi-cell TDD systems," *IEEE Transactions on Wireless Communications*, vol. 10, no. 8, pp. 2640–2651, 2011.

[28] E. Bengtsson, "Massive MIMO from a terminal perspective," Ph.D. dissertation, Department of Electrical and Information Technology, Sep. 2019.

[29] J. Flordelis, F. Rusek, F. Tufvesson, E. G. Larsson and O. Edfors, "Massive MIMO performance—TDD versus FDD: What do measurements say?" *IEEE Transactions on Wireless Communications*, vol. 17, no. 4, pp. 2247–2261, 2018.

[30] C. E. Shannon, "A mathematical theory of communication," *The Bell System Technical Journal*, vol. 27, no. 3, pp. 379–423, 1948.

[31] E. Björnson, E. G. Larsson and T. L. Marzetta, "Massive MIMO: Ten myths and one critical question," *IEEE Communications Magazine*, vol. 54, no. 2, pp. 114–123, 2016.

[32] A. Paulraj and C. Papadias, "Space-time processing for wireless communications," *IEEE Signal Processing Magazine*, vol. 14, no. 6, pp. 49–83, 1997.

[33] J. Choi, D. J. Love and P. Bidigare, "Downlink training techniques for FDD massive MIMO systems: Open-loop and closed-loop training with memory," *IEEE Journal of Selected Topics in Signal Processing*, vol. 8, no. 5, pp. 802–814, 2014.

[34] J. Vieira, F. Rusek, O. Edfors, S. Malkowsky, L. Liu and F. Tufvesson, "Reciprocity calibration for massive MIMO: Proposal, modeling, and validation," *IEEE Transactions on Wireless Communications*, vol. 16, no. 5, pp. 3042–3056, 2017.

[35] J. Vieira, "Algorithms and proofs of concept for massive MIMO systems," Ph.D. dissertation, Broadband Communication, Department of Electrical and Information Technology, 2017.

[36] K. T. Truong and R. W. Heath, "Effects of channel aging in massive MIMO systems," *Journal of Communications and Networks*, vol. 15, no. 4, pp. 338–351, 2013.

[37] E. Björnson, J. Hoydis and L. Sanguinetti, "Massive MIMO has unlimited capacity," *IEEE Transactions on Wireless Communications*, vol. 17, no. 1, pp. 574–590, 2018.

[38] M. Joham, W. Utschick and J. Nossek, "Linear transmit processing in MIMO communications systems," *IEEE Transactions on Signal Processing*, vol. 53, no. 8, pp. 2700–2712, 2005.

[39] E. Björnson, J. Hoydis, M. Kountouris and M. Debbah, "Massive MIMO systems with non-ideal hardware: Energy efficiency, estimation, and capacity limits," *IEEE Transactions on Information Theory*, vol. 60, no. 11, pp. 7112–7139, 2014.

[40] E. Björnson, J. Hoydis, M. Kountouris and M. Debbah, "Massive MIMO systems with non-ideal hardware: Energy efficiency, estimation, and capacity limits," *IEEE Transactions on Information Theory*, vol. 60, no. 11, pp. 7112–7139, 2014.

[41] H. Q. Ngo and E. G. Larsson, "No downlink pilots are needed in TDD massive MIMO," *IEEE Transactions on Wireless Communications*, vol. 16, no. 5, pp. 2921–2935, 2017.

[42] X. Gao, O. Edfors, F. Rusek and F. Tufvesson, "Linear pre-coding performance in measured very-large MIMO channels," in *2011 IEEE Vehicular Technology Conference (VTC Fall)*, 2011, pp. 1–5.

[43] P. Bello, "Characterization of randomly time-variant linear channels," *IEEE Transactions on Communications Systems*, vol. 11, no. 4, pp. 360–393, 1963.

[44] M. Shafi, J. Zhang, H. Tataria *et al.*, "Microwave vs. millimeter-wave propagation channels: Key differences and impact on 5G cellular systems," *IEEE Communications Magazine*, vol. 56, no. 12, pp. 14–20, 2018.

[45] C. Jansen, S. Priebe, C. Moller *et al.*, "Diffuse scattering from rough surfaces in THz communication channels," *IEEE Transactions on Terahertz Science and Technology*, vol. 1, no. 2, pp. 462–472, 2011.

[46] R. Piesiewicz, C. Jansen, D. Mittleman, T. Kleine-Ostmann, M. Koch and T. Kurner, "Scattering analysis for the modeling of THz communication systems," *IEEE Transactions on Antennas and Propagation*, vol. 55, no. 11, pp. 3002–3009, 2007.

[47] E. K. Smith, "Centimeter and millimeter wave attenuation and brightness temperature due to atmospheric oxygen and water vapor," *Radio Science*, vol. 17, no. 06, pp. 1455–1464, 1982.

[48] M. Schmieder, F. Undi, M. Peter, E. Koenig and W. Keusgen, "Directional wideband channel measurements at 28 GHz in an industrial environment," in *2019 IEEE Global Communications Conference (GLOBECOM)*, 2019, pp. 1–6.

[49] M. Cheffena, "Propagation channel characteristics of industrial wireless sensor networks [wireless corner]," *IEEE Antennas and Propagation Magazine*, vol. 58, no. 1, pp. 66–73, 2016.

[50] O. Al-Saadeh, K. Hiltunen, K. Kittichokechai *et al.*, "5G ultra-reliable low-latency communication for factory automation at millimetre wave bands," in *2019 IEEE Global Communications Conference (GLOBECOM)*, 2019, pp. 1–6.

[51] K. S. Low, W. Win and M. J. Er, "Wireless sensor networks for industrial environments," in *International Conference on Computational Intelligence for Modelling, Control and Automation and International Conference on Intelligent Agents, Web Technologies and Internet Commerce (CIMCA-IAWTIC'06)*, vol. 2, 2005, pp. 271–276.

[52] K. Blackard, T. Rappaport and C. Bostian, "Measurements and models of radio frequency impulsive noise for indoor wireless communications," *IEEE Journal on Selected Areas in Communications*, vol. 11, no. 7, pp. 991–1001, 1993.

[53] S. Jaeckel, N. Turay, L. Raschkowski *et al.*, "Industrial indoor measurements from 2-6 GHz for the 3GPP-NR and QuaDRiGa channel model," in *2019 IEEE 90th Vehicular Technology Conference (VTC2019-Fall)*, 2019, pp. 1–7.

[54] J. Karedal, S. Wyne, P. Almers, F. Tufvesson and A. F. Molisch, "A measurement-based statistical model for industrial ultra-wideband channels," *IEEE Transactions on Wireless Communications*, vol. 6, no. 8, pp. 3028–3037, 2007.

[55] E. Tanghe, W. Joseph, J. D. Bruyne, L. Verloock and L. Martens, "The industrial indoor channel: Statistical analysis of the power delay profile," *AEU - International Journal of Electronics and Communications*, vol. 64, no. 9, pp. 806–812, 2010.

[56] E. Tanghe, D. P. Gaillot, M. Liénard, L. Martens and W. Joseph, "Experimental analysis of dense multipath components in an industrial environment," *IEEE Transactions on Antennas and Propagation*, vol. 62, no. 7, pp. 3797–3805, 2014.

[57] X. Chen, S. Zhang and Q. Li, "A review of mutual coupling in MIMO systems," *IEEE Access*, vol. 6, pp. 24 706–24 719, 2018.

[58] S. Malkowsky, "Massive MIMO: Prototyping, proof-of-concept and implementation," Ph.D. dissertation, Apr. 2019.

[59] R. Thoma, D. Hampicke, A. Richter *et al.*, "Identification of time-variant directional mobile radio channels," *IEEE Transactions on Instrumentation and Measurement*, vol. 49, no. 2, pp. 357–364, 2000.

[60] M. Steinbauer, A. Molisch and E. Bonek, "The double-directional radio channel," *IEEE Antennas and Propagation Magazine*, vol. 43, no. 4, pp. 51–63, 2001.

[61] J. Vieira, S. Malkowsky, K. Nieman *et al.*, "A flexible 100-antenna testbed for massive MIMO," in *2014 IEEE Globecom Workshops (GC Wkshps)*, IEEE, 2014, pp. 287–293.

[62] S. Malkowsky, J. Vieira, L. Liu *et al.*, "The world's first real-time testbed for massive MIMO: Design, implementation, and validation," *IEEE Access*, vol. 5, pp. 9073–9088, 2017.

[63] M. Chung, L. Liu, A. Johansson *et al.*, "Millimeter-wave massive MIMO testbed with hybrid beamforming," in *2020 54th Asilomar Conference on Signals, Systems, and Computers*, 2020, pp. 309–313.

[64] M. Chung, L. Liu, A. Johansson *et al.*, "LuMaMi28: Real-time millimeter-wave massive MIMO systems with antenna selection," 2021. arXiv: `2109.03273 [eess.SP]`.

[65] C. Chen, V. Volski, L. Van der Perre, G. A. E. Vandenbosch and S. Pollin, "Finite large antenna arrays for massive MIMO: Characterization and system impact," *IEEE Transactions on Antennas and Propagation*, vol. 65, no. 12, pp. 6712–6720, 2017.

[66] A. Bourdoux, C. Desset, L. van der Perre *et al.*, "D1.2 MaMi channel characteristics: Measurement results," MAMMOET, Report, 2015.

[67] *5G for smart manufacturing (5G-SMART)*, `https://5gsmart.eu/`.

[68] E. D. Carvalho, A. Ali, A. Amiri, M. Angjelichinoski and R. W. Heath, "Non-stationarities in extra-large-scale massive MIMO," *IEEE Wireless Communications*, vol. 27, no. 4, pp. 74–80, 2020.

[69] Z. Chen and E. Björnson, "Channel hardening and favorable propagation in cell-free massive MIMO with stochastic geometry," *IEEE Transactions on Communications*, vol. 66, no. 11, pp. 5205–5219, 2018.

[70] A.-S. Bana, E. de Carvalho, B. Soret *et al.*, "Massive MIMO for Internet of Things (IoT) connectivity," *Physical Communication*, vol. 37, p. 100 859, 2019.

Part II

Included papers

Paper I

Massive MIMO channels

Massive MIMO Channels

Sara Gunnarsson[1,2], *Liesbet Van der Perre*[1,2], *and Fredrik Tufvesson*[1]

[1] *Lund University, Lund, Sweden*
[2] *KU Leuven, Leuven, Belgium*

Introduction

Massive MIMO (multiple-input multiple-output) has emerged as a new technology to be used in wireless systems for the fifth generation and beyond (Marzetta 2010; Rusek et al. 2013; Larsson et al. 2014). When designing channel models for these systems, it is important to capture the most prominent propagation characteristics. The models need to be accurate and tractable in terms of complexity such that they can be used for developing algorithms and assessing system performance.

In massive MIMO systems, the number of base station antennas is radically increased from just a few and is growing, possibly even into the hundreds. With the increased degrees of freedom, capacity can be increased by using spatial multiplexing. Alternatively, by using beamforming techniques, pathloss can be combated. The latter will be essential, as the trend for future generations is to also exploit higher frequencies in addition to the sub-6 GHz bands. Therefore, in addition to investigating how micro-wave propagation affects massive MIMO performance, an understanding of the fundamental aspects of mm-wave propagation is necessary for proper system design. Another effect caused by the evolution of increasing the number of base station antennas is that the complexity of the user terminals can be reduced (Larsson et al. 2014). However, the user equipment and interaction with nearby surroundings still impose limitations on the overall system performance (Björnson et al. 2014; Bengtsson et al. 2015), and a realistic channel model should, therefore, capture these aspects as well.

In order to characterize massive MIMO channels, several measurement campaigns have been carried out. Analysis of these measurements has provided insights about the effects of deploying large antenna systems in real-world scenarios. Firstly, due to the physically large arrays, the assumption of planar wavefronts does not necessarily hold anymore and near-field effects can be experienced. Secondly, nonstationarity and large-scale fading effects over the array can be present. Finally, when deploying an order of magnitude more antennas at the base station side, the possibilities to even further extract spatial and polarization diversity from the environment open up. Then 3D propagation and polarization effects in the channel become noticeable and thus important to consider (Gao 2016).

Wiley 5G Ref. Edited by Rahim Tafazolli, Chin-Liang Wang and Periklis Chatzimisios.

DOI: 10.1002/9781119471509.w5GRef040

Taking the whole massive MIMO system into account, some channel-dependent characteristics can be identified, which relates to how the channel is experienced. For the base station, the experienced channel depends on the uplink pilot transmission and how the users experience the channel is affected by the applied precoding. Two significant channel-dependent characteristics in massive MIMO systems are that user separability increases (Flordelis et al. 2018), as a result of favorable propagation conditions, and system reliability increases due to the channel hardening effect. Favorable propagation is defined as the mutual orthogonality between the user channels (Ngo et al. 2014). The channel hardening effect refers to that the variations of channel gain decrease in both time and frequency domain when increasing the number of antennas (Ngo and Larsson 2017; Payami and Tufvesson 2013).

The most commonly used channel model for theoretical massive MIMO analyses is the independent and identically distributed (i.i.d.) complex Gaussian channel model. The model is convenient to use and beneficial from a complexity point of view but has its limitations with respect to accurately representing the channel behavior. For conventional MIMO systems, different stochastic and deterministic channel modeling approaches exist. A common deterministic channel model approach is ray tracing. In the first category, there are correlation-based channel models, such as the Kronecker (Kermoal et al. 2002) and Weichselberger (2003) channel models, and different types of geometry-based channel models, including geometry-based reference models and geometry-based stochastic channel models (GSCMs). The stochastic channel models are generally tractable in terms of complexity while deterministic channel models accurately can represent the channel in a specific environment. Even though the underlying propagation channel remains the same independent of the system deployed, some characteristics that affect the system performance become more pronounced and therefore these need to be accounted for when designing and using an appropriate channel model for massive MIMO systems.

Many of the conventional MIMO models have been evaluated and extended for massive MIMO, taking into account the propagation characteristics that have been shown to be more prominent in massive MIMO channels. Although efficiently providing simulated channel realizations, the performance based on channels from correlation-based channel models generally diverges from the performance of measured channels. A more realistic and extensively used channel modeling approach for massive MIMO system simulations is based on geometry-based channel models, providing a good trade-off between accuracy and complexity. Research efforts have been invested in extending the conventional geometry-based MIMO channel models to better capture the characteristics of massive MIMO channels. Also the map-based approach, which is based on simplified ray tracing, has gained interest as a viable option for accurate, although feasible in terms of complexity, modeling of massive MIMO channels.

This article provides a comprehensive overview of the state-of-the-art related to massive MIMO channels. The following section describes the fundamentals of massive MIMO propagation. Originating from measurements, prominent Massive MIMO Channel Characteristics are described and is followed by Channel-Dependent Massive MIMO Characteristics. Channel Modeling for Massive MIMO first reviews channel modeling approaches currently being used for conventional MIMO systems. For each approach, their applicability for developing and assessing the performance of massive

MIMO systems is evaluated and extensions are presented. Lastly, a discussion of future opportunities and challenges is provided.

Fundamentals of Massive MIMO Propagation

In a basic massive MIMO system, K single-antenna users are spatially multiplexed by using M base station antennas, as shown in Figure 1. Although earlier systems, in general, are using frequency division duplex (FDD), massive MIMO systems are typically serving users in the same time-frequency resource in a time division duplex (TDD) manner. The system is relying on channel reciprocity, where the channel coefficients for each antenna pair in the downlink channel matrix H, can be acquired by using the transpose of the uplink channel matrix H^{T}. This matrix is estimated based on uplink pilots and affects how the base station experiences the channel. Before base station transmission, the channel state information is used for precoding at the base station side and this will affect how the user experiences the channel. With precoding, signals can be transmitted from all base station antennas such that they add up constructively at the intended user, resulting in an array gain. There are also other forms of massive MIMO relying on explicit beamforming, such as 3D-MIMO technology, but here the focus is on reciprocity-based massive MIMO for aggressive spatial multiplexing.

The underlying assumption about the propagation channel in massive MIMO is that as M grows large, the channels between different users will become orthogonal. Moreover, in the asymptotic case, the effects of uncorrelated noise and fast fading disappear (Marzetta 2010). This means that as M goes to infinity, the correlation between H and its Hermitian transpose approaches the $K \times K$ identity matrix I_K as

$$\frac{1}{M} HH^H \rightarrow I_K$$

With orthogonal user channels, linear precoding schemes become nearly optimal (Marzetta 2010; Gao et al. 2011; Rusek et al. 2013). To measure user orthogonality, the singular value spread, also called the channel condition number, can be used as the metric of interest. The singular value spread is defined as the ratio between the largest and smallest singular value of the channel matrix H, obtained by applying the singular value decomposition, that is

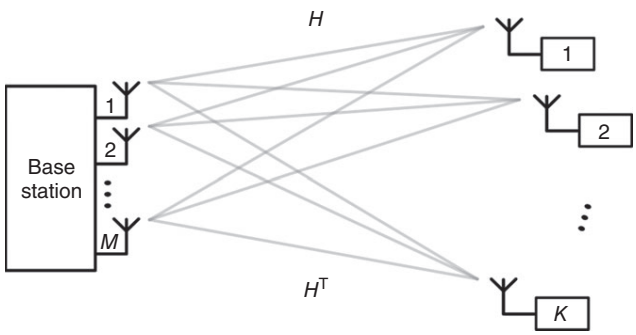

Figure 1 System with a large array at one side and single-antenna users spatially multiplexed at the other side for both uplink and downlink transmission.

$$\kappa = \frac{\sigma_1}{\sigma_K}$$

A large k implies that some user channel vectors are close to parallel and therefore will be hard to separate, meanwhile a value close to 1 means that all channel vectors are pairwise orthogonal. The inverse of k could also be used to get a bounded value between 0 and 1. The singular value spread provides information about the performance of the worst user; to better reflect the behavior of all users, the normalized sum of the squared singular values could be used as given by

$$\frac{1}{\sigma_1^2}\sum_{k=1}^{K}\sigma_k^2$$

Another measure when evaluating how orthogonal the channels between user i and j are is through the pairwise correlation coefficient, defined as

$$\delta_{i,j} = \frac{|h_i^H \cdot h_j|^2}{\|h_i\|^2 \cdot \|h_j\|^2}$$

where $\|\cdot\|$ is the Euclidean norm. Naturally, a low correlation is desired and a value of 0 would mean orthogonal user channels.

Micro-Wave vs Mm-Wave Massive MIMO

As micro-wave and mm-wave propagation channels behave fundamentally different (Rappaport et al. 2015), this will impact the system performance and how a massive MIMO system should be implemented in these different bands (Björnson et al. 2019). In mm-wave bands, pathloss and shadowing losses become larger. To still get sufficient signal levels, mm-wave massive MIMO would benefit from the beamforming gain acquired from explicit 3D-beamforming. Meanwhile, in massive MIMO systems operating in the sub-6 GHz bands, the focus is generally on multiuser operation enabled by aggressive spatial multiplexing. Such a system rather relies on coherent signal combining through channel state information and channel reciprocity, as previously described, rather than using explicit beamforming directions.

Influence of Users and Device Antennas

Most novel ideas for massive MIMO are related to the base station side and consequently, these aspects have received much attention. However, the terminals have an impact on the overall system performance, as neither the user equipment nor the interaction with the user will be ideal. In fact, performance is mainly limited by the hardware impairments in the user equipment, while the effect of impairments from the large array asymptotically disappears (Björnson et al. 2014). Further on the user interaction, in terms of shadowing and loading of the antenna, will make the system less efficient (Harrysson et al. 2010).

To decrease the effect of user loading, antenna diversity could also be motivated at the terminal side. For example, Martinez et al. (2018a) showed a capacity improvement of 43% when adding a second user antenna. Also using multiple user antennas, Bengtsson

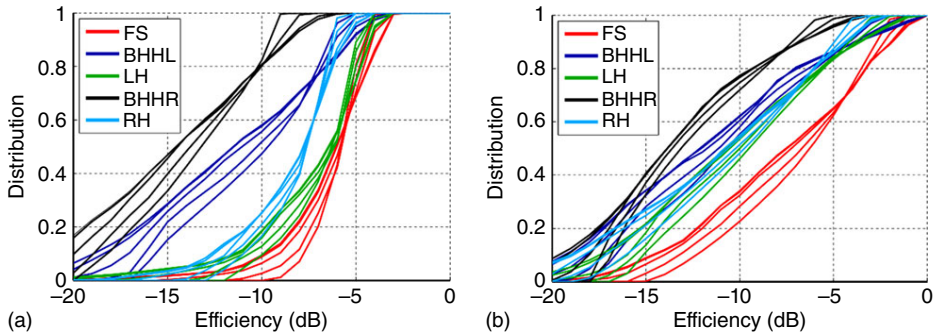

Figure 2 Cumulative distribution functions for the angular spread impact on antenna *E*-field patterns, for two different antennas, in different load scenarios. Source: Bengtsson et al. (2015). Reproduced with permission of IEEE.

et al. (2015) investigated the influence of different antenna loadings, showing that the influence of the left and right hand (LH/RH) or beside head with hand left and right (BHHL/BHHR) decreases the average power and increase the sensitivity to the channel angular spread, in comparison to free space (FS), as seen in Figure 2.

Massive MIMO Channel Characteristics

When increasing the number of base station antennas, some channel characteristics become more pronounced in comparison to conventional MIMO systems. In measurement campaigns, the key characteristics that should be captured by a suitable channel model for massive MIMO, have been identified to be spherical wavefronts, nonstationarity, 3D-propagation, and polarization effects. Depending on the array deployed, these characteristics will affect the system in different ways. However, for different sub-6 GHz bands, the characteristics seem to remain stable (Li et al. 2016; Martinez et al. 2016a).

Spherical Wavefronts

When increasing the number of antennas in a massive MIMO system, the system will experience near-field effects as the physical dimensions of the array usually become large. This means that the plane wave approximation does not necessarily hold anymore and spherical wavefronts can be experienced over the array (Payami and Tufvesson 2012). The phase differences between different antenna elements do not only depend on the angle of the incoming wave but also the distance to users or scatterers, meaning that this can be used for better spatial separation of user signals (Zhou et al. 2015). One way to determine whether spherical wavefronts occur is through the Rayleigh distance, a metric depending on the largest dimension of the antenna array D_a and the wavelength λ, as

$$d_R = \frac{2D_a^2}{\lambda}$$

As an example, it has been validated in a measurement campaign at 2.6 GHz, with 50 MHz of bandwidth, that the plane wave assumption no longer holds by analyzing the

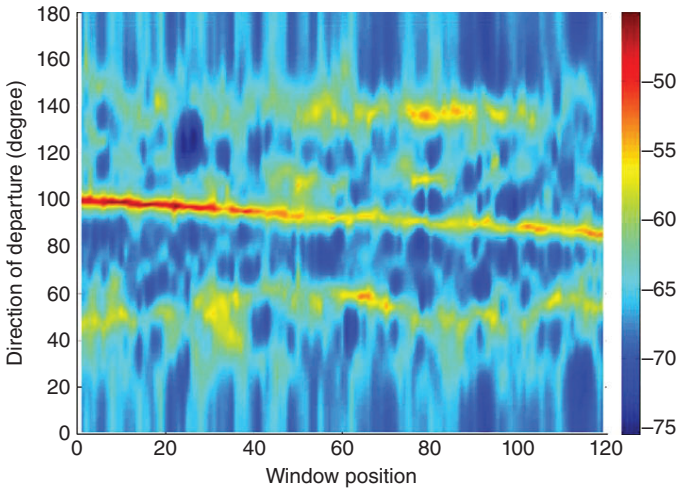

Figure 3 Angular power spectrum over the array for a user in a LOS scenario. Source: Payami and Tufvesson (2012). Reproduced with permission of IEEE.

angular power spectrum; the angle of the line-of-sight (LOS) component is shown to vary with approximately 20 degrees over a 128 element linear array (Payami and Tufvesson 2012), as seen in Figure 3.

Nonstationarity

Nonstationarities over the array mean that the received signal strengths at different antenna elements can differ significantly. In (Gao et al. 2013b) it was shown in a measurement campaign at 2.6 GHz, with 50 MHz bandwidth and a virtual linear array in an outdoor LOS scenario, that the wide-sense stationarity assumed for conventional MIMO systems was not satisfied (Gao et al. 2013a). The angular power spectrum in Figure 4 shows the spatial variations observed over the array; the LOS component is much stronger in the beginning and is shadowed towards the end. Another measurement campaign at 5.8 GHz with 100 MHz of bandwidth, taking place in an indoor LOS scenario with a very large array and a compact 2D array (Martinez et al. 2014), evaluated their differences in average power variations and between different users. In Figure 5, it can be observed that the power variations are smaller in the compact array, but even for this smaller aperture, there are variations in the order of 10 dB.

3D Propagation and Polarization Effects

With many antennas, different configurations, such as linear, planar, cylindrical, or even distributed arrays, are realizable. Extending the array in both vertical and horizontal domains increases the possibility to further extract spatial diversity due to the increased spatial resolution. To fully extract the diversity in the environment and to add a further dimension to separate users in, dual-polarized antenna elements need to be deployed at the base station. However, when users only have one polarization, a dual-polarized base station could degrade the performance.

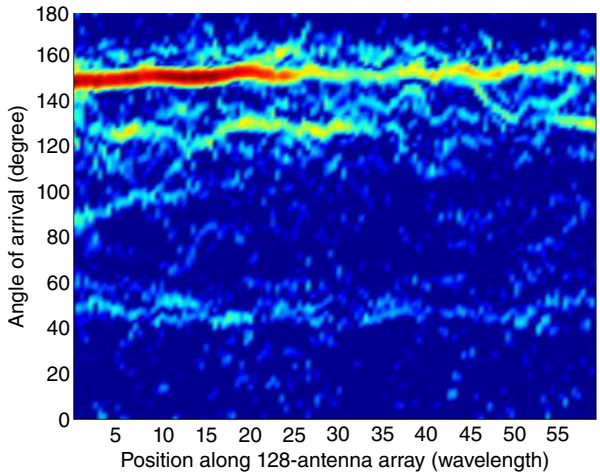

Figure 4 Angular power spectrum over the large base station array from an outdoor LOS scenario. Source: From Gao et al. (2013b). Reproduced with permission of IEEE.

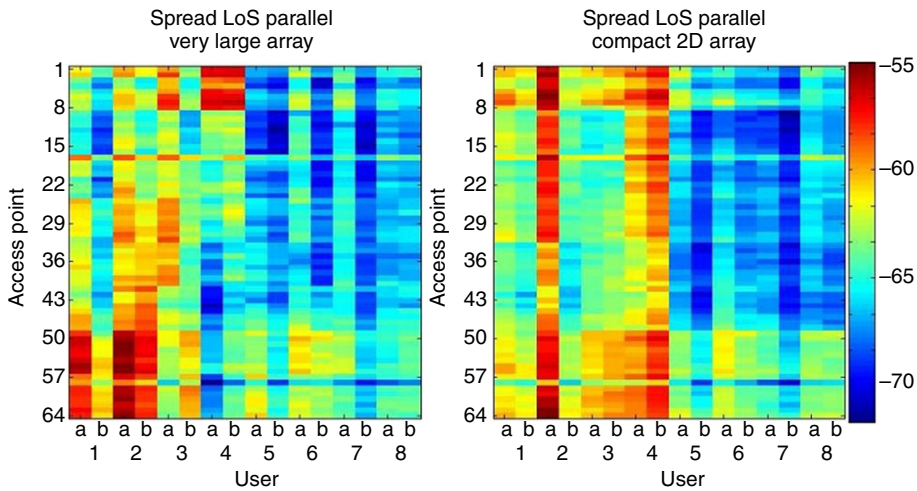

Figure 5 Comparison of the average power variations over a very large array and a compact 2D array from an indoor LOS scenario. Source: Martinez et al. (2014). Reproduced with permission of IEEE.

In one measurement campaign, the ratios of received power between vertically and horizontally polarized antenna ports were shown to be approximately log-normal distributed with a mean of 2.2 dB and standard deviation of 8 dB (Gao et al. 2015b).

In general, the orientation of the user equipment is unknown and deploying dual-polarized arrays can usually support improvement of user orthogonality (Flordelis et al. 2015) showed in a measurement campaign that with randomly oriented users, a system with 16 dual-polarized antenna elements, i.e. $M = 32$, could give the same performance as a system with 64 antennas having the same polarization.

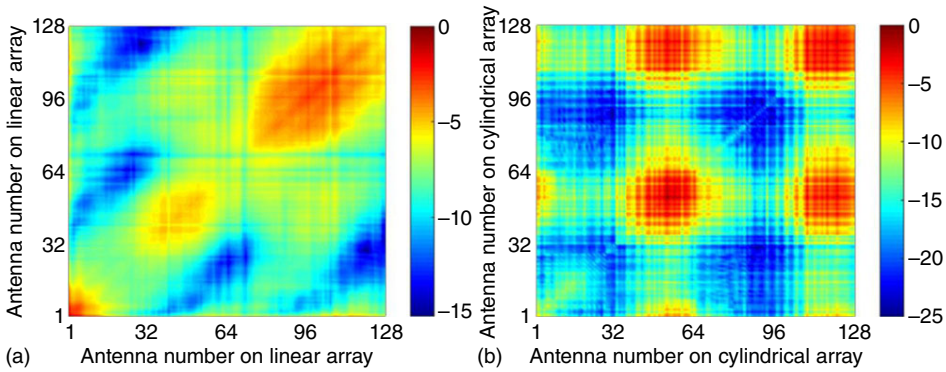

Figure 6 Correlation matrix in a LOS scenario for (a) a linear array with 128 antenna elements and (b) a cylindrical array with 128 antenna elements. Source: Gao et al. (2016). Reproduced with permission of IEEE.

In conventional MIMO systems with regular arrays, where the number of antennas is small, the correlation matrices can be modeled as Toeplitz structures (Zelst and Hammerschmidt 2002). Although, as previously described, nonstationarities can be experienced in a massive MIMO array and therefore the correlation matrices may not follow the same structure. This is seen in Figure 6a for a linear array and in Figure 6b for a cylindrical array. For the linear array, the correlation is reduced since it is a physical large array, and for the cylindrical array it is due to its circular structure extending also in the vertical dimension and the directive antenna arrangement with dual-polarized antennas (Gao et al. 2014; Gao 2016). As the number of antennas grows and as the antenna spacing increases the antenna correlation decreases, although having a larger impact in the vertical domain than in the horizontal (Li et al. 2014).

Channel-Dependent Massive MIMO Characteristics

At a massive MIMO system level, some characteristics related to the underlying propagation channel appear as an effect of the applied signal processing. These characteristics become important due to their effect on the system performance and relate to how the base stations and users experience the channel. In this section, theory and measurements related to user separability, as an effect of favorable propagation conditions, and channel hardening are outlined.

User Separability

In massive MIMO systems, user separability increases as an effect of the channel offering favorable propagation. A definition of favorable propagation is given in Ngo et al. (2014) and it means that the channel vectors between two users become pairwise orthogonal and thus, a channel offers favorable propagation if

$$h_i^H h_j = \begin{cases} 0, & i,j = 1,\ldots,K, \quad i \neq j \\ \|h_k\|^2 \neq 0, & k = 1,\ldots K \end{cases}$$

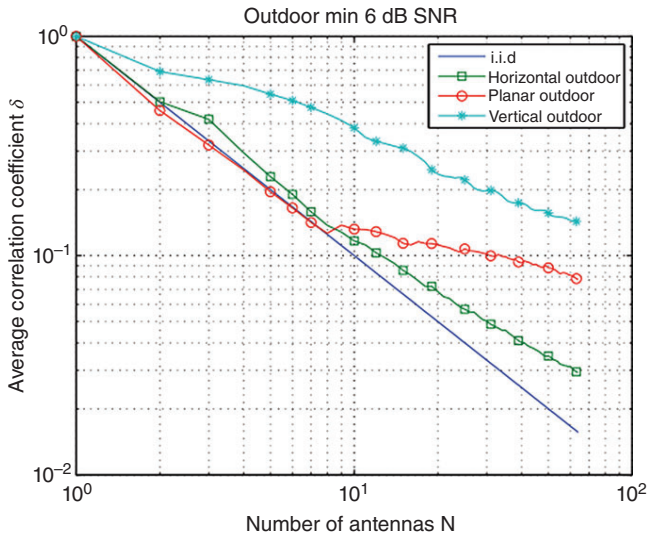

Figure 7 The average correlation coefficient for randomly picked channel vector pairs for three different antenna arrangements. Source: Gauger et al. (2015). Reproduced with permission of IEEE.

In general, this does not hold in reality although a channel can asymptotically offer favorable propagation when M goes to infinity if

$$\frac{1}{M}h_i{}^H h_j \to 0, \quad i \neq j$$

Analysis of measurement data has shown that favorable propagation can be harvested in real environments. By comparing singular value spreads, inverse condition numbers, and correlation coefficients, it has been shown that the channel vectors between different users do become more orthogonal to each other as the number of base station antennas increases. However, not to the same extent as for the i.i.d. complex Gaussian channel (Hoydis et al. 2012; Gao et al. 2015a). The decreasing singular value spread has also been evaluated in mobile channels, showing that decorrelation of user channels is a prominent effect even in dynamic environments where the 100 antenna case decorrelated by 20%, seven times faster than the eight antenna case (Harris et al. 2017). Considering different antenna array geometries, the average correlation coefficient was investigated in an outdoor scenario, observing that the horizontal antenna arrangement is the most beneficial one, while the vertical arrangement performed the worst (Gauger et al. 2015), as seen in Figure 7.

The comparison of the normalized sum of squared singular values in Figure 8 shows that it is more difficult to separate users in LOS with closely spaced users in comparison to having widely spread users (Martinez et al. 2014). However, even in the more difficult scenario, massive MIMO can separate users; the user channels do become more orthogonal (Flordelis et al. 2015, 2018). Figure 9 shows the cumulative distribution functions (CDFs) of the singular value spreads for two different measurement sites when using different number of antennas. For example, a 10 dB difference when increasing the number of antennas from 8 to 16 can be observed. To increase the capacity in this type of scenario, distributed arrays could be beneficial; distributing the arrays orthogonally to each

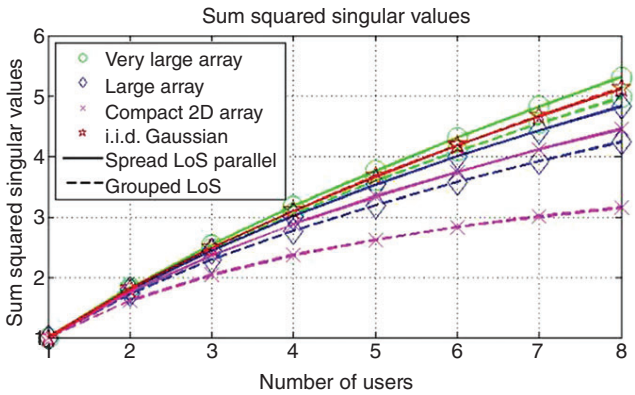

Figure 8 Normalized sum of squared singular values for different number of users in an LOS scenario, with users either spread and parallel to the base station or grouped. Source: Martinez et al. (2014). Reproduced with permission of IEEE.

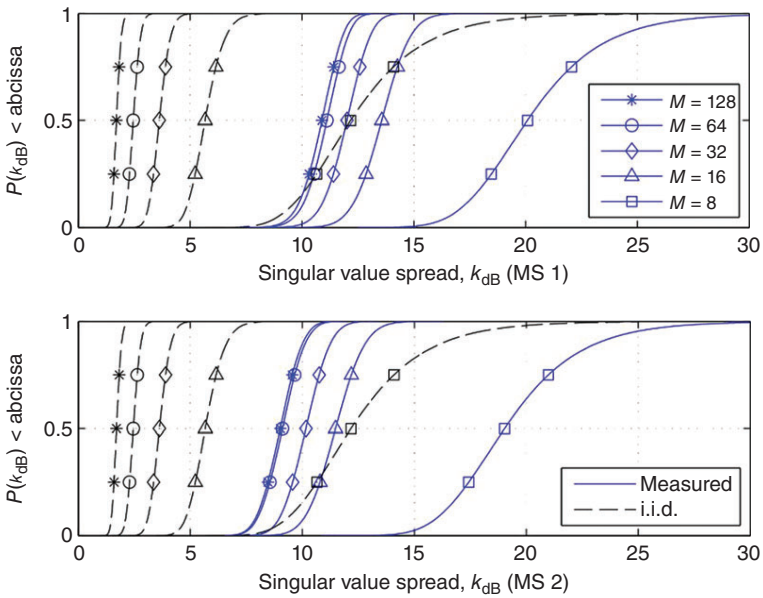

Figure 9 CDFs of the singular value spread when using different number of antennas at two different measurement sites. Source: Flordelis et al. (2015). Reproduced with permission of IEEE.

other was shown in one measurement campaign to provide up to 140% capacity increase in comparison to a collocated array (Chen et al. 2016).

Channel Hardening

As the number of antennas increases, the variations of channel gain decrease in both time and frequency domain and therefore get more concentrated around its

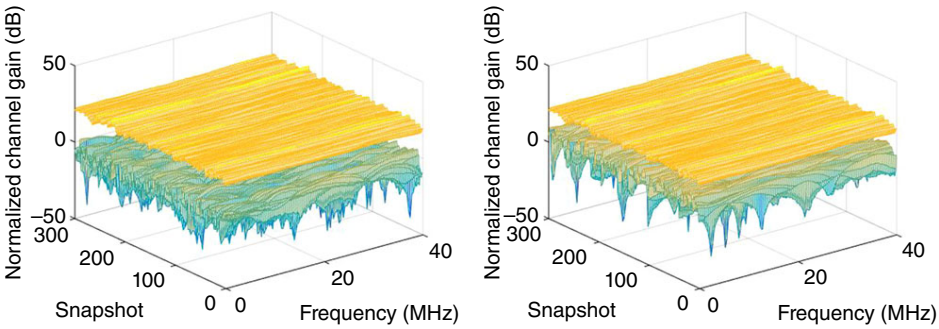

Figure 10 Normalized channel gain for a general user showing the single-antenna with the lowest mean channel gain (left, lower), highest mean channel gain (right, lower) and the channel gain for 128 base station antennas (both, upper). Source: Gunnarsson et al. (2018). Reproduced with permission of IEEE.

mean. This effect, visualized in Figure 10, is called channel hardening. The more stable channels lead to increased system reliability. With the small-scale fading decreasing, the system design can be simplified as operations, such as scheduling (Hochwald et al. 2004), can be done over a time scale controlled by large-scale fading instead.

Theoretically, the channel hardening effect has been dealt with in several studies (Marzetta 2010; Ngo and Larsson 2017; Björnson et al. 2017; Roy et al. 2018). Ngo et al. (2017) defined channel hardening as that the channel h_k offers hardening for user k if

$$\frac{\mathrm{Var}\{\|h_k\|^2\}}{E\{\|h_k\|^2\}^2} \to 0, \text{as } M \to \infty$$

Roy et al. (2018) further derived closed-form expressions for the coefficient of variation of channel gain that provides further insights about the channel characteristics that affects channel hardening.

The theoretical i.i.d. complex Gaussian channel clearly offers channel hardening as the number of antennas increases. However, channel hardening has also been validated experimentally for measured massive MIMO channels, where the effect is not as prominent as for the theoretical case (Payami and Tufvesson 2013; Gunnarsson et al. 2018; Ghiaasi et al. 2018; Martinez et al. 2018b). In Figure 11, the standard deviation of mean power across the array, averaged over subarray positions and users, in a LOS scenario for different array configurations is shown. The curves for the different arrays clearly decay as the number of antennas increases up until a point where the effect of power variation across the array instead increases the standard deviation. The very large array offers the most channel hardening, which is likely due to the larger aperture, which leads to less correlated channels. (Ghiaasi et al. 2018) showed, by analyzing the root mean square (rms) delay spread and the ratio of the normalized subcarrier to average single input single output (SISO) power of the equivalent channel, that the channel hardening effect has a consistent behavior throughout four frequency bands, ranging from 1 to 4 GHz.

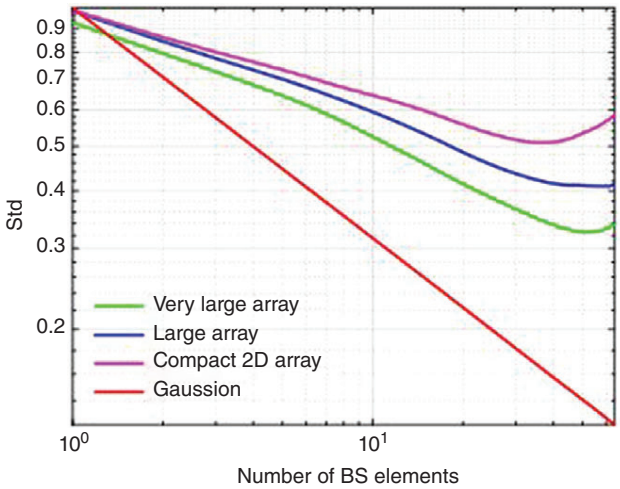

Figure 11 Standard deviation of mean power, averaged over subarray position and users for spread users, holding the two user antennas perpendicular to the base station, in a LOS scenario. Source: Martinez et al. (2018b). Reproduced with permission of IEEE.

Channel Modeling for Massive MIMO

Starting from the general channel modeling approaches, these can be divided into the categories of stochastic and deterministic channel models, see Figure 12. Stochastic channel models aim at reproducing the statistical behavior of important channel characteristics and include correlation-based and geometry-based channel models. Deterministic channel models are based on physical propagation mechanisms and are connected to specific environments; the most accurate solution is given by solving Maxwell's equations. The deterministic models, such as ray tracing, require a detailed and accurate description of the environment and are, therefore, usually accurate for a specific environment. However, the ray-tracing models are in general more complex in comparison to stochastic channel models. As a trade-off between accuracy and complexity, hybrid solutions could also be feasible.

Correlation-Based Channel Models

In studies about massive MIMO, a Rayleigh fading model is commonly used, i.e. the i.i.d. complex Gaussian channel $H_{\text{i.i.d.}}$. This theoretical model is often used as a benchmark

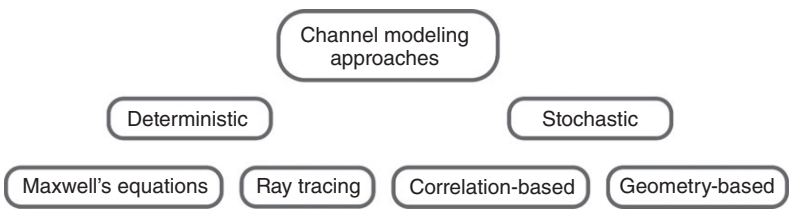

Figure 12 Channel modeling approaches.

when analyzing measured massive MIMO channels. The reason for using this model is that the assumption in massive MIMO is that it is a rich scattering environment with incoming signals from all directions. However, in practice, channels are typically correlated and there are often power imbalances between antennas. Measurements confirm this and have shown that although a great portion of the performance can be harvested in measured channels; the Rayleigh fading model is over-optimistic (Gao et al. 2011, 2015a; Hoydis et al. 2012; Li et al. 2014; Gunnarsson et al. 2018).

Two other simple correlation-based channel models that includes correlation between antennas at the transmitter and/or receiver side are the Kronecker channel model (Kermoal et al. 2002; Chizhik et al. 2003; Ozcelik et al. 2003) and the Weichselberger channel model (Weichselberger 2003; Weichselberger et al. 2006; Wood and Hodgkiss 2008). The Kronecker channel model assumes independent scattering on each side and, for the correlation matrices R_{Rx} and R_{Tx}, the channel matrix H_{kron} is given by

$$H_{\text{Kron}} = R_{Rx}^{1/2} H_{i.i.d.} R_{Tx}^{1/2}$$

The Weichselberger model includes coupling between the two sides by performing the element-wise square-root of a coupling matrix, contained in $\widetilde{\Omega}$, with U_{Rx} and U_{Tx}, being the eigenbases of the previously introduced correlation matrices. Performing the element-wise product with $H_{\text{i.i.d.}}$, the resulting channel matrix is given by

$$H_{\text{Weichsel}} = U_{Rx}(\widetilde{\Omega} \odot H_{i.i.d.})U_{Tx}$$

Both the Kronecker and Weichselberger channel models have been shown to underestimate massive MIMO capacity (Gao et al. 2014), with as much as 20–50% for the first model and up to 20% for the latter (Gao 2016). To better capture channel characteristics representing massive MIMO channels, a Kronecker-based stochastic model, which considers a birth–death process along the array has been developed (Wu et al. 2015a).

Geometry-Based Channel Models

There are two types of geometry-based channel models, the geometry-based reference models and GSCMs (Molisch et al. 2003). The first type of models, originally include models such as Lee's model, the geometrically based circular model and the geometrically based elliptical model (Ertel et al. 1998).

Other theoretical geometry-based reference models that aim for capturing massive MIMO characteristics, such as spherical wavefronts and nonstationarities, have been developed and analyzed. Examples are a 3D wideband twin-cluster model (Wu et al. 2014) and a 2D wideband multi-confocal ellipse channel model (Wu et al. 2015b).

There are two main approaches within GSCMs, the ones based on the WINNER-approach where scatterers are described based on their angle of arrival and departure (WINNER 2005) and the models based on the COST-approach where the physical positions of the scatterers are defined (Liu et al. 2012). The drawback with the first approach is that is not spatially consistent while for the latter approach, the extraction of parameters can be difficult. In all these models, the channels are created from the superposition of multipath components coming from different clusters distributed in the environment. To model a time-variant channel, GSCMs can make use of either the concept of visibility regions, where clusters become visible as users move inside the corresponding region or the concept of birth–death processes of clusters.

In general, the massive MIMO channel models are not focusing on the evaluation of different antenna designs and loading effects on the user side, although this has shown to have a big influence on performance (Bengtsson et al. 2015). To fill this gap, Bengtsson et al. (2017) developed a framework, which similarly to GSCMs also uses the concept of clusters. This framework can simulate multiple-antenna terminals in massive MIMO systems and shows a close match to measured results.

Among massive MIMO channel models, the GSCM-approach is the most common one. Examples of such models are the COST 2100 channel model (Liu et al. 2012) with massive MIMO extensions (Gao et al. 2015c; Flordelis et al. 2019), the QuaDRiGa channel model (Jaeckel et al. 2014, 2017), where extensions applicable for WINNER-type models has been proposed (Martinez et al. 2016b), the 3GPP channel model (TR 38.901; 3GPP 2017) and the IMT-2020 channel model (ITU-R M.2412-0 2017).

Ray Tracing and Map-Based Approaches

Ray tracing is based on an accurate representation of a specific simulated environment where either rays are launched and interact with objects in the simulation environment or the simulation environment is analyzed to determine where different forms of wave interaction can take place. An up to date tutorial of ray tracing for 5G applications is given in (He et al. 2019), and we refer the interested reader to this paper and the references therein. One should also mention a simplified ray-tracing technique, referred to as the map-based model (Medbo et al. 2016). Based on this, the METIS channel model (Nurmela et al. 2015) was developed to capture important channel characteristics for massive MIMO. There also exists a stochastic version that does not include all massive MIMO features.

Conclusions

Going from a theoretical concept to being a part of the standard for the fifth generation of wireless systems, massive MIMO has shown to bring great benefits to the overall capacity in cellular communication. As the underlying propagation channel determines the limits of what is achievable, the research efforts on massive MIMO channels provide valuable insights for system design. Interestingly, massive MIMO channels are not only promising for capacity improvements, but also for other performance factors such as reliability, range, and low-power user terminals.

The potential of increased reliability in massive MIMO systems is partly due to the effect of channel hardening. With more stable channels, there is potential for new applications that the infrastructure of today might not be able to support. Other aspects of reliability are the impact of shadowing and to minimize the probability of outage, where measurements and channel modeling is still lacking. One application where this increased reliability would be needed is in future connected factories, often referred to as Industry 4.0. This type of environment is assumed to provide very rich scattering, which is beneficial in order to get channel hardening, but could also potentially be problematic in terms of shadowing. The effect of these two propagation characteristics in this type of environment remains open questions.

In the future, more and more devices are expected to be connected, building up to huge internet-of-things (IoT) networks. These networks will also benefit from increased reliability, depending on the application. Although, in many scenarios, increased range and the possibility to use low-power user terminals might be more important. Another game-changing aspect of IoT networks is that the devices will also use lower frequency bands, i.e. below 1 GHz. In this band, the pathloss is lower and the coherence time is longer, which will be beneficial for low-power devices that are communicating over a long range. As most of the studies have been focusing on the frequency band 1–6 GHz and research below this band is rare, measurement campaigns need to be carried out in order to explore the impact of using massive MIMO in this scenario.

Going up in frequency instead, many details of the mm-wave massive MIMO channel are to a large extent not explored enough (Huang et al. 2017). Massive MIMO as an enabler for vehicular communication also remains an open question to be investigated; the number of mobility measurements for massive MIMO are very few. Further ideas, that are taking a step beyond the contemporary massive MIMO concept, are large intelligent surfaces (Hu et al. 2018), and cell-free massive MIMO (Ngo et al. 2017). With both concepts the number of radiating and sensing elements are expected to grow beyond the numbers considered for massive MIMO; the measurements presented here have included a number of 64–144 antennas. With an array that increases the spatial dimension even further, the near field effects are assumed to be even more prominent as the Rayleigh distance grows. The challenge will include practical difficulties to realize these large systems but further performance improvements are expected. Performance improvements are also expected for cell-free massive MIMO where the implementation complexity rather lies in the backhaul.

Having distributed antenna systems, such as in cell-free massive MIMO and large intelligent surfaces, will result in fundamentally different channels and will cause power imbalances between the antennas in the system. Already in massive MIMO systems, it is common with power imbalances between the different antennas in the array. This effect could be caused by large-scale fading, such as having obstacles shadowing a part of the array, or be a result of the influence of antenna characteristics; the interplay between the channel and antenna pattern will affect the received power levels. Power imbalances affect the overall system performance and further research on how to realistically capture this in channel models is needed.

What also needs to be captured in the channel models is the influence of antenna patterns. In a few studies, this has been shown to have a substantial impact on the performance of a massive MIMO system, although more extensive research is lacking. It is common to consider ideal antenna patterns. However, parameters such as the specific antenna pattern, influence of the users and mutual coupling will impact the system performance. One important effect related to antennas concerns polarization, which is rarely the focus in studies. With further knowledge in this area, diversity in this dimension could further accelerate performance.

Considering the development of channel models for massive MIMO in general, many of the emerging standard models are based on the GSCM approach; this has been considered as a good trade-off between accuracy and complexity. However, parameterization and validation with more measurements are still needed for many of the models in order to be able to assess how well they represent real measured channels. A new trend that can be expected to continue is the combining of different channel modeling

approaches in order to get an even better accuracy-complexity trade-off; the hybrid modeling using the map-based approach with stochastic elements has started to pave the way in this direction.

Overall, much of the fundamental understanding of the behavior of massive MIMO channels is there; now it is mostly a matter of improving channel models to even better reflect the measured channels and to include more scenarios. Ongoing research topic is to explore the deployment of massive MIMO in new frequency bands and also the potential of using massive MIMO to achieve more reliable systems, increased range and using low-power user terminals. Also, moving beyond today's contemporary massive MIMO systems to large intelligent surfaces and cell-free massive MIMO are foreseen to be a part of the development of future wireless systems.

Related Articles

Energy-Efficient and Spectrally-Efficient MIMO
Spatial Division Multiplexing
Precoding/Beamforming
Multiuser MIMO
Massive MIMO Fundamentals
Channel Estimation for Massive MIMO
3D MIMO Channels
Millimeter Wave Channels
METIS Channel Model
QuaDRiGa Channel Model
3GPP Channel Model (TR 38.901)
IMT-2020 Channel Model
Massive MIMO Antenna Designs
Massive MIMO RF Designs
Testbeds
URLLC Achieved by using Massive MIMO Link Operation Design for Wireless Networked Control System
Massive MIMO
Massive IoT Connections
mm-Wave
URLLC and Tactile Internet Networks
Machine-Type Communications

References

3GPP (2017). Study on Channel Model for Frequencies From 0.5 to 100 GHz. 3GPP TR 38.901, *Tech. Rep*. v14.1.0.

Bengtsson, E.L., Tufvesson, F., and Edfors, O. (2015). UE antenna properties and their influence on massive MIMO system performance. 2015 9th European Conference on Antennas and Propagation (EuCAP), Lisbon, Portugal (13–17 April 2015). IEEE.

Bengtsson, E.L., Rusek, F., Malkowsky, S. et al. (2017). A simulation framework for multiple-antenna terminals in 5G massive MIMO systems. *IEEE Access* 5: 26819–26831.

Björnson, E., Hoydis, J., Kountouris, M., and Debbah, M. (2014). Massive MIMO systems with non-ideal hardware: Energy Efficiency, Estimation, and Capacity Limits. *IEEE Transactions on Information Theory* 60 (11): 7112–7139.

Björnson, E., Höydis, J., and Sanguinetti, L. (2017). Massive MIMO networks: spectral, energy, and hardware efficiency. *Foundations and Trends in Signal Processing* 11 (3–4): 154–655.

Björnson, E., Van der Perre, L., Buzzi, S., and Larsson, E.G. (2019). Massive MIMO in sub-6 GHz and mmWave: physical, practical, and use-case differences. *IEEE Wireless Communications* 26 (2): 100–108.

Chen, C., Volskiy, V., Chiumento, A. et al. (2016). Exploration of user separation capabilities by distributed large antenna arrays. 2016 IEEE Globecom Workshops (GC Wkshps), Washington, DC (1–8 December 2016). IEEE.

Chizhik, D., Ling, J., Wolniansky, P.W. et al. (2003). Multiple-input-multiple-output measurements and modeling in Manhattan. *IEEE Journal on Selected Areas in Communications* 21 (3): 321–331.

Ertel, R.B., Cardieri, P., Sowerby, K.W. et al. (1998). Overview of spatial channel models for antenna array communication systems. *IEEE Personal Communications* 5 (1): 10–22.

Flordelis, J., Gao, X., Dahman, G. et al. (2015). Spatial separation of closely-spaced users in measured massive multi-user MIMO channels. 2015 IEEE International Conference on Communications (ICC), London, UK (8–12 June 2015). IEEE.

Flordelis, J., Rusek, F., Gao, X. et al. (2018). Spatial separation of closely-located users in measured massive MIMO channels. *IEEE Access* 6: 40253–40266.

Flordelis, J., Li, X., Edfors, O., and Tufvesson, F. (2019). Massive MIMO extensions to the COST 2100 channel model: modeling and validation. *IEEE Transactions on Wireless Communication* doi: 10.1109/TWC.2019.2945531, also available at arXiv e-prints, arXiv:1905.04931.

Gao, X. (2016). Massive MIMO in real propagation environments. Doctoral thesis. Lund University.

Gao, X., Edfors, O., Rusek, F., and Tufvesson, F. (2011). Linear pre-coding performance in measured very-large MIMO channels. 2011 IEEE Vehicular Technology Conference (VTC Fall), San Francisco, CA, USA (5–8 September 2011). IEEE.

Gao, X., Edfors, O., Liu, J., and Tufvesson, F. (2013a). Antenna selection in measured massive MIMO channels using convex optimization. 2013 IEEE Globecom Workshops (GC Wkshps), Atlanta, GA, USA (9–13 December 2013). IEEE.

Gao, X., Tufvesson, F., and Edfors, O. (2013b). Massive MIMO channels – Measurements and models. 2013 Asilomar Conference on Signals, Systems and Computers, Pacific Grove, CA, USA (3–6 November 2013). IEEE.

Gao, X., Zhu, M., Rusek, F. et al. (2014). Large antenna array and propagation environment interaction. 2014 48th Asilomar Conference on Signals, Systems and Computers, Pacific Grove, CA, USA (2–5 November 2014). IEEE.

Gao, X., Edfors, O., Rusek, F., and Tufvesson, F. (2015a). Massive MIMO performance evaluation based on measured propagation data. *IEEE Transactions on Wireless Communications* 14 (7): 3899–3911.

Gao, X., Edfors, O., Tufvesson, F., and Larsson, E.G. (2015b). Massive MIMO in real propagation environments: do all antennas contribute equally? *IEEE Transactions on Communications* 63 (11): 3917–3928.

Gao, X., Flordelis, J., Dahman, G. et al. (2015c). Massive MIMO channel modeling – extension of the COST 2100 model. Joint NEWCOM/COST Workshop on Wireless Communications.

Gauger, M., Hoydis, J., Hoek, C. et al. (2015). Channel measurements with different antenna array geometries for massive MIMO systems. 10th International ITG Conference on Systems, Communications and Coding (SCS), Hamburg, Germany (2–5 February 2015). VDE.

Ghiaasi, G., Abraham, J., Eide, E., and Ekman, T. (2018). Measured channel hardening in an indoor multiband scenario. 2018 IEEE 29th Annual International Symposium on Personal, Indoor and Mobile Radio Communications (PIMRC), Bologna, Italy (9–12 September 2018). IEEE.

Gunnarsson, S., Flordelis, J., Van der Perre, L., and Tufvesson, F. (2018). Channel hardening in massive MIMO – a measurement based analysis. 2018 IEEE 19th International Workshop on Signal Processing Advances in Wireless Communications (SPAWC), Kalamata, Greece (25–28 June 2018). IEEE.

Harris, P., Malkowsky, S., Vieira, J. et al. (2017). Performance characterization of a real-time massive MIMO system with LOS mobile channels. *IEEE Journal on Selected Areas in Communications* 35 (6): 1244–1253.

Harrysson, F., Medbo, J., Molisch, A. et al. (2010). Efficient experimental evaluation of a MIMO handset with user influence. *IEEE Transactions on Wireless Communications* 9 (2): 853–863.

He, D., Ai, B., Guan, K. et al. (2019). The design and applications of high-performance ray-tracing simulation platform for 5G and beyond wireless communications: a tutorial. *IEEE Communications Surveys & Tutorials* 21 (1): 10–27.

Hochwald, B.M., Marzetta, T.L., and Tarokh, V. (2004). Multiple-antenna channel hardening and its implications for rate feedback and scheduling. *IEEE Transactions on Information Theory* 50 (9): 1893–1909.

Hoydis, J., Hoek, C., Wild, T., and ten Brink, S. (2012). Channel measurements for large antenna arrays. 2012 International Symposium on Wireless Communication Systems (ISWCS), Paris, France (28–31 August 2012). IEEE.

Hu, S., Rusek, F., and Edfors, O. (2018). Beyond massive MIMO: the potential of data transmission with large intelligent surfaces. *IEEE Transactions on Signal Processing* 66 (10): 2746–2758.

Huang, J., Wang, C., Feng, R. et al. (2017). Multi-frequency mmWave massive MIMO channel measurements and characterization for 5G wireless communication systems. *IEEE Journal on Selected Areas in Communications* 35 (7): 1591–1605.

ITU-R (2017). Guidelines for evaluation of radio interface technologies for IMT-2020. ITU-R M.2412-0. ITU-R Tech Rep. Ser. M.

Jaeckel, S., Raschkowski, L., Borner, K., and Thiele, L. (2014). QuaDRiGa: a 3-D multi-cell channel model with time evolution for enabling virtual field trials. *IEEE Transactions on Antennas and Propagation* 62 (6): 3242–3256.

Jaeckel, S., Raschkowski, L., Borner, K. et al. (2017). QuaDRiGa: Quasi Deterministic Channel Generator, User Manual and Documentation. Frauenhofer Heinrich Hertz Institute, *Tech. Rep*. v2.0.0.

Kermoal, J., Schumacher, L., Pedersen, K. et al. (2002). A stochastic MIMO radio channel model with experimental validation. *IEEE Journal on Selected Areas in Communications* 20 (6): 1211–1226.

Larsson, E., Edfors, O., Tufvesson, F., and Marzetta, T. (2014). Massive MIMO for next generation wireless systems. *IEEE Communications Magazine* 52 (2): 186–195.

Li, J., Zhao, Y., and Tan, Z. (2014). Indoor channel measurements and analysis of a large-scale antenna system at 5.6 GHz. 2014 IEEE/CIC International Conference on Communications in China (ICCC), Shanghai, China (13–15 October 2014). IEEE.

Li, J., Ai, B., He, R. et al. (2016). Measurement-based characterizations of indoor massive MIMO channels at 2 GHz, 4 GHz, and 6 GHz frequency bands. 2016 IEEE 83rd Vehicular Technology Conference (VTC Spring). Nanjing, China (15–18 May 2016). IEEE.

Liu, L., Oestges, C., Poutanen, J. et al. (2012). The COST 2100 MIMO channel model. *IEEE Wireless Communications* 19 (6): 92–99.

Martinez, A.O., De Carvalho, E., and Nielsen, J.Ø. (2014). Towards very large aperture massive MIMO: a measurement based study. 2014 IEEE Globecom Workshops (GC Wkshps), Austin, TX, USA (8–12 December 2014). IEEE.

Martinez, A.O., De Carvalho, E., Nielsen, J.Ø., and Jing, L. (2016a). Frequency dependence of measured massive MIMO channel properties. 2016 IEEE 83rd Vehicular Technology Conference (VTC Spring), Nanjing, China (15–18 May 2016). IEEE.

Martinez, A.O., Eggers, P., and De Carvalho, E. (2016b). Geometry-based stochastic channel models for 5G: extending key features for massive MIMO. 2016 IEEE 27th Annual International Symposium on Personal, Indoor, and Mobile Radio Communications (PIMRC), Valencia, Spain (4–8 September 2016). IEEE.

Martinez, A.O., Nielsen, J.Ø., De Carvalho, E., and Popovski, P. (2018a). An experimental study of massive MIMO properties in 5G scenarios. *IEEE Transactions on Antennas and Propagation* 66 (12): 7206–7215.

Martinez, A., Popovski, P., Nielsen, J.Ø., and De Carvalho, E. (2018b). Experimental study of the benefits of a second antenna at the user side in a massive MIMO system. *IEEE Access* 6: 2899–2907.

Marzetta, T. (2010). Noncooperative cellular wireless with unlimited numbers of base station antennas. *IEEE Transactions on Wireless Communications* 9 (11): 3590–3600.

Medbo, J., Kyosti, P., Kusume, K. et al. (2016). Radio propagation modeling for 5G mobile and wireless communications. *IEEE Communications Magazine* 54 (6): 144–151.

Molisch, A.F., Kuchar, A., Laurila, J. et al. (2003). Geometry-based directional model for mobile radio channels – principles and implementation. *European Transactions on Telecommunications* 14 (4): 351–359.

Ngo, H.Q. and Larsson, E. (2017). No downlink pilots are needed in TDD massive MIMO. *IEEE Transactions on Wireless Communications* 16 (5): 2921–2935.

Ngo, H.Q., Larsson, E.G., and Marzetta, T.L. (2014). Aspects of favorable propagation in massive MIMO. 2014 22nd European Signal Processing Conference (EUSIPCO), Lisbon, Portugal (1–5 September 2014). IEEE.

Ngo, H.Q., Ashikhmin, A., Yang, H. et al. (2017). Cell-free massive MIMO versus small cells. *IEEE Transactions on Wireless Communications* 16 (3): 1834–1850.

Nurmela, V., Karttunen, A., Roivainen, A. et al. (2015). Deliverable D1.4 METIS Channel Models. Mobile and wireless communications Enablers for the Twenty-twenty Information Society (METIS), *Tech. Rep*. v1.0, https://metis2020.com.

Ozcelik, H., Herdin, M., Weichselberger, W. et al. (2003). Deficiencies of 'Kronecker' MIMO radio channel model. *Electronics Letters* 39 (16): 1209–1210.

Payami, S. and Tufvesson, F. (2012). Channel measurements and analysis for very large array systems at 2.6 GHz. 2012 6th European Conference on Antennas and Propagation (EUCAP), Prague, Czech Republic (26–30 March 2012). IEEE.

Payami, S. and Tufvesson, F. (2013). Delay spread properties in a measured massive MIMO system at 2.6 GHz. 2013 IEEE 24th Annual International Symposium on Personal, Indoor, and Mobile Radio Communications (PIMRC), London, UK (8–11 September 2013). IEEE.

Rappaport, T.S., MacCartney, G.R., Samimi, M.K., and Sun, S. (2015). Wideband millimeter-wave propagation measurements and channel models for future wireless communication system design. *IEEE Transactions on Communications* 63 (9): 3029–3056.

Roy, M., Paquelet, L., Magoarou, L., and Crussiere, M. (2018). MIMO channel hardening for ray-based models. 2018 14th International Conference on Wireless and Mobile Computing, Networking and Communications (WiMob), Limassol, Cyprus (15–17 October 2018). IEEE.

Rusek, F., Persson, D., Lau, B.K. et al. (2013). Scaling Up MIMO: opportunities and challenges with very large arrays. *IEEE Signal Processing Magazine* 30 (1): 40–60.

Weichselberger, W. (2003). Spatial structure of multiple antenna radio channels a signal processing viewpoint. Doctoral thesis. Technische Universität Wien.

Weichselberger, W., Herdin, M., Özcelik, H., and Bonek, E. (2006). A stochastic MIMO channel model with joint correlation of both link ends. *IEEE Transactions on Wireless Communications* 5 (1): 90–100.

WINNER (2005). Final Report on Link Level and System Level Channel Models. IST-2003-507581 WINNER. D5.4 *Tech. Rep*. v. 1.4.

Wood, L. and Hodgkiss, W. (2008). Understanding the Weichselberger model: a detailed investigation. IEEE Military Communications Conference (MILCOM), San Diego, CA, USA (16–19 November 2008). IEEE.

Wu, S., Wang, C., Aggoune, E.M. et al. (2014). A non-stationary 3-D wideband twin-cluster model for 5G massive MIMO channels. *IEEE Journal on Selected Areas in Communications* 32 (6): 1207–1218.

Wu, S., Wang, C., Aggoune, E.M., and Alwakeel, M.M. (2015a). A novel Kronecker-based stochastic model for massive MIMO channels. 2015 IEEE/CIC International Conference on Communications in China (ICCC), Shenzhen, China (2–4 November 2015). IEEE.

Wu, S., Wang, C., Haas, H. et al. (2015b). A non-stationary wideband channel model for massive MIMO communication systems. *IEEE Transactions on Wireless Communications* 14 (3): 1434–1446.

Zelst, A.V. and Hammerschmidt J.S. (2002). A single coefficient spatial correlation model for multiple-input multiple-output (MIMO) radio channels. URSI XXVIIth General Assembly.

Zhou, Z., Gao, X., Fang, J., and Chen, Z. (2015). Spherical wave channel and analysis for large linear array in LoS conditions. 2015 IEEE Globecom Workshops (GC Wkshps), San Diego, CA, USA (6–10 December 2015). IEEE.

Further Reading

Wang, C.-X., Wu, S., Bai, L. et al. (2016). Recent advances and future challenges for massive MIMO channel measurements and models. *Science China Information Sciences* 59 (2): 021301.

Wu, S., Wang, C., Yang, Y. et al. (2016). Performance comparison of massive MIMO channel models. 2016 IEEE/CIC International Conference on Communications in China (ICCC), Chengdu, China (27–29 July 2016). IEEE.

Zhang, P., Chen, J., Yang, X. et al. (2018). Recent research on massive MIMO propagation channels: a survey. *IEEE Communications Magazine* 56 (12): 22–29.

Zheng, K., Ou, S., and Yin, X. (2014). Massive MIMO channel models: a survey. *International Journal of Antennas and Propagation* 2014: 1–10.

Paper II

Channel hardening in massive MIMO: Model parameters and experimental assessment

Reliability is becoming increasingly important for many applications envisioned for future wireless systems. A technology that could improve reliability in these systems is massive MIMO (Multiple-Input Multiple-Output). One reason for this is a phenomenon called channel hardening, which means that as the number of antennas in the system increases, the variations of channel gain decrease in both the time- and frequency domain. Our analysis of channel hardening is based on a joint comparison of theory, measurements and simulations. Data from measurement campaigns including both indoor and outdoor scenarios, as well as cylindrical and planar base station arrays, are analyzed. The simulation analysis includes a comparison with the COST 2100 channel model with its massive MIMO extension. The conclusion is that the COST 2100 model is well suited to represent real scenarios, and provides a reasonable match to actual measurements up to the uncertainty of antenna patterns and user interaction. Also, the channel hardening effect in practical massive MIMO channels is less pronounced than in complex independent and identically distributed (i.i.d.) Gaussian channels, which are often considered in theoretical work.

I Introduction

Mission-critical applications such as remote surgery, intelligent transportation systems and industry automation are envisioned to be based on wireless connectivity in the future. To realize these applications, reliable communication is required. Massive MIMO [1][2] has in theory shown a potential to increase reliability; by deploying a massive number of antennas at the base station side, an unprecedented level of spatial diversity can be exploited. Additional advantages are that both spectral and energy efficiency increase. However, the enhanced reliability is the main focus of this paper.

Stable channels are essential in order to achieve reliability in communication systems. In massive MIMO systems, the channel gain becomes more concentrated around its mean when increasing the number of base station antennas. This phenomenon, where a fading channel behaves more deterministically, is called channel hardening. The decreasing fading variations will also render a more stable capacity. The channel hardening effect can be studied from two points of view. The first point is that the fading over frequency is reduced due to the decrease of experienced delay spread. The second point is channel hardening in the time domain, where the temporal fading decreases as a result of the coherent combination of the signals from the many base station antennas.

The theory of channel hardening has been discussed in many papers, see e.g. [1], [3]–[7]. In [3] and [4] a definition of channel hardening is given and the authors in [5] introduce and derive closed form results for the coefficient of variation of channel gain, which further relates to the characteristics of the channel, which are affecting channel hardening. In [7], a proof of complete convergence of channel hardening in massive MIMO with uncorrelated Rayleigh fading is presented. Although co-located massive MIMO systems are shown to provide channel hardening, this might not be the case in cell-free massive MIMO [8]. Much research has been carried out on the theoretical aspects of channel hardening, not as many studies have investigated this phenomenon experimentally [9]–[14].

Early theoretical massive MIMO studies and proofs of channel hardening have been relying on the assumption that the channels experience such rich scattering that they can be modeled as complex independent and identically distributed (i.i.d.) Gaussian channels. However, it has been shown in measurements that this is not the case [15][16] in practice. In general, real massive MIMO channels are spatially correlated. This phenomenon has been acknowledged and recently it has also been taken into account in theoretical analyses of channel hardening [3][17]. The other extreme channel is the keyhole channel, which is shown to not provide any channel hardening [4]. Any real massive MIMO system will experience a channel hardening somewhere in between; here we investigate what actually can be expected in different real scenarios.

To develop and assess the system performance of future mission-critical

applications, adequate channel models that can capture the relevant channel characteristics are needed. However, the relation between experiments and models has not been studied so far. Several channel models could be used for this purpose, such as the QuaDRiGa channel model [18][19] with extensions for WINNER-type models [20], the 3GPP channel model (TR 38.901) [21], the IMT-2020 channel model [22], and the METIS channel model [23]. Here, the COST 2100 channel model [24][25] is chosen as it is a geometry-based stochastic channel model (GSCM) with the important property that it can consistently describe the channel in space, time and frequency. It also realistically captures the behavior at a multipath level. The model has recently been extended with features such that it realistically can reflect characteristics that are prominent in measured massive MIMO channels [26][27]. To serve as an adequate channel model for the intended applications, all important channel aspects that affect system performance should be caught by the model; this leads to the questions if and how the channel model realistically can capture the channel hardening effect as well, and what are appropriate model parameters.

The contribution of this paper is twofold. First, channel hardening has been validated by experiments; this being a key part in the process of extracting relevant parameters that can be used for accurate channel modeling. We extend our analysis in [9] with evaluation of more parameters and thereby providing further insights; the number of analyzed scenarios has been extended and the analysis is now also including outdoor environments as well as different antenna arrays. We present generalized values for what can be expected in terms of channel hardening in a co-located massive MIMO system. The second contribution, novel in relation to [9], is an assessment of the capabilities of the COST 2100 channel model with its massive MIMO extension to capture the channel hardening effect and an evaluation of its model parameters. This is evaluated by relating simulated results from the model to our experimental findings. We highlight key parameters, related to propagation and antenna characteristics, that affect the channel hardening. With this knowledge, appropriate channel models and parameter sets can be selected and used to acquire realistic massive MIMO channels; consequently, these could be appropriate for development and assessment of future wireless applications.

The structure of the paper is as follows; Section II describes the measurement campaigns, including both the scenarios and the equipment used. Section III presents theory and the definition of channel hardening. The measurement results, including generalized values for channel hardening in different scenarios, are presented in Section IV. Section V describes the COST 2100 channel model and the performed simulations. Section VI presents a joint comparison between theory, measurements and simulations in order to give a more thorough and complete analysis of channel hardening in co-located massive MIMO systems. In Section VII, the paper is summarized and conclusions are presented.

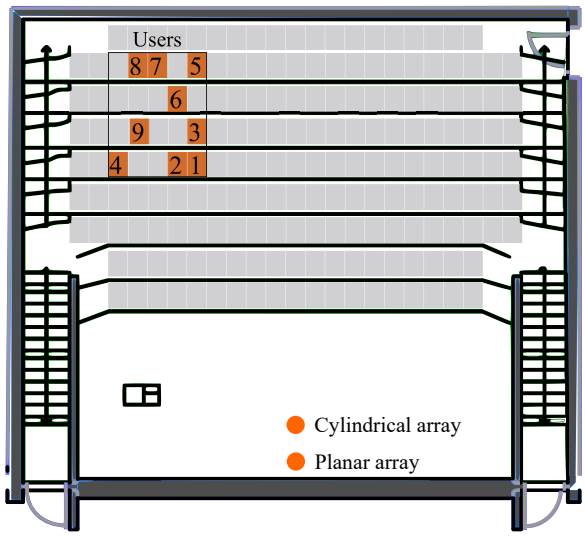

Figure 1: The auditorium where the indoor scenario took place. The base station is standing in the front of the room, at different positions depending on the array used in the measurements, and the users are sitting in the back of the room to the left.

II Measurement scenarios and equipment

The main focus of this work is on indoor propagation, as this typically is the scenario with the richest scattering, and therefore the environment where channel hardening is most pronounced. Only single-antenna user equipment is considered, limiting this study to focus on how channel hardening is affected when only changing the number of base station antennas. For this primary scenario, the base station is situated in the front of an indoor auditorium, and is serving a group of nine closely-spaced users. We also consider another scenario, which is an outdoor scenario where a base station is located on a roof serving nine closely-spaced users. Two different measurement campaigns have been conducted and the measured channels have been analyzed in terms of channel hardening. The first measurement campaign considered both scenarios and the measurements were performed with a channel sounder deployed with a cylindrical array. This campaign and the performed measurements therein is further described in [28]. The second measurement campaign aimed at repeating and validating some of the measurements in the indoor scenario with a real-time testbed equipped with a planar array. For all measurements the user equipment antenna was a vertically polarized SkyCross SMT-2TO6MB-A.

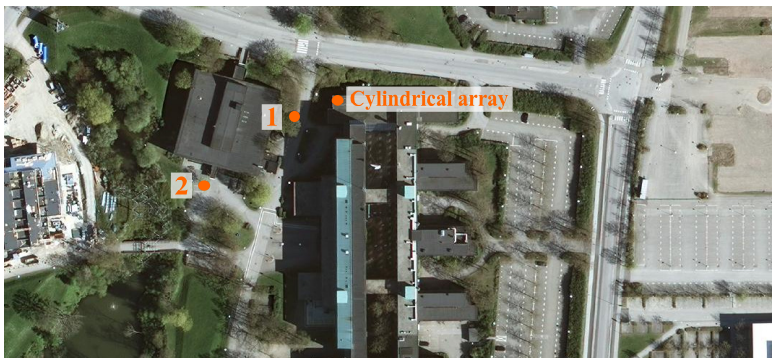

Figure 2: The outdoor scenario for both LOS (position 1) and NLOS (position 2). The base station has a cylindrical array and is positioned on the roof. The users were moving within a circle with a diameter of 5 m.

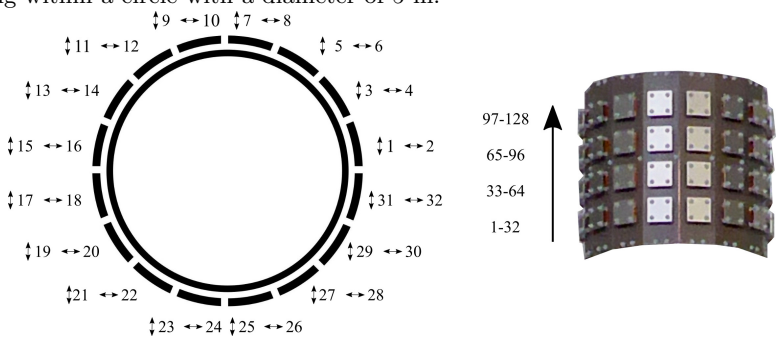

Figure 3: The cylindrical base station antenna array as seen from above (left) with the numbering of the antenna elements in the first ring, both vertically and horizontally polarized. The cylindrical array seen from the side (right) with the numbering per ring.

A Indoor scenario

The indoor measurement campaign was carried out in an auditorium located at Lund University. As seen in Fig. 1, a base station is standing in the front of the room and is serving users sitting in the left back corner. With the cylindrical array, simultaneous measurements were done when serving all nine users. With the planar array, evaluations were performed for user 1 and 5, which serve as representatives of users in the front and in the back rows, respectively. The users were mostly static during the measurements but were moving the antennas slowly back and forth, tilted approximately 45 degrees, with a speed lower than 0.5 m/s. The measurement campaigns also included, for both antenna arrays, the case when the rectangle in Fig. 1 was almost full with people in the vicinity of the active users.

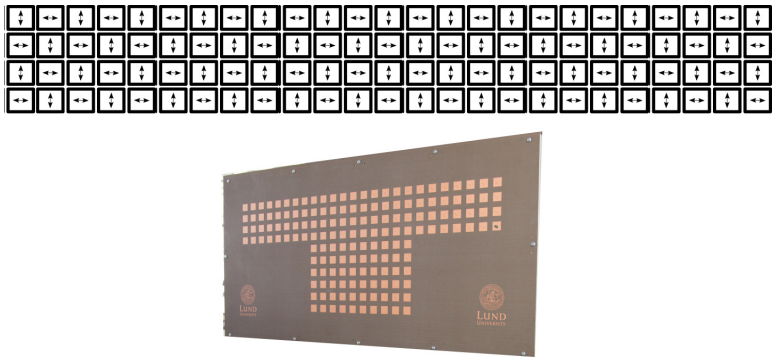

Figure 4: The planar base station antenna array as seen from the front (lower). Every other antenna is vertically and horizontally polarized (upper), where the 100 connected antennas are shown with their corresponding polarizations.

B Outdoor scenario

In the outdoor scenario, the measurement campaign was carried out in an open area at the campus of Lund University. A base station was placed at the roof on top of the second floor and measurements were performed both for a Line-Of-Sight (LOS) scenario (position 1 in Fig. 2) and for a non-LOS (NLOS) scenario (position 2 in Fig. 2). In both cases, nine closely-spaced users were moving around within a circle having a diameter of 5 m. The users were holding the antennas tilted approximately 45 degrees.

C Channel sounder

The RUSK LUND MIMO channel sounder was used for the first measurement campaign with the cylindrical array. This channel sounder is a multiplexed-array channel sounder, meaning that the transfer functions for each transmit-receive antenna pair is measured at a fast pace one after the other. The cylindrical array connected to the channel sounder is shown in Fig. 3. The array consists of 64 dual-polarized patch antennas spaced half a wavelength apart at the carrier frequency of 2.6 GHz, resulting in 128 antenna ports in total. The bandwidth is 40 MHz. The antenna elements are in the measurement data numbered according to Fig. 3, i.e. starting with the lower ring and finishing with the upper ring as seen to the right in the figure. To the left in Fig. 3, the lower ring is seen as from above. Important to note is that odd-numbered antenna ports are vertically polarized, even-numbered ones have a horizontal polarization. For the indoor scenario the measurements produced 129 frequency points and 300 snapshots taken over 17 seconds. This was also done for the outdoor scenario, with the exception that here 257 frequency points were measured. For the indoor scenario, the time for sounding is 3.2 μs for one

transmit-receive antenna pair, leading to a time per snapshot of approximately 7.37 ms. For the outdoor scenario, these values doubles due to measuring twice as many frequency points.

D Real-time testbed

The Lund University Massive MIMO testbed (LuMaMi) was used for the second measurement campaign with the planar array. This testbed is based on software-defined radio technology and is operating in real-time at a carrier frequency of 3.7 GHz with 20 MHz of bandwidth. More information about the technical details of the testbed can be found in [29] and [30]. The planar array connected to the testbed is shown in Fig. 4, where the lower part shows the array from the front. The upper four rows with 25 antennas at each row are connected to one transceiver chain each, resulting in 100 antenna elements, spaced half a wavelength apart. Every other antenna element is vertically polarized while the other element has a horizontal polarization. The measurements when using the testbed produced 100 frequency points per user and for 20 seconds, 2000 snapshots were stored[1].

III Channel hardening in theory

Following [4], let $\mathbf{h}_k$ be the channel vector between the base station and user k. The channel $\mathbf{h}_k$ offers hardening if

$$\frac{\mathrm{Var}\{\|\mathbf{h}_k\|^2\}}{\mathrm{E}\{\|\mathbf{h}_k\|^2\}^2} \to 0, \quad \text{as } M \to \infty, \tag{1}$$

where M is the number of base station antennas. In [5], the coefficient of variation (CV^2) is introduced and further derived as

$$\begin{aligned} CV^2 &= \frac{\mathrm{Var}\{\|\mathbf{H}\|_F^2\}}{\mathrm{E}\{\|\mathbf{H}\|_F^2\}^2} \\ &= \mathcal{E}^2(\mathcal{A}_{tx}, \mathcal{D}_{tx})\mathcal{E}^2(\mathcal{A}_{rx}, \mathcal{D}_{rx})\frac{\mathrm{E}\{\|\mathbf{c}\|^4 - \|\mathbf{c}\|_4^4\}}{\mathrm{E}\{\|\mathbf{c}\|^2\}^2} + \frac{\mathrm{Var}\{\|\mathbf{c}\|^2\}}{\mathrm{E}\{\|\mathbf{c}\|^2\}^2}, \end{aligned} \tag{2}$$

where $\|\mathbf{H}\|_F$ is the Frobenius norm of $\mathbf{H}$, $\mathcal{E}^2(\mathcal{A}_{tx}, \mathcal{D}_{tx})$ and $\mathcal{E}^2(\mathcal{A}_{rx}, \mathcal{D}_{rx})$ are the second moments of the inner products between the steering vectors of two different physical paths for the transmitter and receiver, respectively, and $\|\mathbf{c}\|^2$ is the accumulated channel gain from all physical paths. In our case $\mathbf{H} = \mathbf{h}_k$.

[1] For completeness, it should be noted that 9 snapshots were lost during the measurements with user 1, and 7 snapshots during the measurements with user 5, possibly due to bad synchronization. These snapshots were therefore removed when analysing the data.

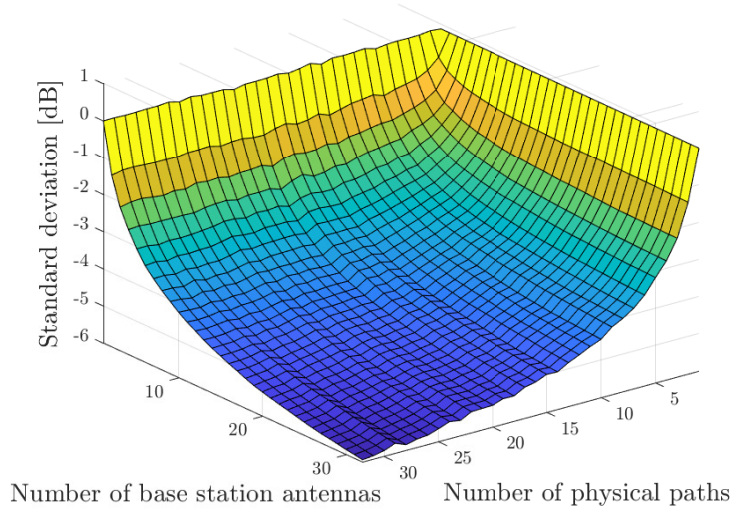

Figure 5: Standard deviation of channel gain as a function of number of base station antennas and the number of physical paths. Interpretation based on [5].

The first term in (2) can be considered as a small-scale fading factor. The second term can be considered as a large-scale fading factor, which for channel coefficients with independent channel gains with variance σ^2 and mean μ is shown to be equal to $\frac{1}{P}(\frac{\sigma}{\mu})^2$ [5], where P is the number of physical paths in the environment. Under the assumptions that the channel coefficients for all physical paths are $\mathcal{CN}(0,1)$ and that the steering vectors of the physical paths are distributed uniformly over the unit sphere, (2) can be further rewritten as

$$CV^2 = \frac{1}{M}(1 - 1/P) + 1/P \tag{3}$$

where we here consider M base station antennas and 1 user antenna [5]. The standard deviation of the channel gain as a function of the number of base station antennas and physical paths is shown in Fig. 5, obtained through a simulation based on (3) and then taking the square-root of the results. As expected, more base station antennas increase the channel hardening, although this is only true if there are enough physical paths in the environment. The achievable channel hardening in a specific environment will therefore be limited either by the number of base station antennas or the number of physical paths, assuming a fixed number of antennas for the user equipment. It is worth noting in (3) that if the number of physical paths $P \to \infty$, then the coefficient of variation $CV^2 \to \frac{1}{M}$. If also the number of antennas $M \to \infty$ then $CV^2 \to 0$,

and the channel offers hardening as defined in (3).

The data, acquired as previously described for the two measurement campaigns, has been analyzed in order to validate the theoretical channel hardening results. This is done in the same way as in [9], and similar to the investigation in [11][12]. Specifically, the measured channel transfer functions have been normalized according to

$$\overline{\mathbf{h}}_k(n,f) = \frac{\mathbf{h}_k(n,f)}{\sqrt{\frac{1}{NFM}\sum_{n=1}^{N}\sum_{f=1}^{F}\sum_{m=1}^{M}|h_{km}(n,f)|^2}}, \tag{4}$$

where N is the number of snapshots, F is the number of frequency points and M is the number of *selected* base station antennas, i.e. those over which the standard deviation is later computed in order to obtain a measure of the experienced channel hardening. This normalization makes sure that the average power of each entry in $\overline{\mathbf{h}}_k$, averaged over frequency, time, and base station antennas, is equal to one.

For M selected base station antennas, the instantaneous channel gain for each user is defined as

$$\overline{G}_k(n,f) = \frac{1}{M}\sum_{m=1}^{M}|\overline{h}_{km}(n,f)|^2, \tag{5}$$

such that the average channel gain

$$\mu_k = \frac{1}{NF}\sum_{n=1}^{N}\sum_{f=1}^{F}\overline{G}_k(n,f) = 1 \tag{6}$$

is independent of the number of antennas selected at the base station. This means that the base station can reduce the total output power with a factor of M, i.e. the beamforming gain. The standard deviation of channel gain is computed for each user according to

$$\mathrm{std}_k = \sqrt{\frac{1}{NF}\sum_{n=1}^{N}\sum_{f=1}^{F}|\overline{G}_k(n,f)-\mu_k|^2}, \tag{7}$$

where the instantaneous channel gain for user k, $\overline{G}_k(n,f)$, is given in (5) and the average channel gain for user k, μ_k, is given in (6). The standard deviation in (7) is indeed an estimate, $\hat{CV}(M)$, of the (square root of the) coefficient of variation (3), for some $M \geq 1$. In the following, when quantifying the channel hardening for some subset of antennas of size M, we use the difference

$$\hat{CV}(M) - \hat{CV}(1) \tag{8}$$

of the standard deviation as given in (7). This means that depending on which antenna element that is chosen as the reference element, the channel hardening will result in different values. How this reference element is chosen in our analysis will be elaborated on in the next section.

IV Channel hardening in practice

This section presents our contribution to the experimental research on channel hardening in real environments, extending the initial results in [9] to include more scenarios, array geometries and propagation characteristics. In addition, we extend the analysis and provide further insights on aspects that impact the experienced channel hardening and hence, the overall reliability in massive MIMO systems.

For the indoor scenario with the cylindrical array, see Fig. 1 and Fig. 3, the un-normalized average channel gain for each of the 128 base station antennas is shown in Fig. 6, for all nine users. Since the channels are not normalized, what is seen are the actual measured differences in average channel gain between users and antenna elements in the array. As expected, there are for each user large variations over the array which can be seen as the four larger peaks and dips, one for each ring of antennas, due to some antennas experiencing a LOS condition while some are not. Fig. 3 is used as reference for the numbering of the antennas in the rings as well as the numbering between the two polarizations. The latter explains the more local variations in Fig. 6, where the average channel gain is alternating between every two consecutive antennas. Both these variations contributes to an imbalance between the antenna elements in the array. The results in Fig. 6 can also be explained as an effect of the interaction between the cylindrical dual-polarized array and the environment. The variations that are seen show that the multipath components are not coming in with equal strength from all directions. They are rather coming dominantly from some distinct angles, in line with other experimental studies [15][16], and the previous analysis in [28], where also the distribution of channel coefficients can be found. Detailed cluster analysis can be found in [27] This observation questions the appropriateness of modeling massive MIMO channels with the complex Gaussian channel model and strengthens the conclusion that massive MIMO channels are indeed spatially correlated.

A Channel hardening in time and frequency

A clear visualization of the channel hardening effect is seen in Fig. 7, where the normalized channel gain with a single base station antenna versus the channel gain when using all 128 base station antennas is shown for user 1 in the indoor scenario. For the single antenna case, $M = 1$, the antenna element in the base

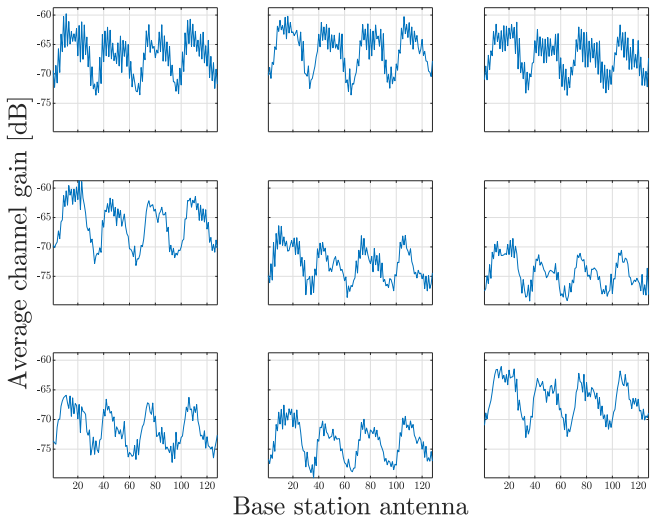

Figure 6: Unnormalized average channel gain for the 128 base station antennas in the cylindrical array shown for all nine users. Numbering of the users is row-wise, starting from the top left corner.

station array which has the median average channel gain is chosen. For this single antenna, there are large dips in both time and frequency. The combination of all 128 antennas results in both array gain, yielding a higher average, and smaller variations relative to this average. It is evident that in the time domain, there is a channel hardening effect. The channel flattens out when using a large number of base station antennas; the remaining variations are caused by the movements of the user equipment. The channel hardening is even more evident in the frequency domain; for the measured scenario and the considered bandwidth, the channel response becomes almost entirely flat. For comparison, in this scenario, the difference between the maximum and minimum normalized channel gain in the time domain, averaged over subcarriers and for $M = 1$ and $M = 128$ respectively, is 36 dB and 9 dB. The corresponding values for the frequency domain are 16 dB and 2 dB. In general in massive MIMO systems, the result will be similar as it is straight-forward to apply precoding to flatten out the channel in the frequency domain. However, shadowing effects in the time domain can not easily be compensated for.

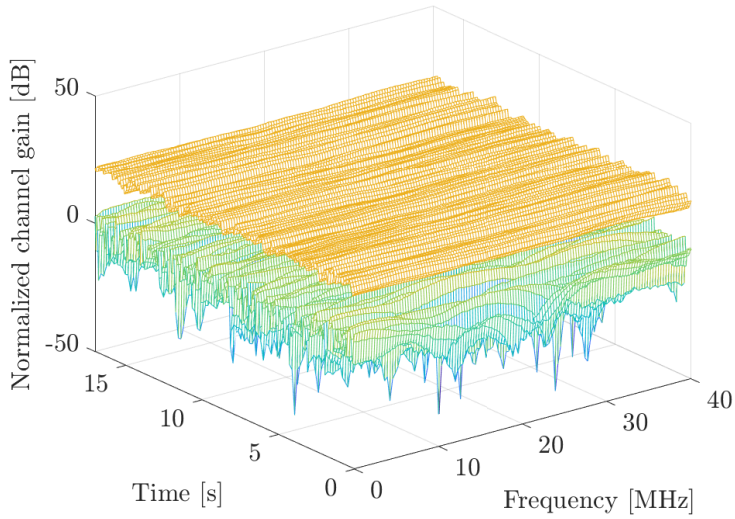

Figure 7: Normalized channel gain for user 1 showing the single antenna with the median average channel gain (lower) and the total channel gain for all 128 base station antennas in the cylindrical array (upper).

B Channel hardening with different subsets of antennas

The standard deviation of channel gain as the number of base station antennas M increases from 1 to 128 is shown in Fig. 8 for user 1. The channels are normalized according to (4) and the instantaneous channel gain for every subset is computed for all frequencies and snapshots as in (5) before the standard deviation of channel gain for each subset is computed using (7). The blue solid line shows the result for the complex Gaussian channel, which for 128 base station antennas has a channel hardening, measured as the decrease in standard deviation of channel gain when going from 1 to 128 base station antennas as in (8), of around 10.5 dB. This is close to the theoretical value of $10\log_{10}(\sqrt{128})$ dB. The standard deviation of channel gain is also shown in Fig. 8 when selecting the antennas in different orders as the number of base station antennas increases. All the curves for the measured responses end up at the same point but they evolve differently as the number of antennas increases and have different reference elements and therefore different starting points.

The case 'Original' is where the antennas are chosen in the order shown in Fig. 3. For the indoor scenario, the first few selected antennas are in NLOS and then some antennas in LOS get included in the selected subset resulting in a temporary increase of the standard deviation, as seen for the black dashed line. The case 'Strongest first' means choosing the antennas with the highest average

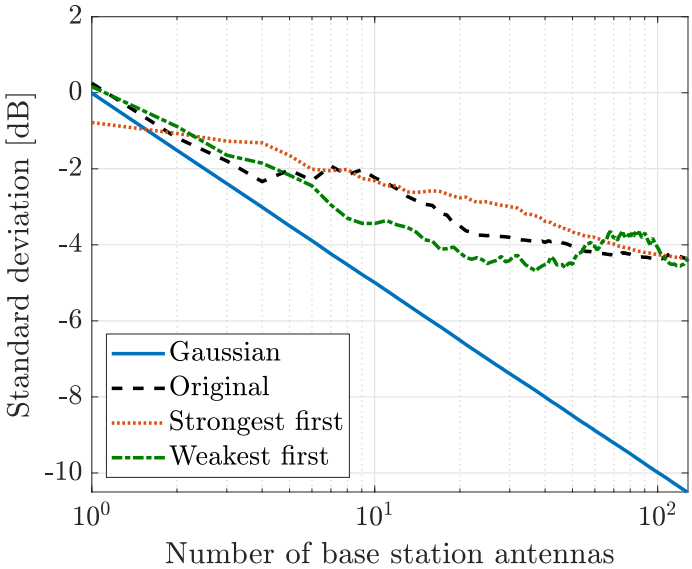

Figure 8: Standard deviation of channel gain as a function of number of base station antennas when selecting antennas in different orders, for user 1 and the cylindrical base station array, and the complex Gaussian channel as reference.

channel gain first, as computed for all frequency points and snapshots. This seems to be the most reasonable choice and leads to quite a steady decrease of the standard deviation in logarithmic scale. For comparison, the case 'Weakest first' is also shown, which is simply the reverse of the 'Strongest first' label. This results in a increase of the standard deviation when the antennas with higher channel gain, relative to the already included antennas, also are included in the subset. An observation from Fig. 8 is that whether the subset of selected antennas is in LOS, NLOS or a combination therefore, affects the behavior of the standard deviation curve, both in terms of starting point and regarding the course of the curve. For further analysis see [9]. An additional remark is that even though the order 'Weakest first' has the least variations around its average for M in the range from 5 to 50 antennas, and thus offers the most channel hardening, one should note that this still may not be the option to go for since the power level is normalized for the selected antennas. This makes them comparable in terms of variations relative to their respective means but that does not guarantee that choosing the weakest antenna first results in a good enough channel in terms of absolute channel gain. As an example, for $M = 10$, the un-normalized total channel gain, as summed for the first ten

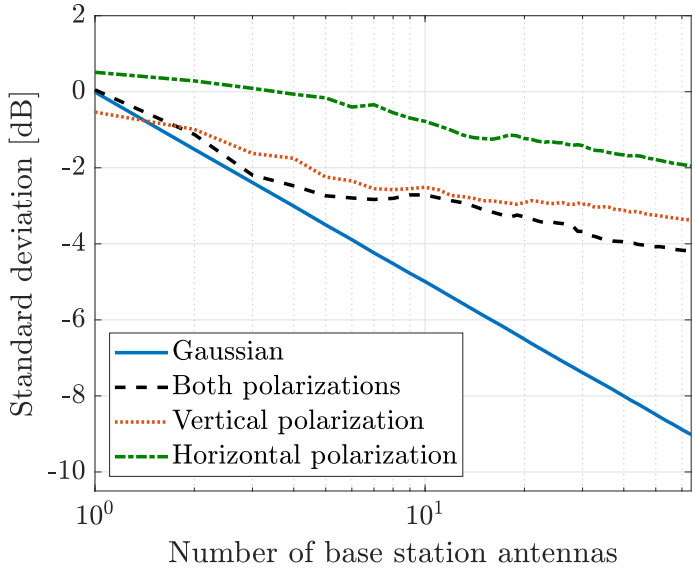

Figure 9: Standard deviation of channel gain as a function of number of base station antennas when using one of the polarizations or a combination of both, for user 1 and the cylindrical base station array, and the complex Gaussian channel as reference.

antennas and the whole bandwidth, is -30 dB for 'Strongest first' and -42 dB for 'Weakest first', averaged over snapshots. Therefore, only the 'Strongest first' order will be used in the analysis from now on, in order to avoid any confusion.

As previously indicated, the polarization state is causing variations in the channel gain over the array. Computing the standard deviation for $M = 1, \ldots, 64$ when using one of the polarizations or a combination of both yields the results in Fig. 9. For 'Both polarizations', the set of antennas are selected as one polarization per antenna, starting with vertical polarization, and then alternating between the two polarizations as it traverses through the rings. This means that the three options have the same aperture. The experienced channel hardening depends on the polarization set selected, and thereby also on the selected reference element. Fig. 9 shows the decrease of standard deviation when going from 1 to 64 antennas, using the definition in (8). When using the 64 horizontally polarized antennas, the channel hardening is 2.7 dB, while the case with the 64 vertically polarized antennas gives a channel hardening of 2.8 dB. It is worth noting that even though the channel hardening is almost the same for these two curves, the specific value of the standard deviation of channel gain at each point is smaller when using the vertical polarization since

these antennas already have smaller variations relative to its average compared to the horizontally polarized antennas. An interpretation of this is that the channel already can be considered as 'pre-hardend', which could be a result of the LOS component being mainly vertically polarized. This is supported by the fact that when computing the mean of the un-normalized average channel gain, this results in -64 dB for the vertically polarized antennas and -68 dB for the horizontally polarized antennas. The most channel hardening, and also the lowest standard deviation of channel gain for $M = 128$, is achieved when using a combination of both polarizations; then the channel hardening is 4.2 dB. This is partly explained by the ability to exploit polarization diversity in the environment, i.e. an increased number of physical paths, but is also an effect of having different reference elements.

C Analysis of different scenarios

To investigate differences and similarities between scenarios, the channel hardening is also analysed for measurements from the outdoor scenario, both in LOS and NLOS, as depicted in Fig. 2. For all three scenarios, the users with the most and least channel hardening are shown in Fig. 10a and Fig. 10b, respectively. Note that these are not necessarily the users with the smallest and largest standard deviation for a specific subset of antennas, such as for $M = 128$. In Fig. 10a it can be seen that the user with the most channel hardening is in the outdoor NLOS scenario. However, the channel from the indoor scenario could already be interpreted as being 'pre-hardened', as it for each subset of antennas already has a smaller standard deviation of channel gain relative to its mean. The users with the least channel hardening, and also the largest standard deviation of channel gain for $M = 128$, are in general found in the outdoor LOS scenario. Recalling that the channels for the different users are normalized, it should be noted that even though users in the outdoor LOS scenario have the least channel hardening it does not necessarily imply that it is a bad channel since the un-normalized channel could still have a considerable high received channel gain and that a strong LOS in general gives good communication performance. A comparison of the mean and maximum un-normalized channel gain in the three scenarios is found in Table 1. It can be observed that it is indeed the case that both the mean and the maximum channel gain, as per antenna, are as expected higher in the outdoor LOS scenario than in the NLOS scenario, although lower than in the indoor scenario. However, the distances are different and thereby also the pathloss.

Fig. 11 shows the empirical CDFs of their channel gains when $M = 128$ for all scenarios and users, providing further insights about the behaviour of the curves in the different scenarios. The marked users experience the least and most channel hardening, also shown in Fig. 10a and 10b, respectively. Evidently, the steeper the CDF is, the more channel hardening. Another ob-

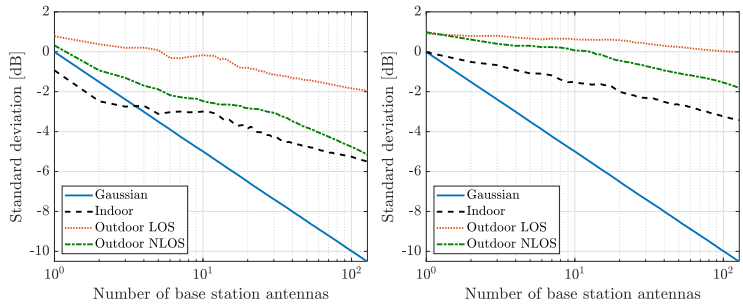

(a) The users with the most channel hardening

(b) The users with the least channel hardening

Figure 10: Standard deviation of channel gain as a function of number of base station antennas for the three different scenarios with the cylindrical array, and the complex Gaussian channel as reference.

servation is that if there are strong outliers, the standard deviation level is increased; this is the case for the outdoor scenarios. As a reference, the exponential distribution with $\lambda = 1$ is also provided, corresponding to the channel gain, i.e. $|h|^2$, with a mean of 1 for the one-antenna case where the channel is complex Gaussian distributed; this means that there is no channel hardening. Given this, the observation is that although the outdoor LOS scenario is to a large extent similar to the reference curve for higher channel gains, the risk of lower gains, affecting the probability of outage, is reduced when combining the many antennas. As a final remark on the comparison between different scenarios, a quantification of the average channel hardening results in 3.9 dB for the indoor scenario, 1.7 dB for the outdoor LOS scenario and 4.3 dB for the outdoor NLOS scenario.

D Influence of polarization

After exploring the influence of LOS and NLOS on the experienced channel hardening, further investigations included a revisit to take a closer look into

	Scenario	Mean	Maximum
Fig. 10a	Indoor	-71	-66
	Outdoor LOS	-100	-93
	Outdoor NLOS	-107	-104
Fig. 10b	Indoor	-72	-66
	Outdoor LOS	-88	-81
	Outdoor NLOS	-105	-99

Table 1: Comparison of the antennas with the mean and maximum average unnormalized channel gain in the different scenarios.

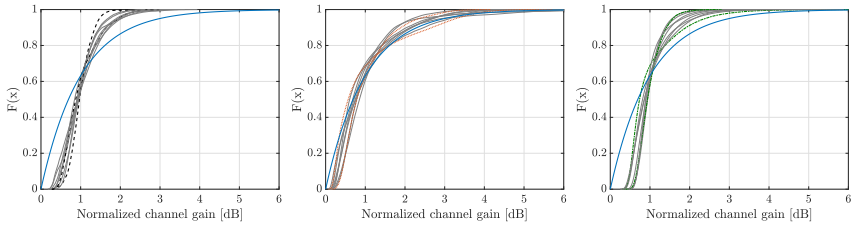

(a) Indoor **(b)** Outdoor LOS **(c)** Outdoor NLOS

Figure 11: Empirical CDFs of the normalized channel gain when using all 128 antennas in the cylindrical array, for all scenarios and users. The users marked in (a) black dashed, (b) orange dotted and (c) green dash-dotted lines have the least and the most channel hardening, and correspond to the users shown in Fig. 10. To serve as reference, the exponential distribution ($\lambda = 1$) is in blue full line.

the polarization aspect. In Table 2, the mean and standard deviation of the ratio between the channel gains of the vertical and horizontal polarization, as per snapshot, frequency point and antenna element, are shown for the users in Fig. 10. Although, they all seem to have similar standard deviation, the mean is in general closer to zero for the users with the most channel hardening; this is likely contributing to a more even distribution of the channel gain.

E Interaction between environment and antenna array

The last aspect we want to further investigate is the interaction between the environment and the array. Therefore, measurements were also performed in the indoor scenario, as previously has been described (see Fig. 1), with the planar array shown in Fig. 4 for user 1 and 5. The resulting channel hardening curves are shown in Fig. 12. For these measurements the users were surrounded with a crowd, such that the square in Fig. 1 was almost filled with people. The results in Fig. 12 show that significantly smaller standard deviations of channel gain, i.e. down to -6.8 dB, are achieved for both users when using the planar array in comparison to using the cylindrical array. This demonstrates that for a

	Scenario	Mean ratio	Std ratio
Fig. 10a	Indoor	-0.7	8.0
	Outdoor LOS	-0.2	7.8
	Outdoor NLOS	-0.3	7.8
Fig. 10b	Indoor	1.5	7.9
	Outdoor LOS	1.4	7.9
	Outdoor NLOS	1.1	7.9

Table 2: Mean and standard deviation (std) of the ratio between the channel gains of the vertical and horizontal polarization for the users in Fig. 10.

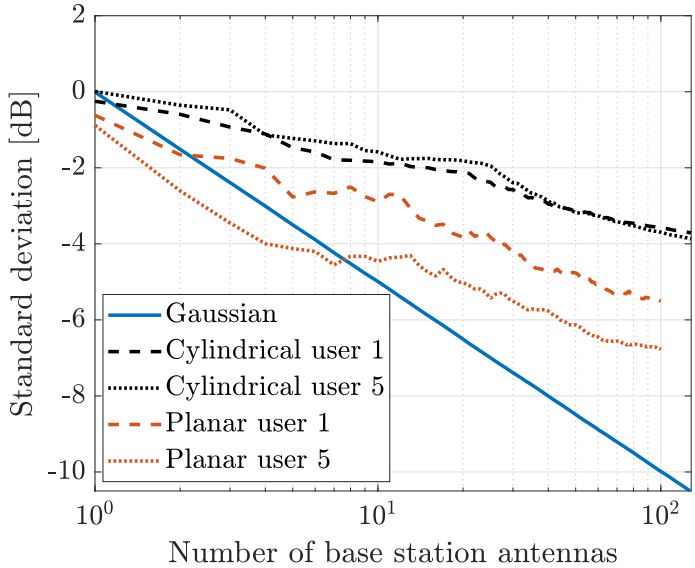

Figure 12: Standard deviation of channel gain as a function of number of base station antennas for user 1 and 5, and the complex Gaussian channel as reference. The scenario is the indoor scenario where the users are surrounded by a crowd with the cylindrical and the planar array, respectively.

typical deployment geometry, the planar array can better exploit the diversity in the environment as more of the antennas are effective and the distribution of channel gain over the array is more even; the latter can be seen in Fig. 13 where the slopes of the empirical CDFs of the normalized channel gain for the scenario with the planar array are steeper.

V Channel hardening in the COST 2100 channel model

This section provides a short description of the COST 2100 channel model, the simulations performed with the model, which are later used for comparison, and an example result from the simulations. Initial answers to the questions if and how well the COST 2100 channel model with its model parameters in general can capture the channel hardening effect are also given. This is further elaborated on in the comparison in Section VI.

The COST 2100 channel model [24], including the massive MIMO extension described in [27], is a GSCM that can stochastically describe massive MIMO

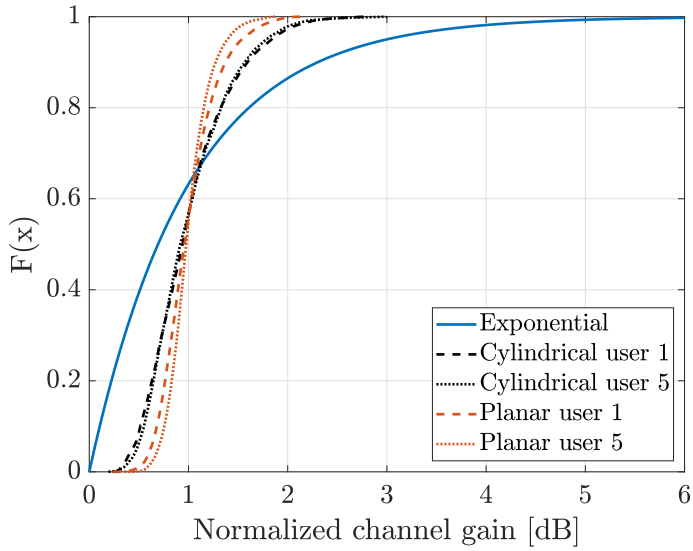

Figure 13: Empirical CDFs of the normalized channel gain when using all 100 or 128 antennas for the two arrays and users in Fig. 12. and the exponential distribution ($\lambda = 1$) as reference.

channels over time, frequency and space in a spatially consistent manner. The goal with the extension is to capture channel characteristics that become more prominent in massive MIMO channels. These extensions are:

- 3D propagation,
- the possibility for different parts of a physically large array to experience different clusters, and
- a gain-function regulating the gain for individual multipath components, which is of particular importance to closely-spaced users.

For the evaluation in this paper we use the indoor scenario with the cylindrical array and closely-spaced users at 2.6 GHz. This scenario has been parameterized based on the measurement data used in previous experimental analysis and the complete model can be found at [25]. More specifically, the chosen settings when running the simulations are outlined in Table 3.

In the simulations, 300 snapshots were generated at a rate of 50 snapshots per second with a user velocity of 0.25 m/s; this means that samples are taken over a distance of 1.5 m in total. 129 points in frequency are computed. The simulated propagation environment is combined with a synthetic antenna pattern of a cylindrical array with 128 antennas at the base station side. At the

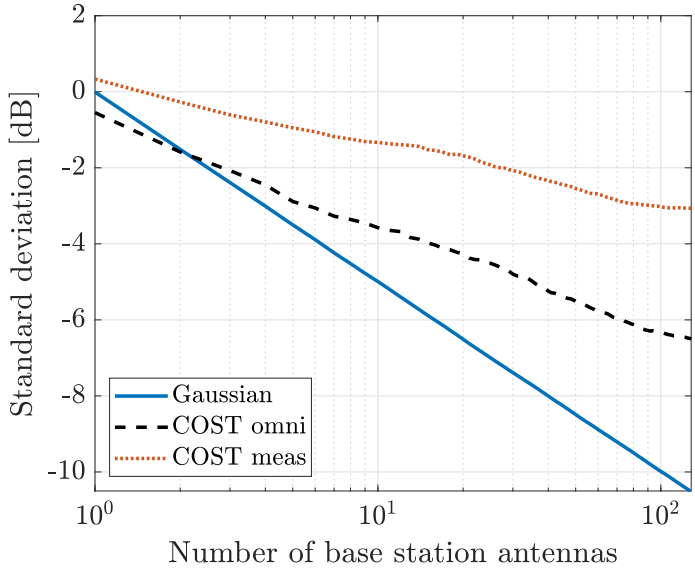

Figure 14: Standard deviation of channel gain as a function of number of base station antennas with an omni-directional antenna (COST omni) or an antenna pattern with user effect (COST meas) in the COST 2100 channel model for a typical user, and the complex Gaussian channel as a reference.

user side, the multipath components obtained from the simulated environment are combined with either an antenna pattern with user effect or an omni-directional antenna, for comparison. A description of the antenna pattern with user effect can be found in [31].

Each user antenna starts with a random initial orientation uniformly generated between $[-\pi\ \pi)$, and during the simulation each user antenna undergoes a randomly generated rotation between $[-\pi\ \pi)$ in total in the azimuth plane. For the obtained transfer function, the channels are normalized as in (4) and the standard deviation of channel gain is computed as in (7), in the same manner as for the measurement data. Running the simulation ten times, and averaging the resulting standard deviation of channel gain over these ten simulations,

	Setting
Network	'Indoor_CloselySpacedUser_2_6GHz'
Link	'Multiple'
Antenna	'MIMO_Cyl_patch'
Band	'Wideband'

Table 3: Settings chosen for the simulations with the COST 2100 channel model.

gives the result in Fig. 14 for a typical user.

As an example result from the simulations, Fig. 14 shows the resulting standard deviation both when using the omni-directional and measured antenna pattern with user effect, for the same propagation environment. The complex Gaussian channel is also shown as a reference. The difference of the starting point of the two curves with different antenna patterns is almost 0.9 dB while at the end point, the difference is about 3.4 dB. The result here is only for one specific user antenna pattern, and changing this pattern would affect the channel hardening. However, it shows that there is both a limitation on the channel hardening that is imposed by the simulated environment, in line with the presented theory in Section III, but also that the antenna pattern of the user can reduce the experienced channel hardening as much as to half of the channel hardening experienced with an omni-directional antenna, on a linear scale. In general, any user equipment with a non omni-directional antenna pattern will likely degrade the experienced channel hardening as not all scatterers will be effective.

VI Comparison between theory, measurements and simulations

The last part of this study is a joint comparison of the three levels at which channel hardening has been analyzed: theory, measurements and simulations. This provides a more thorough analysis of channel hardening and synthesizes the three points of view. We discuss aspects which are relevant when designing reliable massive MIMO systems and highlight channel and antenna characteristics important for channel hardening.

In Fig. 15, a comparison between theory, measurements and simulation results from the COST 2100 channel model is shown. The users shown from the measurements and simulations are the users with the most channel hardening (Fig. 15a) and the least channel hardening, (Fig. 15b) among the nine users when using all 128 base station antennas. As reference, the complex Gaussian channel is included.

Quantifying the general behaviour of the curves from the simulations, Fig. 16 shows the decrease (Δ) of standard deviation when increasing the number of antennas, averaged over all users. Here, it can be seen that on average, the slopes resulting from the measurements and the COST simulations with measured antenna pattern have very similar behaviors and that the model in general shows good correspondence. Meanwhile, the COST simulations with an omni-directional antenna have in general a larger slope, although not as high as in the complex Gaussian case due to the limitations in the environment. Considering the average channel hardening in the three cases, the measurements

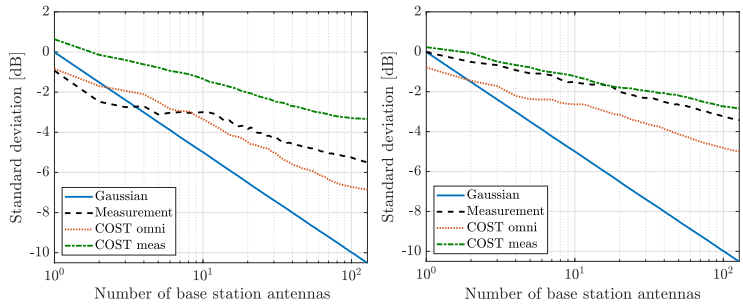

(a) The users with the most channel hardening

(b) The users with the least channel hardening

Figure 15: Standard deviation of channel gain as a function of number of base station antennas for one user from (i) the measurements, (ii) the simulation with an omni-directional antenna and (iii) the simulation with an antenna pattern with user effect in the indoor scenario with the cylindrical array, and the complex Gaussian channel as reference.

give a channel hardening of 3.9 dB, while the COST simulations on average give, for the measured and omni-directional antenna, a channel hardening of 3.5 dB and 5.3 dB, respectively. Looking at the average starting points for the three cases, the measurements start at 0.3 dB while the COST simulations with the measured antenna pattern start at 0.6 dB and the omni-directional antenna at
-0.8 dB. Below we summarize the results and discussions from three important aspects.

The complex Gaussian channel model is overoptimistic: Starting the discussion from a theoretical point of view, the complex Gaussian channel, which is only limited by the number of antennas, gives a channel hardening of 10.5 dB when having 128 base station antennas. This channel has often been assumed in theoretical studies of massive MIMO and is shown in this study to be more optimistic than real measured massive MIMO channels, which in general are spatially correlated. In reality the environment does generally not create as rich scattering as assumed in the complex Gaussian channel. As a result, channel responses are rather spatially correlated, and thus the environment also imposes a limitation on the achievable channel hardening; this fact is captured by (3). Moreover, the interactions between the array and the environment can result in quite different received power levels at the antenna elements.

The channel gain distribution over the array is essential: Repeating the assumptions made in [5] in order to get to (3), it was assumed that the channel coefficients for all physical paths are $\mathcal{CN}(0,1)$ and that the steering vectors of the physical paths are distributed uniformly over the unit sphere. If the mean μ and the variance σ^2 would deviate from this assumption, then

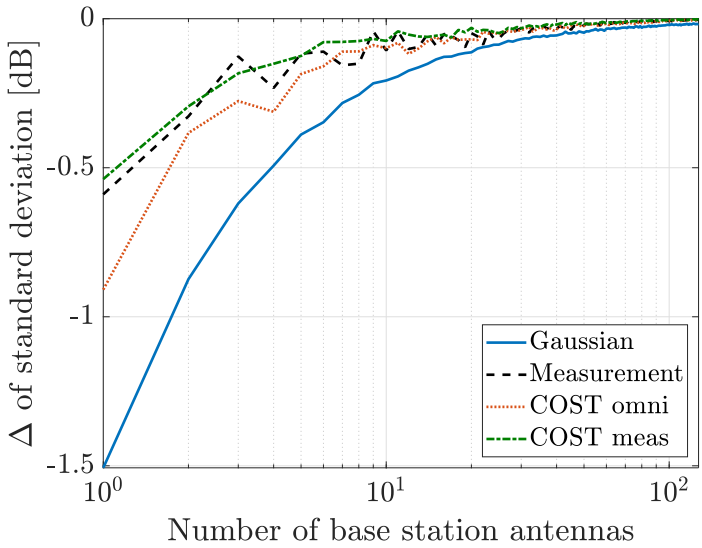

Figure 16: Decrease (Δ) of standard deviation of channel gain as a function of the increasing number of base station antennas for the average user in (i) the measurements, (ii) the simulation with an omni-directional antenna and (iii) the simulation with an antenna pattern with user effect, and the complex Gaussian channel as reference.

the large-scale fading term in (3) would be bounded by $\frac{1}{P}(\frac{\sigma}{\mu})^2$, see [5]. With a large variance, relative to the mean, the standard deviation curves would move up. The curves would move down if the variance is small relative to the mean. What can be seen in e.g. Figs 8-10 is indeed that when having a higher mean, the standard deviation curves in the indoor scenario move down; this is likely due to having a strong LOS component. Having a large imbalance in the channel gain over the array causes variations and can hence move the standard deviation curves up; causes of these variations can be due to having some antennas experiencing a strong LOS while others are not. This imbalance can also occur between the polarization modes. These aspects could as well change over time and thereby much of the remaining variations of channel gain come from the time domain.

The user movements and antenna patterns are uncertain: The large variation of channel gain in the time domain can be hard to predict as there is always an uncertainty in the user movements and as a result of this, in the interaction between the environment and the antenna patterns of the user equipment. It is clear that the user antenna pattern and behaviour can be a limiting factor for the channel hardening. This can be seen in Fig. 15 as the

simulated curves with the antenna pattern with user effect are close to the user with the least channel hardening in the measurements in Fig. 15b, while a user with an omni-directional antenna experiences more channel hardening. Assuming a non-beneficial scenario from the user aspect, then this type of simulation, where the user equipment is rotating, could be used while in reality it could happen that conditions are more favourable and thus a smaller standard deviation could be achieved. For example, the user from the measurements with the most channel hardening in Fig. 15a, experiences a similar channel hardening as the simulations with the omni-directional antenna in Fig. 15b. Overall, the most significant reasons for the differences between the measurements and the simulations in Fig. 15 are the different antenna patterns and movements of the users; to further align the results, then these parameters should be the same. Further on, since the COST 2100 channel model is a stochastic channel model, comparisons with particular measurements are difficult. However, on average the channel hardening curves resulting from the model show very similar behavior as for the measurements, as seen in Fig. 16.

VII Conclusion

From our experiments and analysis, we can conclude that there is a clear channel hardening effect in massive MIMO, which flattens out the channel fading in frequency and time as the number of antennas increases. However, the complex i.i.d. Gaussian channel model, which is commonly assumed in theoretical studies, is shown to be overoptimistic and does not provide an accurate model for channel hardening in massive MIMO. This is due to the fact that real environments do not provide as rich scattering as assumed in the model but are rather spatially correlated, as recently acknowledged in literature. Moreover, interactions between the array and the environment will cause variations of the received power levels between the different antenna elements. Therefore, by investigating the mechanisms that build up the distribution of channel gain over the array, the channel hardening effect can be better understood. Power imbalances can be due to having a set of antennas where some have a stronger LOS and some not; this imbalance could also be between the polarization modes. As these imbalances change over time, there will still be variations of the channel gain that are originating from the time domain. These changes are hard to predict as there is always an uncertainty of user movements and antenna pattern.

We have also shown that the COST 2100 model with its massive MIMO extension statistically can capture the channel hardening effect well, given appropriate propagation parameters and a realistic antenna pattern and user behavior. As a final remark, in order to maximize the experienced channel hardening, one needs to find strategies to cope with the power imbalances over

the array and design the massive MIMO system such that it can best exploit the diversity of the considered environment. However, channel hardening is only one part of the complex story of achieving reliable communication and in future work other aspects, such as received power levels and coverage, should also be considered.

References

[1] T. L. Marzetta, "Noncooperative cellular wireless with unlimited numbers of base station antennas," *IEEE Trans. Wireless Commun.*, vol. 9, pp. 3590–3600, 11 Nov. 2010.

[2] E. G. Larsson, O. Edfors, F. Tufvesson and T. L. Marzetta, "Massive MIMO for next generation wireless systems," *IEEE Communications Magazine*, vol. 52, no. 2, pp. 186–195, 2014.

[3] E. Björnson, J. Hoydis and L. Sanguinetti, *Massive MIMO Networks: Spectral, Energy, and Hardware Efficiency (Foundations and Trends in Signal Processing)*. Now Publishers Inc, 2018.

[4] H. Q. Ngo and E. G. Larsson, "No downlink pilots are needed in TDD massive MIMO," *IEEE Trans Wireless Commun*, vol. 16, no. 5, pp. 2921–2935, 2017.

[5] M. Roy, S. Paquelet, L. L. Magoarou and M. Crussière, "MIMO channel hardening for ray-based models," in *2018 14th International Conference on Wireless and Mobile Computing, Networking and Communications (WiMob)*, 2018, pp. 1–7.

[6] D. Dardari, "Channel hardening, favorable equalization and propagation in wideband massive MIMO," in *2019 27th European Signal Processing Conference (EUSIPCO)*, 2019, pp. 1–5.

[7] N. Pourjafar and J. Seifali Harsini, "On the complete convergence of channel hardening and favorable propagation properties in massive-MIMO communications systems," *Journal of Mathematical Modeling*, vol. 7, no. 4, pp. 429–443, 2019. eprint: `https://jmm.guilan.ac.ir/article_3671_196ad0a7087d462ce7e945c273d98f22.pdf`.

[8] Z. Chen and E. Björnson, "Channel hardening and favorable propagation in cell-free massive MIMO with stochastic geometry," *IEEE Transactions on Communications*, vol. 66, no. 11, pp. 5205–5219, 2018.

[9] S. Gunnarsson, J. Flordelis, L. V. der Perre and F. Tufvesson, "Channel hardening in massive MIMO - a measurement based analysis," in *19th IEEE International Workshop on Signal Processing Advances in Wireless Communications (SPAWC)*, 2018.

[10] S. Payami and F. Tufvesson, "Delay spread properties in a measured massive MIMO system at 2.6 GHz," in *2013 IEEE 24th Annual International Symposium on Personal, Indoor, and Mobile Radio Communications (PIMRC)*, IEEE, 2013, pp. 53–57.

[11] A. O. Martinez, E. De Carvalho and J. O. Nielsen, "Massive MIMO properties based on measured channels: Channel hardening, user decorrelation and channel sparsity," in *2016 50th Asilomar Conference on Signals, Systems and Computers*, IEEE, 2016, pp. 1804–1808.

[12] A. O. Martinez, J. O. Nielsen, E. De Carvalho and P. Popovski, "An experimental study of massive MIMO properties in 5G scenarios," *IEEE Transactions on Antennas and Propagation*, vol. 66, no. 12, pp. 7206–7215, 2018.

[13] G. Ghiaasi, J. Abraham, E. Eide and T. Ekman, "Measured channel hardening in an indoor multiband scenario," in *2018 IEEE 29th Annual International Symposium on Personal, Indoor and Mobile Radio Communications (PIMRC)*, 2018, pp. 1–6.

[14] G. Ghiaasi, J. Abraham, E. Eide and T. Ekman, "Effective channel hardening in an indoor multiband scenario," *International Journal of Wireless Information Networks*, 2019.

[15] X. Gao, O. Edfors, F. Rusek and F. Tufvesson, "Massive MIMO performance evaluation based on measured propagation data," *IEEE Transactions on Wireless Communications*, vol. 14, no. 7, pp. 3899–3911, 2015.

[16] X. Gao, O. Edfors, F. Tufvesson and E. G. Larsson, "Massive MIMO in real propagation environments: Do all antennas contribute equally?" *IEEE Transactions on Communications*, vol. 63, no. 11, pp. 3917–3928, 2015.

[17] L. Sanguinetti, E. Björnson and J. Hoydis, "Toward massive MIMO 2.0: Understanding spatial correlation, interference suppression, and pilot contamination," *IEEE Transactions on Communications*, vol. 68, no. 1, pp. 232–257, 2020.

[18] S. Jaeckel, L. Raschkowski, K. Börner and L. Thiele, "QuaDRiGa: A 3-D multi-cell channel model with time evolution for enabling virtual field trials," *IEEE Transactions on Antennas and Propagation*, vol. 62, no. 6, pp. 3242–3256, 2014.

[19] S. Jaeckel, L. Raschkowski, K. Börner, L. Thiele, F. Burkhardt and E. Eberlein, "QuaDRiGa: - quasi deterministic channel generator, user manual and documentation," Frauenhofer Heinrich Hertz Institute, Tech. Rep. v2.0.0, 2017.

[20] A. O. Martínez, P. Eggers and E. De Carvalho, "Geometry-based stochastic channel models for 5G: Extending key features for massive MIMO," in *2016 IEEE 27th Annual International Symposium on Personal, Indoor, and Mobile Radio Communications (PIMRC)*, 2016, pp. 1–6.

[21] "Study on channel model for frequencies from 0.5 to 100 GHz," 3GPP TR 38.901, Tech. Rep. v14.1.0, 2017.

[22] "Guidelines for evalation of radio interface technologies for imt-2020," ITU-R, Tech. Rep. M.2412-0, 2017.

[23] V. Nurmela, A. Karttunen, A. Roivainen *et al.*, "Deliverable D1.4 METIS channel models," Mobile and wireless communications Enablers for the Twenty-twenty Information Society (METIS), Tech. Rep. v1.0, 2015.

[24] L. Liu, C. Oestges, J. Poutanen *et al.*, "The COST 2100 MIMO channel model," *IEEE Wireless Communications*, vol. 19, no. 6, pp. 92–99, 2012.

[25] "The COST 2100 channel model with massive MIMO extensions." (), [Online]. Available: `https://github.com/cost2100`.

[26] X. Gao, J. Flordelis, G. Dahman, F. Tufvesson and O. Edfors, "Massive MIMO channel modeling - extension of the COST 2100 model," English, Joint NEWCOM/COST Workshop on Wireless Communications (JNCW) ; Conference date: 14-10-2015 Through 15-10-2015, 2015.

[27] J. Flordelis, X. Li, O. Edfors and F. Tufvesson, "Massive MIMO Extensions to the COST 2100 Channel Model: Modeling and Validation," *IEEE Trans. Wireless Commun.*, 2019.

[28] A. Bourdoux, C. Desset, L. van der Perre *et al.*, "D1.2 MaMi channel characteristics: Measurement results," MAMMOET, Report, 2015.

[29] J. Vieira, S. Malkowsky, K. Nieman *et al.*, "A flexible 100-antenna testbed for massive MIMO," in *2014 IEEE Globecom Workshops (GC Wkshps)*, IEEE, 2014, pp. 287–293.

[30] S. Malkowsky, J. Vieira, L. Liu *et al.*, "The world's first real-time testbed for massive MIMO: Design, implementation, and validation," *IEEE Access*, vol. 5, pp. 9073–9088, 2017.

[31] F. Harrysson, J. Medbo, A. F. Molisch, A. J. Johansson and F. Tufvesson, "Efficient experimental evaluation of a MIMO handset with user influence," *IEEE Transactions on Wireless Communications*, vol. 9, no. 2, pp. 853–863, 2010.

Paper III

Fading in reflective and heavily shadowed industrial environments with large arrays

One of the use cases for 5G systems and beyond is ultra-reliability low-latency communication (URLLC). An enabling technology for URLLC is massive multiple-input multiple-output (MIMO), which can increase reliability due to improved user separation, array gain and the channel hardening effect. Measurements have been performed in an operating factory environment at 3.7 GHz with a co-located massive MIMO array and a unique randomly distributed array. Channel hardening can appear when the number of antennas is increased such that the variations of channel gain (small-scale fading) is decreased and it is here quantified. The cumulative distribution function (CDF) of the channel gains then becomes steeper and its tail is reduced. This CDF is modeled and the required fading margins are quantified. By deploying a distributed array, the large-scale power variations can also be reduced, further improving reliability. The large array in this rich scattering environment, creates a more reliable channel as it approaches an independent identically distributed (i.i.d.) complex Gaussian channel, indicating that one can rethink the system design in terms of e.g. channel coding and re-transmission strategies, in order to reduce latency. To conclude, massive MIMO is a highly interesting technology for reliable connectivity in reflective and heavily shadowed industrial environments.

Reprinted from S. Gunnarsson, L. Van der Perre, F. Tufvesson,
"Fading in reflective and heavily shadowed industrial environments with large arrays,"
submitted to *IEEE Journal on Selected Areas in Communications 2022.*

I Introduction

Wireless cellular communication is constantly evolving; currently 5G is rolled out and research is aiming towards 6G. One focus area for 5G systems, for which the requirements still partially are unfulfilled and hence will remain a focus area, is the ultra-reliability low-latency communication (URLLC) use case. Therefore, for 6G systems, discussions are ongoing regarding neXt generation URLLC (xURLLC). It has applications within e.g. automotive industry, remote surgery and smart manufacturing. URLLC has gained huge interest and commonly mentioned goals are reliabilities of $10^{-9} - 10^{-5}$ and latencies of 1 ms [1].

To achieve the goals of xURLLC, new technologies are required. From a physical layer point of view, one of these enabling technologies is massive multiple-input multiple-output (MIMO) [2]. The deployment of massive MIMO systems enables characteristics that can improve reliability. First of all, due to favorable propagation conditions – where the channels between two users become pairwise orthogonal – the possibility to separate spatially multiplexed users is improved. Secondly, when combining the many antennas, the array gain results in a stronger received signal. Lastly, the channel becomes more flat in both time and frequency as a channel hardening effect appears; this means that the variations of channel gain decrease as the number of antennas increases. These two characteristics in combination leads to a decreased probability of outage, which can be so low that the way the rest of the communication system is designed needs to be re-considered.

Channel hardening has been investigated in theory[2]–[7] where an independent and identically distributed (i.i.d.) complex Gaussian channel model is commonly used. However, in an indoor scenario, the model has been shown to be overly-optimistic [8] since real massive MIMO channels usually are spatially correlated. Lately, there have been several studies investigating channel hardening in simulations [9], experimentally [8], [10]–[12] and also for systems beyond conventional massive MIMO such as cell-free massive MIMO [13] and intelligent surfaces [14].

With the channel hardening effect, the cumulative distribution function (CDF) of channel gains becomes steeper and its tails smaller. A number of studies have proposed solutions to model the channel and the tails of these CDFs for URLLC purposes. As URLLC is about accounting for the extreme outage events that rarely happen, an extreme value theory approach is applicable to model the channel [15]. In [16] approximations for the tail distribution for a wide range of channel models are presented, consisting of only two parameters: an exponent and an offset. First elaborating on the benefits and challenges when using parametric and non-parametric channel models, [17] concludes that the power law tail approximation in [16] provides a good trade-off. The concept of local diversity, which concerns evaluating the slope of the CDF

at a certain point, is presented in [18]. The CDFs can also be used to relate to the required fading margin, where a definition is provided in [19].

With the small-scale variations significantly reduced due to channel hardening, the reliability becomes mostly related to the large-scale power variations, mainly caused by shadowing. To combat shadowing, a distributed setup can be the solution, resulting in that not all antennas are blocked simultaneously. Various distributed configurations (ranging from semi-distributed to fully distributed) have been investigated in different indoor scenarios [20]–[23] and their performance has been compared to the co-located equivalent [20], [21].

This study contributes to the area by analysing and modeling the channel based on a unique measurement campaign performed in one of Bosch's operating semiconductor factories in Reutlingen, Germany. The factory is an extremely complex environment from a wireless communication perspective. Channels have been collected with a massive MIMO system equipped with both a co-located and a randomly, fully distributed array (within practical constraints). For the two arrays, the channel hardening effect and required fading margins are quantified. The tails of the channel gain CDFs are characterized. Furthermore, an assessment of the decreased large-scale power variations when deploying a distributed setup is made. To the best of our knowledge, no measurement-based study has been performed with a fully distributed massive MIMO setup in these extreme environments. Our experiments in combination with the analysis, characterization and modeling provide valuable insights to enable URLLC in complex factory environments.

The structure of the paper is as follows. The measurement scenario in Section II, followed by measurement setup and data processing are described in Section III. Following these sections, results are presented in Section IV where a high-level inspection is presented, Section V concerns the channel hardening effect and the tails of the CDFs are modeled in Section VI with related fading margins in Section VII. After the elaboration on small-scale fading, the shadowing-related results are presented in Section VIII. Lastly, in Section IX, summary and conclusions are provided.

II Measurement scenario

The measurements have been performed in the Bosch semiconductor factory in Reutlingen, Germany. This factory provides an environment with many walls and long corridors as well as a lot of high metallic machinery, all providing substantial shadowing and reflections of signals, as can be seen in Fig. 1. The above leads to rich scattering. With robots and humans moving around it also makes it a dynamic environment. The scenario investigated here consists of a corridor with tall machinery on the sides. This environment includes many tricky places in terms of coverage, large-scale and small-scale fading.

(a) View towards the co-located array.

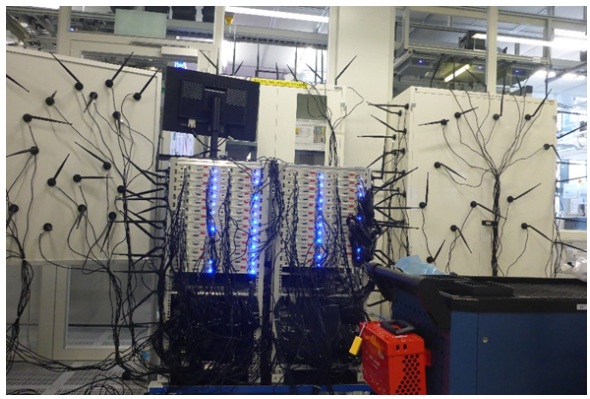

(b) The distributed array.

(c) View towards the left aisle.

Figure 1: Pictures from the measured environment in the Bosch semiconductor factory.

The scenario is described in Fig. 1 where Fig. 1a shows the view from the corridor towards the base station (BS) with the co-located array deployed. Directly in front of the array there is an open space and all antennas have their highest gain in the direction of where the user equipment (UE) is located. Fig. 1b shows the deployed distributed array. Note that this random deployment also means that antennas may have other equipment and/or antennas in the close vicinity and most antennas do not have their highest gain in direction towards the place where the UE is located, which is different from the situation of the co-located array. Lastly, in Fig. 1c, the view from the corridor towards the left aisle in the corridor can be seen.

An overview of where the measurements took place is visualized in Fig. 3, where the BS is placed next to a wall and the UE is in the middle of the corridor (the two UEs representing two different experiments). In the first experiment the blue UE moves from line-of-sight (LoS) to non-line-of-sight (NLoS) to the left (as seen from the BS). The UE antennas are at first pointing as in Fig. 1c, then when moving into NLoS the stick is rotated 90° to the right. The measurements also include scanning the entire area behind the machinery with 6000 time samples, maintaining the antenna orientations. This experiment serves as a basis for collecting statistics of the small-scale fading in heavily shadowed places. For the second experiment, the red UE starts close to the BS and then moves along the corridor while entering the aisles behind the machinery, aiming at collecting large-scale fading statistics. In Fig. 2b the view from the BS towards the UE and the corridor is seen.

III Measurement setup and data processing

The measurement device used in the experiment is the Lund university Massive MIMO (LuMaMi) testbed , a long-term-evolution (LTE)-like and software-defined radio (SDR)-based testbed with 100 coherent radio frequency (RF)-chains, able to serve up to twelve UEs simultaneously. The equipment used as UEs consists of one SDR, each having two RF-chains connected to dipole antennas with vertical and horizontal orientation. The two RF-chains are independently processed and can be seen as two separate users.

The testbed, acting as the BS, is normally equipped with a co-located array, where the connected antenna ports form a rectangular array with four rows and 25 dual-polarized $\lambda/2$-spaced antenna elements in each row. One polarization per antenna element is connected, where the polarization is alternating between two consecutive elements. The second array is a randomly distributed array with random directions and polarizations, with the aim to increase the exploited diversity in the environment. The distributed array consists of 100 omni-directional dipole antennas which, via a cable of three or five meters, are connected to the testbed.

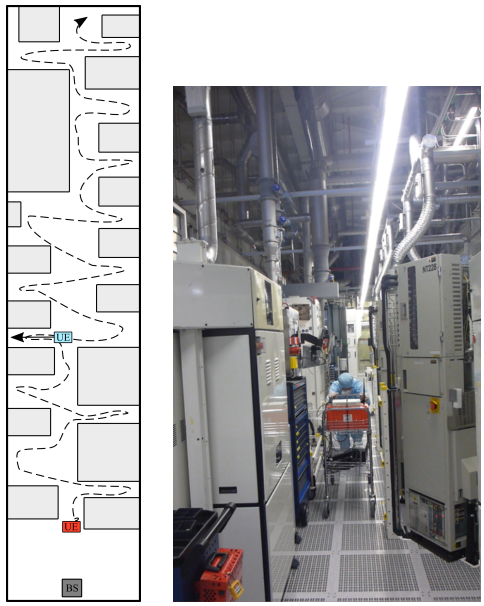

(a) (b)

Figure 2: Overview of the measurement scenario with (a) the map, and (b) the view from the BS towards the UE.

The synchronization between the BS and UEs is over-the-air (OTA) and starts when the BS sends out a synchronization signal in the beginning of each frame. When receiving, the UE uses that signal to synchronize to the BS. During the measurements, samples have occasionally been lost. This is to our best understanding due to the OTA synchronization failing and hence the corresponding channel sample is not stored[2]. The raw channel gain $|h|^2$ over time, as averaged over frequency and summed for all BS antennas when using the vertical UE orientation, is shown in Fig. 3. This shows an example of how the lost samples are witnessed in the response, where dips of more than 25 dB can be seen, randomly distributed over time. Most often, only 1-2 samples in a row are lost. Occasionally but quite rarely, 3-4 samples in a row are lost. There are no signs of fading dips when samples are lost.

The first uplink pilot in each frame is logged for later analysis, meaning that a channel sample is collected every 10 ms (the slowest repetition rate that can be handled by the testbed), i.e. $f_{rep} = 100$ Hz. Channels are continuously recorded for the $M = 100$ BS antennas at a carrier frequency of 3.7 GHz and over 20 MHz bandwidth, with $F = 100$ uniformly distributed frequency

[2]In other experiments where rubidium clocks have been used as frequency reference, then no samples have been lost. This together with visual inspection of the stored transfer functions point to the synchronization as origin for the lost sample problem.

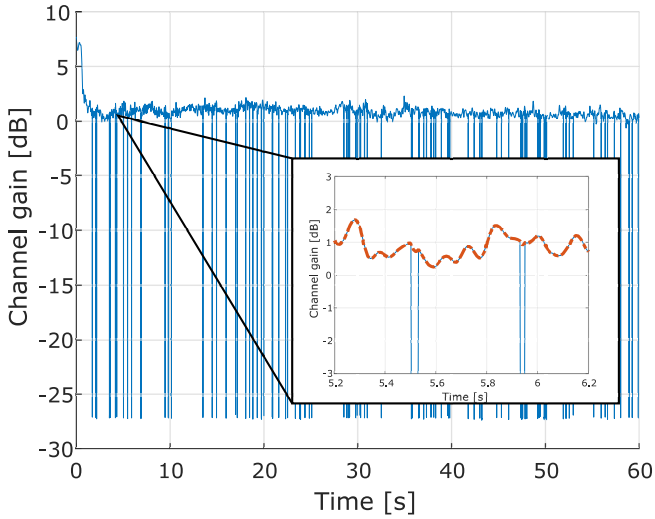

Figure 3: Raw channel gain over time, averaged over frequency and summed for BS antennas, showing lost samples and an example of linear interpolation applied for each frequency point and BS antenna.

samples over the bandwidth. In time, $N = 6000$ samples are collected. This results in, for each UE, a channel matrix of dimensions $H = [N \times F \times M]$.

Considering that the repetition frequency needs to be at least twice the maximum Doppler frequency in order to not violate the Nyquist sampling criterion, i.e. $f_{rep} \geq 2f_{max}$, the maximum speed v_{max} of the UE can be $v_{max} = \frac{cf_{max}}{f_c}$, where c is the speed of light, f_c the carrier frequency and f_{max} is the maximum Doppler frequency that can be handled with this repetition rate. Here this means that the maximum speed of the UE can be 4 m/s; the experiments here are performed below this limit.

The complex time correlation for all BS antennas and frequency samples was investigated. The results showed that the correlation coefficient was less than 0.5 for samples separated 20 ms or more (i.e. two samples) for all frequency points and BS antennas. The samples collected are hence indeed quite independent which is good for the statistical analysis but makes it difficult to make a good interpolation. Therefore, when investigating the channel statistics, the outliers due to the OTA synchronization error are removed. When showing the time series, linear interpolation is applied to each frequency point and BS antenna. An example of this is shown in the smaller box in Fig. 3 where the original signal with outliers is shown in blue and the interpolated signal in dashed red.

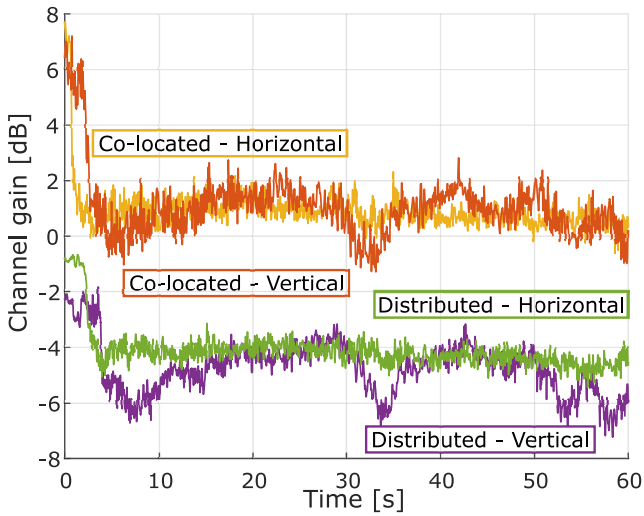

Figure 4: Channel gain for both UE orientations and the co-located and distributed array over time with both UE orientations, when going into the left aisle.

IV High-level inspection

Taking a first look at the channel responses from the first experiment – the UE moving from LoS to NLoS – Fig. 4 shows the interpolated channel gain over time when going into the left aisle for both arrays and UE orientations. The first seconds from the measurement are in LoS, with the higher channel gain, and then the UE is shadowed by the machinery for the rest of the measurements while there scanning the area. The channel gains of the co-located array are higher due to the higher antenna gain and that the distributed setup is also influenced by the attenuation from cables and adaptors. The small dips are when the UE antenna is close to the floor, indicating that coverage can be trickier at these spots.

When being shadowed, the channel gain for the co-located drops about 6 dB and for the distributed setup the gain drops about 2-3 dB, depending on the UE orientation. The LoS can hence be concluded to be less prominent in the distributed case, as expected since the antennas are randomly placed. This leads to somewhat bad placements for this specific measurement, while for the co-located array, all antennas are pointing in the direction where the UE is. In NLoS, the channel gain varies with the movement of the UE, the variations for the vertically oriented antennas are larger than for the horizontally oriented.

For further results and analysis, the first five seconds of each measurement are removed, in order to focus on the heavily shadowed areas. The means

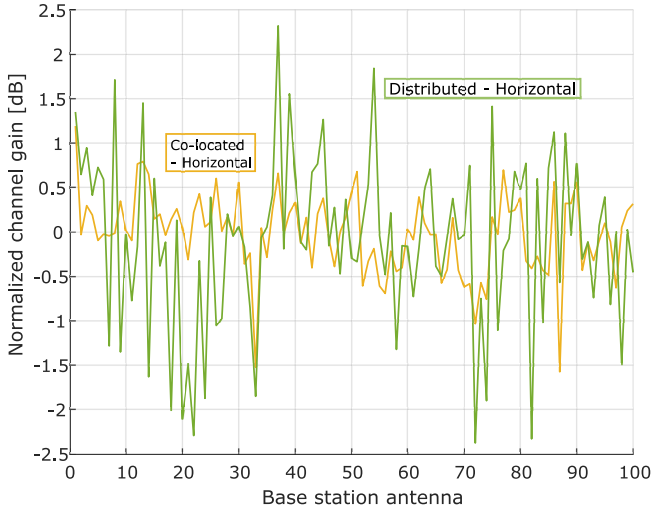

Figure 5: Normalized channel gain, as per BS antenna, in the co-located and distributed array when scanning the left aisle with horizontal UE orientation.

and standard deviations of the gain in dB, as starting from five seconds are summarized in Table. 1

Looking closer into the similarities and differences between the BS antennas of the two arrays, the mean (as averaged over time and frequency) of the normalized channel gain is shown in Fig. 5. It can be seen for the co-located array, most antennas are centered closely around the mean (which is 0 dB due to the normalization) while for the distributed array, the power variations over the array are larger. For the co-located array the standard deviation is 0.10 dB and for the distributed array it is 0.22 dB. The corresponding values for the vertical UE orientation is 0.18 dB and 0.24 dB, respectively. This is in line with the assumption that for the distributed case, some antenna will have beneficial placements, while some will contribute very little.

		$\hat{\mu}$	$\hat{\sigma}$
Co-located	V	0.88	0.70
	H	0.86	0.38
Distributed	V	-4.87	0.80
	H	-4.25	0.32

Table 1: Estimated parameters starting from 5 seconds in Fig. 4 (in dB).

V Channel hardening

Starting the analysis, the channel hardening effect in this environment is investigated and quantified. The definition of channel hardening, as given in [4], is that the channel vector $\mathbf{h}_k$ between the BS and a user k offers channel hardening if

$$\frac{\mathrm{Var}\{\|\mathbf{h}_k\|^2\}}{\mathrm{E}\{\|\mathbf{h}_k\|^2\}^2} \to 0, \quad \text{as } M \to \infty, \tag{1}$$

where M is the number of base station antennas. The evaluation of channel hardening is performed in the same manner as in [8], and with similarities to the work in [10], [11]. Before analysis, the channel matrix for each UE antenna is normalized as

$$\overline{\mathbf{h}}_k(n,f) = \frac{\mathbf{h}_k(n,f)}{\sqrt{\frac{1}{NFM}\sum_{n=1}^{N}\sum_{f=1}^{F}\sum_{m=1}^{M}|h_{km}(n,f)|^2}}, \tag{2}$$

for N snapshots, F frequency points and M *selected* BS antennas, where *selected* means those antennas for which the channel hardening is later evaluated. This normalization is also the one used in Fig. 5 and means that each entry in $\overline{\mathbf{h}}_k$, as averaged over frequency, time, and BS antennas, has an average power equal to one. The channel hardening is then evaluated as the standard deviation (square root of the variance) of channel gain for each UE as

$$\mathrm{std}_k = \sqrt{\frac{1}{NF}\sum_{n=1}^{N}\sum_{f=1}^{F}|\overline{G}_k(n,f) - \mu_k|^2}, \tag{3}$$

where $\overline{G}_k(n,f)$ is the instantaneous channel gain $|\overline{h}_{km}(n,f)|^2$, as summed and divided by M, and μ_k is the average channel gain, as summed and divided by N and F, and hence equal to one (i.e. 0 dB); details can be found in [8]. With (3), the channel hardening can be quantified as the difference in standard deviation when using 1 and M BS antennas.

A visualization of the array gain and channel hardening effect is presented in Fig. 6 for the co-located array in the NLoS part of the first experiment. Here, the channel gain when combining all 100 antennas in comparison to the one antenna case can be seen as a function over time and frequency. When adding up the signals of the 100 antennas, the mean of the channel gain increases, that is the array gain. What also can be seen is that for the one antenna case, there are large variations over both time and frequency, while for the 100 antenna case the variations are just a few dB; this is the channel hardening effect.

To quantify the experienced channel hardening, Fig. 7 shows the decrease of standard deviation as a function of the number of BS antennas. The standard

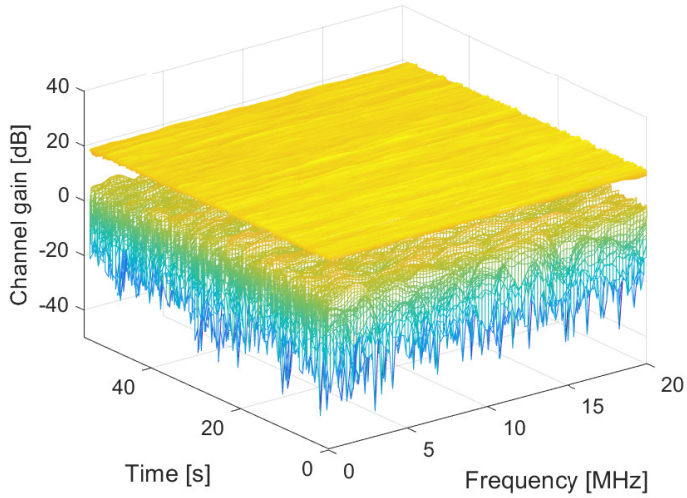

Figure 6: Channel gain over time and frequency for 1 (lower) and 100 BS antennas (upper) when going into the left aisle and the co-located array is deployed and horizontal UE orientation.

deviation for the i.i.d. complex Gaussian is shown for reference. Furthermore, the standard deviation for both the UE with vertical and horizontal orientation are shown and a comparison of the co-located and distributed array. It can be seen that there is indeed a very prominent channel hardening effect as the standard deviation of channel gain decreases as the number of BS antennas increases. It can also be concluded that there are no major differences between the co-located and the distributed array; they behave similarly such that for both arrays, the horizontally oriented UE is experiencing more channel hardening. In general, the vertical UE orientation should be better at picking up signals reflected from machinery on the sides while the horizontal UE orientation ought to be better placed to pick up ceiling and floor reflections.

The measured standard deviations are following the theoretical curve quite closely, or with a small offset, for a smaller number of antennas. For a higher number of BS antennas, the curves start to diverge as the channel hardening effect saturates. However, two of the measured standard deviations in Fig. 7 follow the theoretical one very closely, showing that this is indeed a very rich scattering environment. The resulting channel hardening, measured as the difference between the end and starting points of each curve, is between 7.1 dB and 9.2 dB. This is not that far from the theoretical benchmark, which for 100 BS antennas is 10 dB. Comparing to a more general indoor environment, [8] measured in an indoor auditorium in LoS, reaching standard deviations

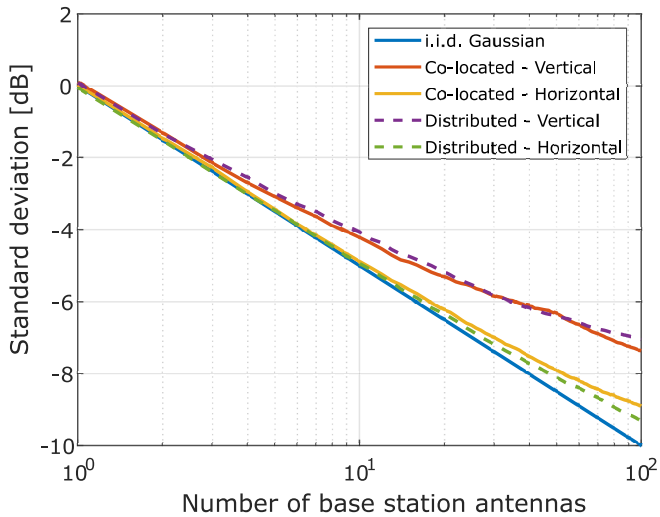

Figure 7: Channel hardening when scanning the left aisle for both arrays and UE orientations. The i.i.d. complex Gaussian channel is shown for reference.

down to -6.8 dB, although less than that in most cases. This indicates that in our indoor rich scattering factory environment, the channels between the UE and the different BS antennas are to a large extent independent, and hence a large portion of the channel hardening effect can be harvested, approaching the theoretical bound.

VI Modeling the tails of the CDFs

Here, the CDFs are modeled by assuming that the underlying channel coefficients h are i.i.d. complex Gaussian, leading to Rayleigh distributed $|h|$ and the channel gain $|h|^2$ resulting in an exponential distribution. Summing up the power for the M BS antennas as done with maximum ratio combining/transmission (MRC/MRT), a gamma distribution $\Gamma(M, 1/M)$ is expected. The shape parameter, here ideally translated to M, can be seen as a measure of the possible degrees of freedom (DoF), which in case of fully independent channel coefficients would be the number of BS antennas.

Visualizing the same measured channel gains but in another analysis, Fig. 8 and 9 show the CDFs of the channel gain for $M = [1, 2, 4, 8, 16, 32, 64, 100]$, for the co-located and the distributed configuration. The array gain, as seen in Fig. 6, can not be seen here, since the gains are normalized by M, meaning that the output power from the BS could be reduced with a factor M. The

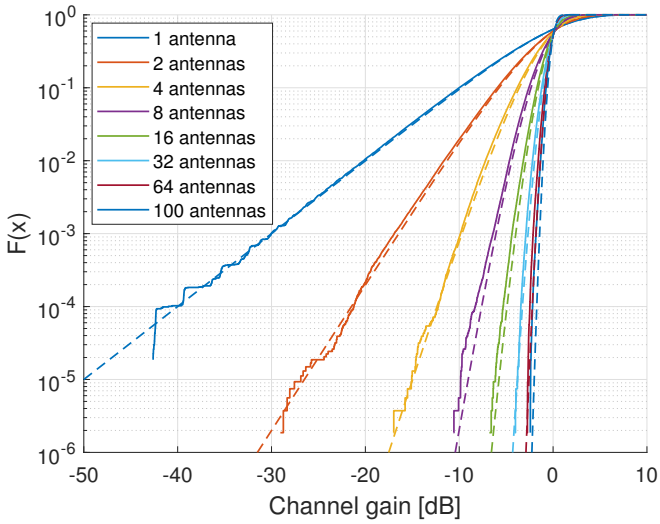

Figure 8: CDF of the channel gain when scanning the left aisle with horizontal UE orientation and the co-located array deployed. The gamma distribution ($\Gamma(M, 1/M)$) is shown for reference.

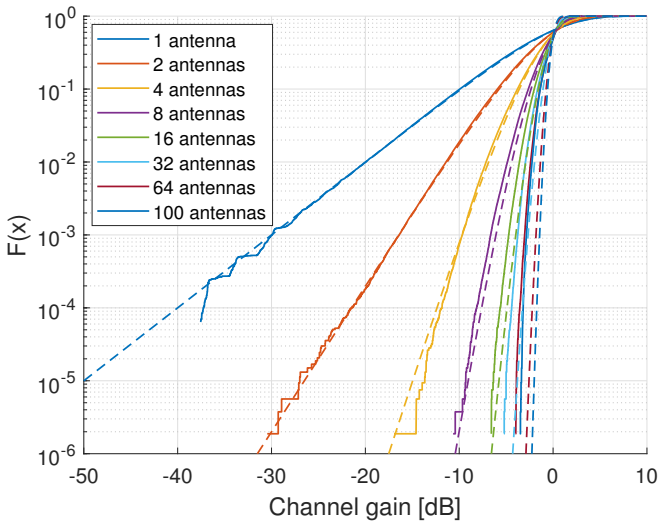

Figure 9: CDF of the channel gain when scanning the left aisle with vertical UE orientation and the distributed array deployed. The gamma distribution ($\Gamma(M, 1/M)$) is shown for reference.

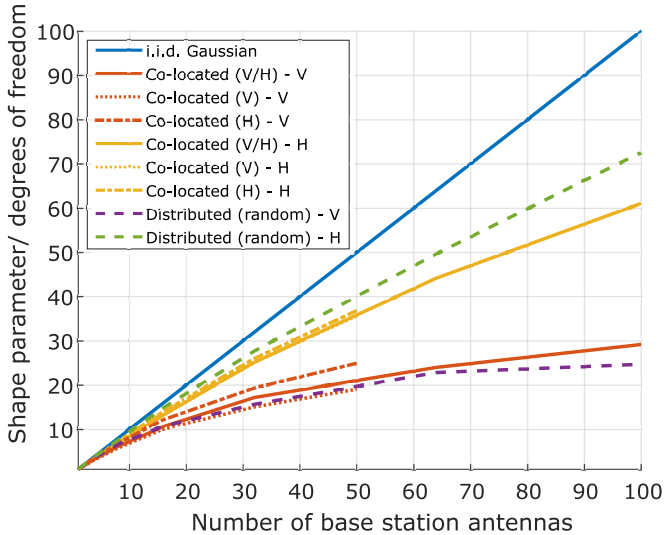

Figure 10: The estimated shape parameter $\hat{M}$ for both the co-located and the distributed array when scanning the left aisle with the vertical or horizontal UE orientation. The i.i.d. complex Gaussian channel is shown for reference.

channel hardening can however be clearly seen as the CDFs get steeper with more antennas. The major improvements happen at the beginning and as the antenna set gets larger, the difference is not as significant, although small improvements are still to be harvested, in line with Fig. 7.

As a reference, the gamma distributions $\Gamma(M, 1/M)$ with the shape parameter M and scale parameter $1/M$ is shown with dashed lines. It can be observed that for a smaller subset of antennas, i.e. up to about 32 BS antennas, both the scale and shape parameter correspond well to the measurements. However, after that, there is a visible difference, indicating that one additional DoF is not gained by adding one more BS antenna and hence, all channels are not independent of each other. This observation can be made for both the co-located and the distributed array. It can also be observed that the slope for the measured curves in general are matching while the offset of the slope at e.g. 10^{-5} for $M > 2$ is between $0.02 - 0.80$ for the co-located array with horizontal UE orientation and $0.52 - 1.37$ in the distributed case with vertical UE orientation.

Elaborating on the previous observation, the shape and scale parameter are shown in Fig. 10 and 11 for the co-located and the distributed setup for both UE orientations. The case when only choosing the vertically or horizontally polarized BS antennas is also included. In the case where the underlying channel coefficient would be i.i.d. complex Gaussian, the shape parameter would

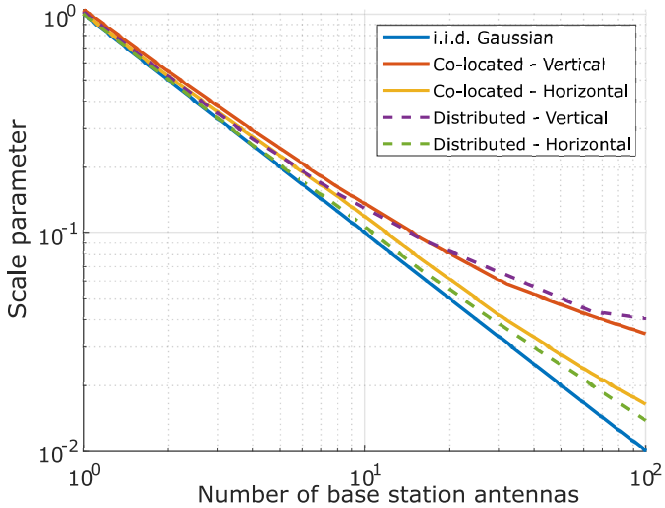

Figure 11: The estimated scale parameter $\frac{1}{M}$ for both the co-located and the distributed array when scanning the left aisle with the vertical or horizontal polarization. The i.i.d. complex Gaussian channel is shown for reference.

increase by 1 when adding 1 antenna, i.e. adding 1 DoF for each new BS antenna. It can be observed that this is indeed not entirely the case, although not too far away for one of the two possible UE orientations. These results can easily be related to the channel hardening in Fig. 7, serving as the link indicating how many independent channels there actually are for a certain subset of antennas. As an example. for the channel hardening curve in Fig. 7, the distributed setup with horizontal UE orientation ends up at the same point as the i.i.d. complex Gaussian for 73 antennas. This can then be seen in the shape parameter in Fig. 10. Interesting to note is also that the slopes when only choosing one polarization at the BS are similar to when alternating, possibly due to the fact that most paths may be reflected. The scale parameter, which can be translated to the standard deviation, is shown in Fig. 11 and can also be used as a measure to quantify the channel hardening effect; here seen as the decreasing slope as the number of BS antennas increases, which is corresponding to the slopes in Fig. 7.

VII Fading margin

In [19], the link between channel hardening and fading margin is elaborated on and a measurement-based definition of the fading margin is introduced by using

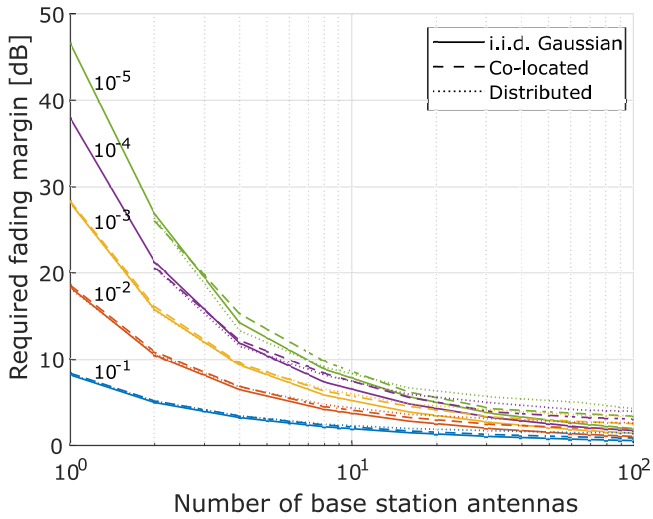

Figure 12: The required fading margin for different outage thresholds for the co-located and the distributed array.

the empirical CDF (ECDF). The definition relates to the median, as dependent on the number of antennas M and with probability p, and is given as

$$F_M(p) = 10\log_{10}(\frac{Q(0.5)}{Q(p)}) \tag{4}$$

where Q is the quantile/inverse CDF function. Naturally, the more channel hardening, the steeper the CDF, and the smaller fading margin is required.

In Fig. 12, the required fading margin, as given in (4) to achieve different outages is shown as a function of the number of BS antennas for the left aisle for the co-located array with horizontal UE orientation and the distributed array with vertical UE orientation. Outages between 10^{-5}–10^{-1} and antenna subsets from $[1, 2, 4, 8, 16, 32, 64, 100]$ are shown, as this is what can be used based on the data, as seen in Figs. 8 and 9. The i.i.d. complex Gaussian channel is shown for reference. What is seen is steadily decreasing required fading margins as the number of BS antennas increases. The co-located and the distributed array are following each other very well. Starting from one antenna, the required fading margins decrease quite rapidly, meaning that there is a lot to gain in terms of fading margin by adding just a few, while the gain in terms of decreased fading margin is not that big when compared to the larger subsets of antennas. It can be noted that at 100 antennas and an outage threshold of 10^{-5}, the required fading margin is not exceeding 4.3 dB.

VIII Shadowing

Changing the focus towards large-scale fading and shadowing effects, the analysis continues with the results from the second experiment, Figs. 13 and 14 show the channel gain for different positions for each BS array, as averaged over frequency and summed for all BS antennas. The effect is as expected a high channel gain when being in LoS in the corridor and a lower channel gain when being shadowed in the aisles. Here the first four to five aisles can be seen for both the vertical and horizontal UE orientation, which show similar behaviour globally but they also show differences when analyzing the details. For example, the horizontal UE does not experience as severe dips when being shadowed, potentially due to being better at picking up reflections from the ceiling. The channel gain is also decreasing from left to right, which is an effect of the path-loss when increasing the distance. However, note that the x-axis is not directly translatable to distance as it is not strictly increasing with the position/measurement time, as seen in Fig. 3.

To investigate the shadowing, the channel gains are fitted to a line ($y = kx + m$) by linear regression in a least-square sense and the values for k and m is shown in Table 2. The shadowing is analysed as the variations around this line and Figs. 15 and 16 show the CDF of channel gain (on a dB-scale) for this shadowing for the two array configurations. For each array, the vertical and horizontal UE are shown with their respective fit to a normal distribution, resulting in a log-normal distribution, with the standard deviation given in Table 2.

In Table 2, the largest standard deviation is found to be with the co-located array, serving the vertical UE, and the smallest variance is with the distributed array serving the horizontal UE. The other two UEs are somewhere in between. For the four cases seen in Figs. 13-16, the normal fit overestimates the tail; the measured shadowing is less severe than this when it comes to the more extremes. For the measured channels, the shadowing variation is between -4 and 6 dB for the co-located array and -3 and 5 dB for the distributed array. These results indicate that the worst cases of shadowing can be avoided and the span can be reduced with a distributed array. Especially since, again reminding of the fact that the co-located array is pointing in the direction of the experiment while the distributed is somewhat random, the UE movement is unknown and therefore

		$\hat{k}$	$\hat{m}$	$\hat{\sigma}$
Co-located	V	-0.0012	22.26	2.41
	H	-0.0010	22.32	1.28
Distributed	V	-0.0011	22.36	1.72
	H	-0.0009	22.13	1.17

Table 2: Estimated parameters as shown in Figs. 13-16.

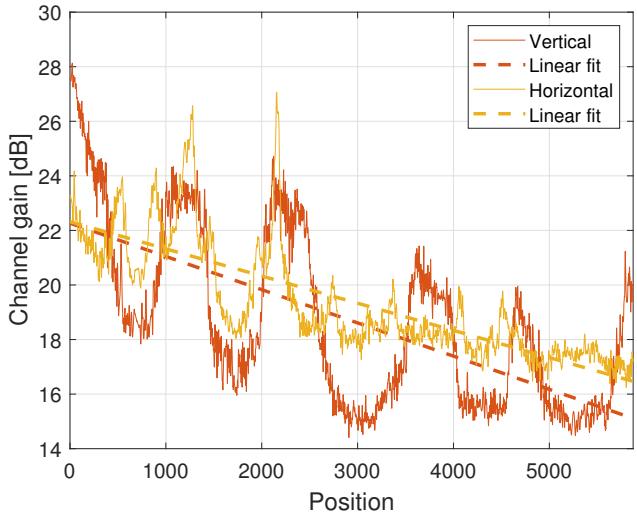

Figure 13: Channel gain over time for the co-located array and both UE orientations with the linear regression line.

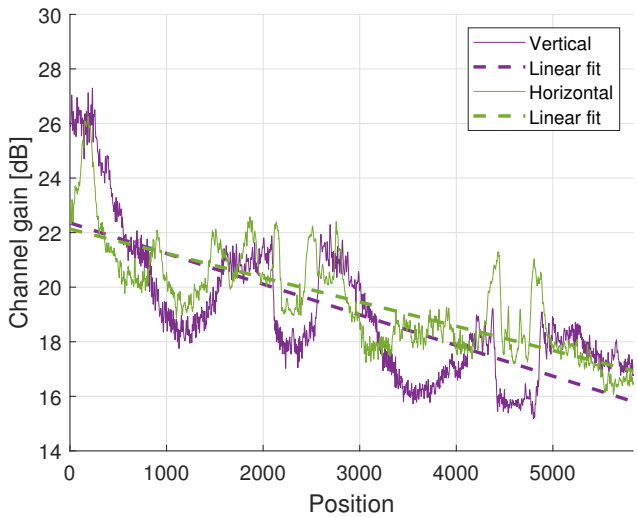

Figure 14: Channel gain over time for the distributed array and both UE orientations with the linear regression line.

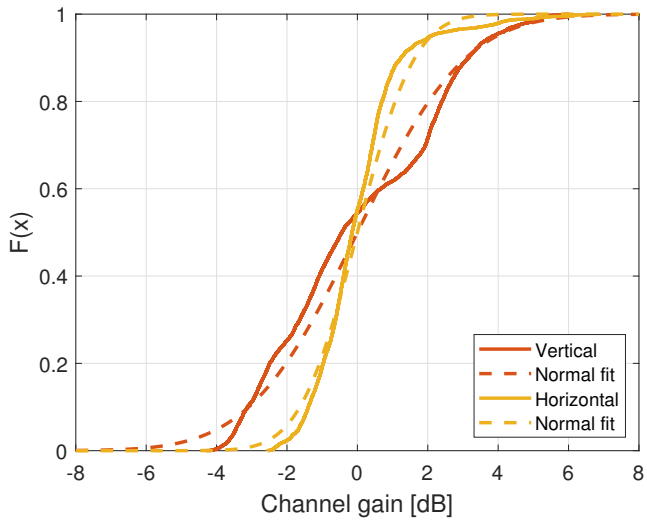

Figure 15: CDF of the shadowing for the co-located array and both UE orientations and the fitted normal distribution.

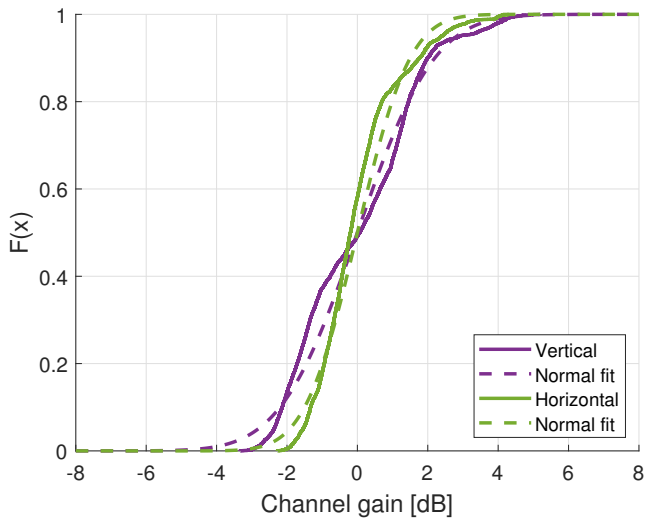

Figure 16: CDF of the shadowing for the distributed array and both UE orientations and the fitted normal distribution.

the best placement of a co-located array would vary while in the distributed case, some of the antennas should always have a more beneficial placement.

IX Conclusions

We have investigated the channel characteristics of massive MIMO, deployed in a real operating factory. The environment provides blocking effects but also extremely rich scattering, leading to the fact that signals are coming from almost every angle and that there are no dominant directions. This results in channel responses being not far from coinciding with the often theoretically assumed i.i.d. complex Gaussian channel.

With massive MIMO, the channel becomes more reliable through the array gain and channel hardening. The channel hardening can also be viewed as the CDF of channel gains becomes steeper, here compared to a gamma distribution, whose parameters have been estimated, giving a slightly different view of this effect and a relation to the number of DoF. The channel hardening effect results in that very small fading margins are required and that has also been quantified. With 100 antennas the required fading margin does not exceed 4.3 dB for any of the two array configurations.

Both a co-located and a fully distributed array have been deployed, aiming at further extracting spatial diversity, and comparisons have been made. The conclusion from this analysis is that the small-scale fading statistics are similar for the two arrays, however, the worst cases in terms of large-scale power variations are avoided and the span of experienced shadowing is reduced with a distributed setup, being beneficial in heavily shadowed environments and unknown UE movement patterns.

Having an almost i.i.d. complex Gaussian channel will impact the whole system architecture, suggesting one to rethink how the channel relates to both the hardware design and the upper layers. From a system perspective, the channel coding can be done with short block lengths and short packets. A very limited number of re-transmissions should also be possible, enabling ultra-low latency. To summarize; xURLLC can be realizable in reflective and heavily shadowed industrial environments with large distributed antenna arrays, but co-located arrays can also be sufficient to achieve this goal.

Acknowledgment

The authors would like to thank Harsh Tataria, Steffen Malkowsky and Anders J Johansson for the help during the measurement campaign and the Bosch staff at the semiconductor factory in Reutlingen for enabling this work.

References

[1] H. Ji, S. Park, J. Yeo, Y. Kim, J. Lee and B. Shim, "Ultra-reliable and low-latency communications in 5G downlink: Physical layer aspects," *IEEE Wireless Communications*, vol. 25, no. 3, pp. 124–130, 2018.

[2] T. L. Marzetta, "Noncooperative cellular wireless with unlimited numbers of base station antennas," *IEEE Trans. Wireless Commun.*, vol. 9, pp. 3590–3600, 11 Nov. 2010.

[3] E. Björnson, J. Hoydis and L. Sanguinetti, *Massive MIMO Networks: Spectral, Energy, and Hardware Efficiency (Foundations and Trends in Signal Processing)*. Now Publishers Inc, 2018.

[4] H. Q. Ngo and E. G. Larsson, "No downlink pilots are needed in TDD massive MIMO," *IEEE Trans Wireless Commun*, vol. 16, no. 5, pp. 2921–2935, 2017.

[5] M. Roy, S. Paquelet, L. L. Magoarou and M. Crussière, "MIMO channel hardening for ray-based models," in *2018 14th International Conference on Wireless and Mobile Computing, Networking and Communications (WiMob)*, 2018, pp. 1–7.

[6] D. Dardari, "Channel hardening, favorable equalization and propagation in wideband massive MIMO," in *2019 27th European Signal Processing Conference (EUSIPCO)*, 2019, pp. 1–5.

[7] N. Pourjafar and J. Seifali Harsini, "On the complete convergence of channel hardening and favorable propagation properties in massive-MIMO communications systems," *Journal of Mathematical Modeling*, vol. 7, no. 4, pp. 429–443, 2019. eprint: `https://jmm.guilan.ac.ir/article_3671_196ad0a7087d462ce7e945c273d98f22.pdf`.

[8] S. Gunnarsson, J. Flordelis, L. Van Der Perre and F. Tufvesson, "Channel hardening in massive MIMO: Model parameters and experimental assessment," *IEEE Open Journal of the Communications Society*, vol. 1, pp. 501–512, 2020.

[9] Y. Miao, S. Pollin and A. A. Glazunov, "Simulation-based investigation on massive multi-antenna system as to spatial channel hardening for mobile single user in a controlled multipath environment," in *2020 14th European Conference on Antennas and Propagation (EuCAP)*, 2020, pp. 1–5.

[10] A. O. Martinez, E. De Carvalho and J. O. Nielsen, "Massive MIMO properties based on measured channels: Channel hardening, user decorrelation and channel sparsity," in *2016 50th Asilomar Conference on Signals, Systems and Computers*, IEEE, 2016, pp. 1804–1808.

[11] A. O. Martinez, J. O. Nielsen, E. De Carvalho and P. Popovski, "An experimental study of massive MIMO properties in 5G scenarios," *IEEE Transactions on Antennas and Propagation*, vol. 66, no. 12, pp. 7206–7215, 2018.

[12] G. Ghiaasi, J. Abraham, E. Eide and T. Ekman, "Effective channel hardening in an indoor multiband scenario," *International Journal of Wireless Information Networks*, 2019.

[13] Z. Chen and E. Björnson, "Channel hardening and favorable propagation in cell-free massive MIMO with stochastic geometry," *IEEE Transactions on Communications*, vol. 66, no. 11, pp. 5205–5219, 2018.

[14] E. Björnson and L. Sanguinetti, "Rayleigh fading modeling and channel hardening for reconfigurable intelligent surfaces," *IEEE Wireless Communications Letters*, vol. 10, no. 4, pp. 830–834, 2021.

[15] N. Mehrnia and S. Coleri, "Wireless channel modeling based on extreme value theory for ultra-reliable communications," *IEEE Transactions on Wireless Communications*, vol. 21, no. 2, pp. 1064–1076, 2022.

[16] P. C. F. Eggers, M. Angjelichinoski and P. Popovski, "Wireless channel modeling perspectives for ultra-reliable communications," *IEEE Transactions on Wireless Communications*, vol. 18, no. 4, pp. 2229–2243, 2019.

[17] M. Angjelichinoski, K. F. Trillingsgaard and P. Popovski, "A statistical learning approach to ultra-reliable low latency communication," *IEEE Transactions on Communications*, vol. 67, no. 7, pp. 5153–5166, 2019.

[18] J. Abraham and T. Ekman, "Local diversity and ultra-reliable antenna arrays," in *2021 55th Asilomar Conference on Signals, Systems, and Computers*, 2021, pp. 1215–1221.

[19] J. Abraham and T. Ekman, "Fading margins for large-scale antenna systems," in *ICC 2021 - IEEE International Conference on Communications*, 2021, pp. 1–5.

[20] T. Choi, P. Luo, A. Ramesh and A. F. Molisch, "Co-located vs distributed vs semi-distributed MIMO: Measurement-based evaluation," in *2020 54th Asilomar Conference on Signals, Systems, and Computers*, 2020, pp. 836–841.

[21] J. R. Pérez, s. Fernández, L. Valle, A. Bedoui, M. Et-tolba and R. P. Torres, "Experimental analysis of concentrated versus distributed massive mimo in an indoor cell at 3.5 GHz," *Electronics*, vol. 10, no. 14, 2021.

[22] S. Kumagai, T. Kobayashi, T. Oyama *et al.*, "Experimental trials of 5G ultra high-density distributed antenna systems," in *2019 IEEE 90th Vehicular Technology Conference (VTC2019-Fall)*, 2019, pp. 1–5.

[23] C.-M. Chen, Q. Wang, A. Gaber, A. P. Guevara and S. Pollin, "User scheduling and antenna topology in dense massive MIMO networks: An experimental study," *IEEE Transactions on Wireless Communications*, vol. 19, no. 9, pp. 6210–6223, 2020.

[24] S. Malkowsky, J. Vieira, L. Liu *et al.*, "The world's first real-time testbed for massive MIMO: Design, implementation, and validation," *IEEE Access*, vol. 5, pp. 9073–9088, 2017.

Paper IV

Massive MIMO goes sub-GHz: Implementation and experimental exploration for LPWANs

Low-Power Wide-Area Networks operating in the unlicensed bands are being deployed to connect a rapidly growing number of Internet-of-Things devices. While the unlicensed sub-GHz band offers favorable propagation for long-range connections, measurements show that the energy consumption of the nodes is still mostly dominated by the wireless transmission affecting their autonomy. We investigate the potential benefits of deploying massive MIMO technology to increase system reliability and at the same time support low-energy devices with good coverage at sub-GHz frequencies. The impact of different antenna configurations and propagation conditions is analyzed. Both actual average experienced array gain and channel hardening are examined. The assessment demonstrates the effect of channel hardening as well as the potential benefits of the experienced array gain. These measurements serve as a first assessment of the channel conditions of massive MIMO at sub-GHz frequencies and are, to the best of our knowledge, the first of its kind.

G. Callebaut, S. Gunnarsson, A. P. Guevara, F. Tufvesson, L. Van der Perre, A. J. Johansson,
"Massive MIMO goes sub-GHz: Implementation and experimental exploration for LPWANs,"
in *IEEE Proc. Asilomar-2020*, Pacific Grove, CA, USA, Nov. 2020.

I Introduction

The Internet-of-Things (IoT) is strongly growing. A variety of applications – each having its own requirements – are being deployed in a fast pace. Consequently, the number of IoT devices are increasing exponentially. Furthermore, a high number of all the applications demand that these devices are autonomous for a couple of years. Low-Power Wide-Area Networks (LPWANs) operating in the unlicensed sub-GHz spectrum are being deployed to connect these devices. However, the current LPWANs are unable to meet the new stringent requirements of a new wave of IoT demanding low-power, massive connectivity and high reliability.

Massive MIMO is a technology where a large number of antennas is used at the base station to serve multiple devices at the same time. By introducing more antennas, the reliability, coverage, energy-efficiency and the number of connected nodes can be enhanced in comparison to when using conventional single-antenna gateways. Hence, there is a potential benefit of using massive MIMO in the unlicensed sub-GHz spectrum to support the growth of IoT applications.

In order to validate the anticipated benefits of using massive MIMO for LPWANs, testbeds or other measurement equipment is required. In Table 1 an overview of current available massive MIMO testbeds operating at sub-6GHz is presented. In contrast to LPWAN applications, most of these testbeds are designed for high throughput. The trend is also to rather explore higher frequencies and therefore a lot of attention is given to designing equipment to operate in the mmWave, or even terahertz, bands. For instance, Facebook introduced Terragraph [1], which is operating at 60 GHz. Although some of the testbeds can operate at sub-GHz frequencies, massive MIMO measurements in this unlicensed band are still lacking and the actual benefit of deploying massive MIMO to support future LPWANs have until now remained unexplored.

To cover this gap, we extended a massive MIMO testbed to be narrowband, operate in the unlicensed sub-GHz band and designed a versatile antenna array. Secondly, we conducted the first sub-GHz massive MIMO measurement campaign to collect channels in an outdoor scenario with two different array configurations and made them available open-source [3]. An initial assessment of the radio propagation characteristics were studied, based on the average array gain and channel hardening, showcasing the potential gain of using massive MIMO to evolve current LPWANs in order to pave the way for the new wave of IoT.

The structure of this paper is as follows. In Section II the versatile antenna array is described, followed by a section elaborating on the implementations made in the framework and in the setup in order to comply to the regulations

[3] `dramco.be/massive-mimo/measurement-selector/#Sub-GHz`

Table 1: Overview of massive MIMO testbeds grouped by frequency band capability.

University/Company	Location	Number of antennas	Frequency range
Sub-GHz			
Eurecom (OAI) [2]	Sophia Antipolis, France	64	depends on RF platform
KU Leuven [3]	Leuven, Belgium	64	400 MHz to 4.4 GHz
Rice University (Argos) [4]	Houston, Texas, USA	64 (v1) 96 (v2) flexible (v3)	50 MHz to 3.8 GHz (v3)
Sub-6GHz			
Norwegian University of Science and Technology [5]	Trondheim, Norway	64	1.2 GHz to 6 GHz
University of Lund (LuMaMi) [6]	Lund, Sweden	100	1.2 GHz to 6 GHz
University of Bristol [7]	Bristol, UK	128	1.2 GHz to 6 GHz
Southeast university [8]	Nanjing, China	128	1.2 GHz to 6 GHz

in the unlicensed band. Section III presents the measurement scenario and Section IV shows the results from the experimental exploration. Finally, the conclusions are given.

II Versatile Large Array

A flexible patch antenna array was developed in-house and deployed at the base station side. The patch was designed for the unlicensed frequency band 865.00 MHz to 869.65 MHz. In this band, an $S_{1,1}$ lower than -10 dB was targeted. As can been seen from Figure 1, the $S_{1,1}$ is lower than -10 dB between 856.25 MHz to 874.25 MHz and is hence meeting the specifications. To lower the impact of mutual coupling between these antennas [9], patch antennas were preferred over dipoles. The radiation pattern of the patch antenna is shown in Fig. 2. The antenna has a gain of 5.9 dBi. Two patch antennas are contained in one antenna holder. The array is made up of antenna holders, where each holder has two patch antennas. The holders were designed to be modular such

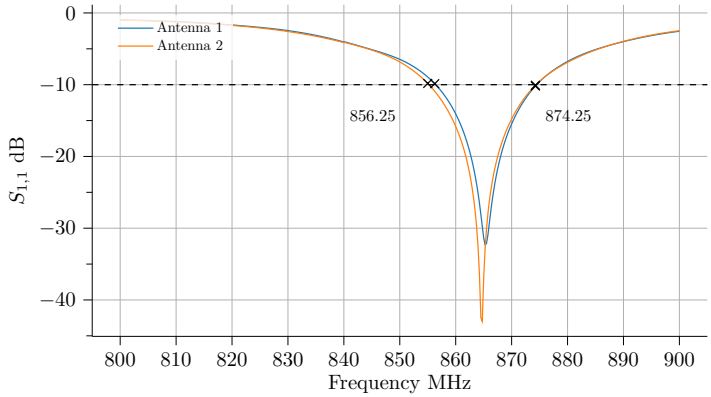

Figure 1: Measured $S_{1,1}$ parameters of two antennas in the same holder.

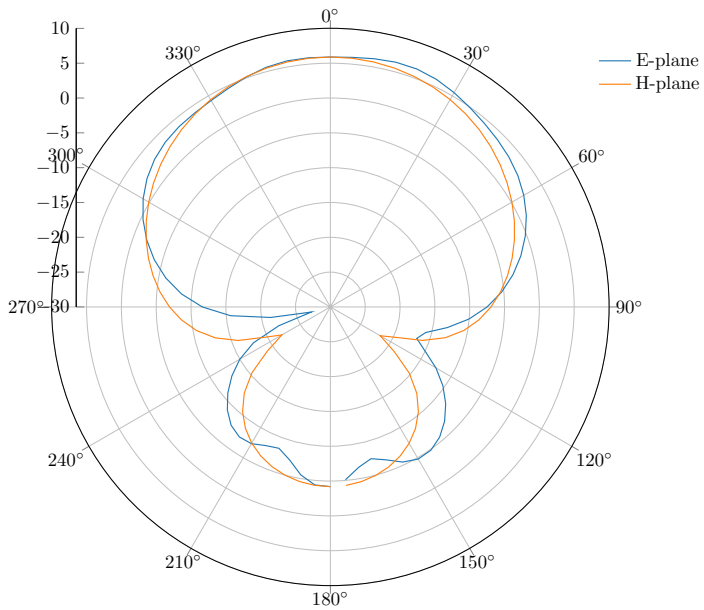

Figure 2: Simulated H- and E-plane of the patch antenna in dBi.

Figure 3: Multiple modular antenna holders connected.

that different configurations could be easily assembled[4]; the back side of these holders and how to connect them can be seen in Fig. 3. Furthermore, our design enforces that the antennas are always spaced by half a wavelength, independent of the the manner in which the holders are connected, i.e., vertically or horizontally. For the experiments we targeted a 32 antenna ULA but also a URA with the 32 antennas split in four rows of eightantennas each. These configurations are shown in Fig. 1. Due to the modular design of the antenna holders, many other configurations could be made including, but not limited to, cylindrical and distributed setups.

III Transmission in the Unlicensed Sub-GHz Band

In order to comply to the regulations of short-range devices (SRD860), the utilized frequency band, the transmit power, bandwidth and duty cycle of the existing massive MIMO framework needed to be adapted. An overview of these limitations are given in [10]. These restrictions apply to specific frequency bands and applications. The allowed bandwidth in the SRD band varies between 5 kHz and 5 MHz. In these bands a maximum transmit power and duty cycle are also specified. The duty cycle ranges from 0.1% (3.6 s per hour) to 10% (36 s per hour). The maximum transmit power is defined as the Effective Radiated Power (ERP). The ERP is the total power that would have been fed to a half-wave dipole to get the same radiation intensity as the actual device at the same distance and in the direction of the antenna's strongest beam. Hence,

[4] `dramco.be/massive-mimo/sub-ghz-array/animation.gif`

(a) 4 × 8 URA

(b) 32-element ULA

Figure 4: Antenna array configurations.

the ERP can be expressed as

$$\mathrm{ERP} = G_\mathrm{d}\, P_\mathrm{in} \quad , \tag{1}$$

where G_d is the gain of the actual antenna compated to a reference half-wave antenna and P_in the input power. The ERP is limited between 5 mW (7 dBm) and 2000 mW (33 dBm).

In this work, we use the SRD band 54[5]. The band is defined between 869.40 MHz and 869.65 MHz, and limits the ERP to 500 mW (27 dBm) and the duty cycle to 10%. We use a carrier frequency of 869.525 MHz.

Transmit Power. As the base station in this measurement setup is only acting as a receiver, the only transmit power that needs to be restricted is the one of the node. This is easily done in the interface of the original framework. The utilized USRP (NI USRP 2952) has a maximum transmit power of 20 dBm, thereby respecting the maximum allowable transmit power of 27 dBm as per SRD860.

Bandwidth. The bandwidth used for real-time operation of the testbed is 20 MHz. Orthogonal frequency-division multiplexing (OFDM) is used and as in LTE, 1200 subcarriers are used for carrying the data, which is further divided into 100 resource blocks and a subcarrier spacing of 15 kHz. To respect the regulations of having a bandwidth of maximum 250 kHz, this has to be reduced. Implementation-wise this was solved by transmitting zeros on all subcarriers

[5]European Union, Commission Decision of 9 November 2006 on harmonisation of the radio spectrum for use by short-range devices (2006). 2006/771/EC. Consolidated version of August 2017.

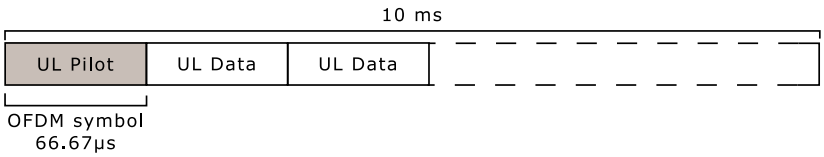

Figure 5: Modified time frame with three OFDM symbols per 10 ms slot.

except for the 13 subcarriers in the middle of the symbols, resulting in a total bandwidth of 195 kHz. This means that uplink pilots were transmitted at two subcarriers in an OFDM symbol and that one resource block of data was utilized.

Duty Cycle. The maximum duty cycle, i.e., transmit-to-silent ratio, depends on the radio frequency (RF) band. The duty cycle is computed as

$$\mathrm{DC}_{max} = \frac{\sum T_{on}}{T_{obs}} \ , \tag{2}$$

over a time window of one hour. In order to respect the duty cycle regulations, the frame structure had to be changed as well. The default frame structure is based on LTE with 10 subframes, each with two slots where each slot is containing seven OFDM symbols. For all experiments, the first OFDM symbol in the first slot was an uplink pilot. The two symbol following symbols were set to be transmitting uplink data, as in Fig. 5 where the first three symbols of the the first slot in the frame structure is shown. All other symbols were empty yielding a duty cycle of 2% ($3 \times 66.67\,\mu s/10\,ms$).

The framework featured Over-the-Air (OTA) synchronization. Due to the modification the original slots dedicated for synchronization were removed. Atomic clocks were instead used for syncing the base station and the mobile station. Therefore, the synchronization source in the framework needed to be changed from the local oscillator to the input clock reference where the atomic clock is connected.

IV Measurement campaign and Open-Source Data

The measurement campaign was performed in front of the Department of Electrical Engineering (ESAT) in Heverlee, Belgium. An overview of this environment can be seen in Fig. 3. The base station was equipped with either an ULA or an URA, as shown in Fig. 1a and 1b, and placed on the balcony of the building at a height of 7 meters. Meanwhile the node, seen in Fig. 7, was moving around along the paths that are also depicted on the map. Measure-

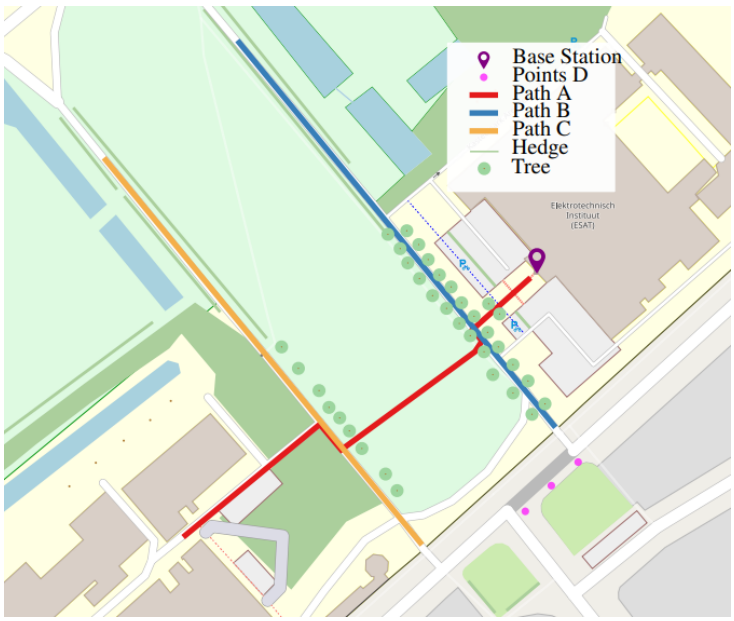

Figure 6: Overview of rural measurement area. All paths have each a total length of approximately 140 m.

ments were collected for all 32 antennas[6] at static points, spaced 10 meters apart, and continuously along the same paths. The chosen paths include positions both in Line-of-Sight (LoS) and non-LoS (NLoS) and also paths that are either perpendicular or parallel to the base station antenna array. The details of the measurement setup can be found in Table 1 and the measurements are available open-source[3].

V Experimental Exploration

In this section a first assessment of the channel conditions of measured massive MIMO at sub-GHz frequencies is presented. The antenna elements are numbered from right to left and from the bottom to the top. A first look of what the average received channel gain for the different antennas can look like for an ULA and an URA in both LoS and NLoS is shown in Fig. 8. The channel gain per antenna at position k is averaged over time and frequency as in

$$\frac{1}{NF}\sum^{N,F}|\mathbf{h}_{k,m}(n,f)|^2 \ , \tag{3}$$

[6]Due to an unexpected issue, only the first 31 channels could be used.

Figure 7: Transmit node.

Table 2: Measurement setup

Parameter	Symbol	Value
Carrier frequency	f_c	869.525 MHz
Number of subcarriers (15 kHz)	F	2
Number of snapshots	N	1000[a]/6000[b]
Transmit power (coerced)	P_{tx}	22.6 dBm
Number of base station antennas	M	32
Number of nodes	K	1
Base station Array configuration		ULA/URA
Type of BS antenna		Patch
Type of UE antenna		Dipole
Sample interval		10 ms
Sample duration		66.67 µs
Measurement duration		10s/60s
Subcarrier modulation		QPSK
BS height		7 m
UE height		1.5 m
Antenna polarization		vertical

[a] For static measurements.
[b] For continuous measurements.

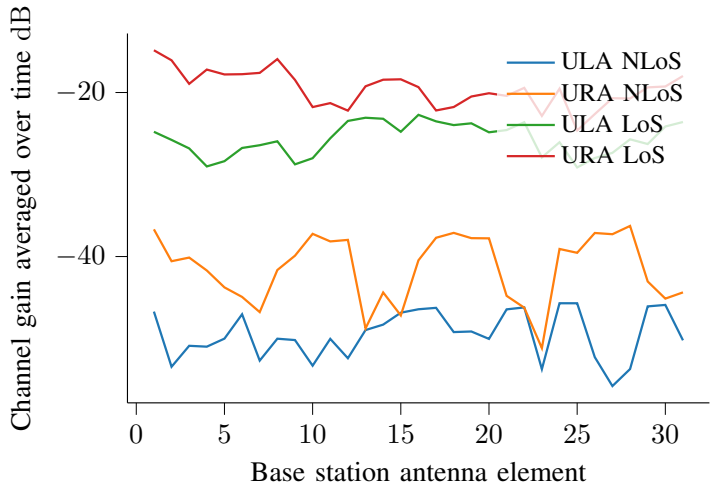

Figure 8: The average channel gain per antenna for the two array configurations in LoS and NLoS. The antenna elements are numbered from right to left and from the bottom to the top.

where $\mathbf{h}_{k,m}(n, f)$ is the channel vector measured at position k at snapshot n, frequency f and at antenna m. By averaging the channel gain over time and frequency, the small-scale effect is averaged out and thus Fig. 8 depicts the large-scale fading coefficient per antenna. The differences between these large-scale fading coefficients per antenna illustrate the large-scale fading over the array. The LoS and NLoS points are chosen as one static point in the beginning of path A, close to the base station array, and one static point 100 meters away along the same path, respectively. Due to the different path losses, the NLoS curves will naturally be lower than the LoS ones. Another difference that can be observed is that for the LoS cases the average channel gain is more similar for the different antennas in both arrays while in NLoS a more prominent large-scale fading effect can be observed over the array; this is especially clear for the URA where four dips of channel gain can be observed – one for each row in the array. Furthermore, the variation of channel gain per antenna is also larger for the NLoS points. The difference between the standard deviation of channell gain per antenna for the ULA between the LoS and NLoS scenario is 1 dB and the corresponding value for the URA is 1.8 dB. The URA experiences a 1.1 dB higher standard deviation than the ULA in the NLoS scenario. Finally, one last observation from Fig. 8 is that the URA in general has a higher average channel gain than the ULA.

One advantage with massive MIMO is the array gain resulting from combining the many antennas, resulting in a potential transmit power reduction at the node side. Moreover, as the number of base station antennas M increases, the

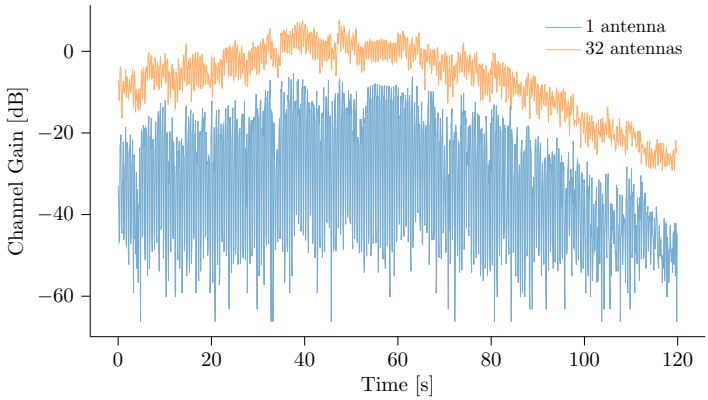

Figure 9: Channel gain over time (along path B) for 1 and 32 base station antennas in the ULA, respectively.

variation of channel gain decreases; this phenomena is called channel hardening and makes a fading channel behave more deterministic. We adopt the definition given in [11], stating that a channel $\mathbf{h}_k$ offers channel hardening when the number of base station antennas M goes to infinity if

$$\frac{\mathbb{V}\left\{\|\mathbf{h}_k\|^2\right\}}{\mathbb{E}\left\{\|\mathbf{h}_k\|^2\right\}^2} \to 0, \qquad \text{as} \;\; M \to \infty, \tag{4}$$

where $\mathbb{V}\{.\}$ is the variance, $\mathbb{E}\{.\}$ the expectation and $\|.\|$ is the Euclidean norm. Both the array gain and the channel hardening can be observed in the experimental results depicted in Fig. 9 where the lower curve corresponds to one antenna and the upper curve is when combining all antennas for the ULA along the continuous path B measurement. Due to the array gain, the latter is moved up and the channel hardening effect can be seen as the variations of channel gain becoming insignificant in comparison to the one antenna case. Both the increased received gain and the smaller fading margin required can reduce the transmit power needed at the node side.

VI Conclusions

In this work, we have presented an experimental setup and the first measurement campaign using massive MIMO at sub-GHz frequencies and made the data available open-source. Our initial assessment shows the potential benefits of using massive MIMO for connecting remote energy-constrained devices. Due to the presence of channel hardening, the reliability of the link can be increased. In addition, the array gain allows to decrease the transmit power of the devices,

or to extend the coverage. The impact of using an ULA in comparison to an URA in LoS and NLoS conditions is investigated. Our study demonstrates the feasibility of using massive MIMO at sub-GHz frequencies to support future LPWANs. These measurements enable further investigation of, e.g., precoding and scheduling algorithms for IoT devices.

Acknowledgment

We would like to thank Vladimir Volski for designing the patch antenna and our colleagues in Dramco for assisting us during the experiments.

References

[1] N. Choubey and A. Panah, "Introducing Facebook's new terrestrial connectivity systems-Terragraph and Project ARIES," *Facebook Research*, 2016.

[2] X. Jiang and F. Kaltenberger, "Demo: an LTE Compatible Massive MIMO Testbed based on OpenAirInterface," in *WSA 2017; 21th International ITG Workshop on Smart Antennas*, 2017, pp. 1–2.

[3] A. O. Martinez, J. Ø. Nielsen, E. De Carvalho and P. Popovski, "An experimental study of massive MIMO properties in 5G scenarios," *IEEE Transactions on Antennas and Propagation*, vol. 66, no. 12, pp. 7206–7215, 2018.

[4] C. W. Shepard, R. Doost-Mohammady, R. E. Guerra and L. Zhong, "ArgosV3: An Efficient Many-Antenna Platform," in *Proceedings of the 23rd Annual International Conference on Mobile Computing and Networking*, 2017, pp. 501–503.

[5] G. Ghiaasi, J. Abraham, E. Eide and T. Ekman, "Effective Channel Hardening in an Indoor Multiband Scenario," *International Journal of Wireless Information Networks*, vol. 26, Jul. 2019.

[6] S. Malkowsky, J. Vieira, L. Liu *et al.*, "The World's First Real-Time Testbed for Massive MIMO: Design, Implementation, and Validation," *IEEE Access*, vol. 5, pp. 9073–9088, 2017.

[7] P. Harris, S. Zang, A. Nix, M. Beach, S. Armour and A. Doufexi, "A Distributed Massive MIMO Testbed to Assess Real-World Performance and Feasibility," in *2015 IEEE 81st Vehicular Technology Conference (VTC Spring)*, 2015, pp. 1–2.

[8] X. Yang, W. Lu, N. Wang *et al.*, "Design and implementation of a TDD-based 128-antenna massive MIMO prototype system," *China Communications*, vol. 14, no. 12, pp. 162–187, 2017.

[9] C. Chen, V. Volski, L. Van der Perre, G. A. E. Vandenbosch and S. Pollin, "Finite Large Antenna Arrays for Massive MIMO: Characterization and System Impact," *IEEE Transactions on Antennas and Propagation*, vol. 65, no. 12, pp. 6712–6720, 2017.

[10] M. Saelens, J. Hoebeke, A. Shahid and E. De Poorter, "Impact of EU duty cycle and transmission power limitations for sub-GHz LPWAN SRDs: an overview and future challenges," eng, *EURASIP JOURNAL ON WIRELESS COMMUNICATIONS AND NETWORKING*, vol. 2019, no. 1, 219:1–219:32, 2019.

[11] H. Q. Ngo and E. G. Larsson, "No downlink pilots are needed in TDD massive MIMO," *IEEE Trans Wireless Commun*, vol. 16, no. 5, pp. 2921–2935, 2017.

Paper V

Experimental exploration of unlicensed sub-GHz massive MIMO for massive Internet-of-Things

Due to the increase of Internet-of-Things (IoT) devices, IoT networks are getting overcrowded. Networks can be extended with more gateways, increasing the number of supported devices. However, as investigated in this work, massive MIMO has the potential to increase the number of simultaneous connections, while also lowering the energy expenditure of these devices. We present a study of the channel characteristics of massive MIMO in the unlicensed sub-GHz band. The goal is to support IoT applications with strict requirements in terms of number of devices, power consumption, and reliability. The assessment is based on experimental measurements using both a uniform linear and a rectangular array. Our study demonstrates and validates the advantages of deploying massive MIMO gateways to serve IoT nodes. While the results are general, here we specifically focus on static nodes. The array gain and channel hardening effect yield opportunities to lower the transmit-power of IoT nodes while also increasing reliability. The exploration confirms that exploiting large arrays brings great opportunities to connect a massive number of IoT devices by separating the nodes in the spatial domain. In addition, we give an outlook on how static IoT nodes could be scheduled based on partial channel state information.

G. Callebaut, S. Gunnarsson, A. P. Guevara, A. J. Johansson, L. Van der Perre, F. Tufvesson,
"Experimental exploration of unlicensed sub-GHz massive MIMO for massive Internet-of-Things,"
in *IEEE Open Journal of the Communications Society*, vol. 2, pp. 2195-2204, Sep. 2021.

I Towards massive and reliable IoT: the potential of multiple antenna systems

Internet-of-Things technology opens up a plethora of new applications and services in various domains. Examples include smart sustainable city services, precision farming, environmental monitoring and efficient utilities. These applications pose requirements on the wireless connectivity beyond what is offered by current networks. In particular, (i) the projected massive number of devices to be supported, (ii) the stringent energy constraints of many of the transmitting nodes, and (iii) the need to establish reliable connections ask for innovative wireless transmission approaches. Low-Power Wide-Area Networks (LPWANs) operating in unlicensed sub-GHz spectrum are of interest to many IoT applications. They incur no or only a small subscription cost, and the operation at relatively low frequencies offers good coverage [1]. In this paper we study the potential of deploying multiple antenna systems to upgrade these LPWANs to support future IoT services. We focus in particular on massive multiple-input and multiple-output (MIMO) technology as it bears a great potential in view of the above listed requirements:

1. It can support an unprecedented number of simultaneous connections through extensive spatial multiplexing.

2. It typically operates with low complexity single antenna terminals. It allows to considerably reduce the transmit power at the node side thanks to the significant array gain at the base station side.

3. It offers an increased reliability of the links due to the experienced channel hardening effect.

New approaches and technologies need to be adopted to accommodate the massive increase of IoT devices. In [2], the authors use a maximum-likelihood strategy to decode two colliding users based on an interference model. This technique further extends the amount of supported devices in the network. Other work has considered diversity techniques to improve IoT technologies. In [3] Snipe is introduced, which is an IoT system deploying two antennas to coherently combine the received signals at the gateway. Spatial diversity is exploited in [4] by coherently combining weak signals of different gateways in the cloud. The system, Charm, improves the range up to three times and the IoT battery-life fourfold. Including multiple antennas at the gateway is also proposed by [5], where this is theoretically analyzed. However, the authors consider only commercially available hardware and are therefore unable to use maximum ratio combining and are hence rather analyzing a selection combing technique.

(a) 32-element ULA

(b) 4 × 8 URA

Figure 1: Antenna array configurations.

The potential benefits of massive MIMO for IoT have been studied in theoretical work such as [6]–[12]. Yet, whether this potential can be realized in real network deployments heavily relies on favorable characteristics of the radio propagation channels [13], [14]. In particular, many studies have assumed independent and identically distributed (i.i.d.) Rayleigh fading channels [5], [7], [12]. Measurement-based studies have shown that the reality deviates from this [15]–[17] and for example significant correlation is often observed over the antennas in the array [16]. Consequently, the channel hardening encountered is less pronounced than predicted by the Rayleigh fading model [15]. Furthermore, different array topologies have been considered as they each favor different environments. For example, in [18] it is demonstrated that an L-structured array outperforms both the uniform linear array (ULA) and the uniform rectangular array (URA) configuration. Hence, they advocate to also consider unconventional array structures.

Previous work has primarily focused on broadband transmission technologies [12], [19]–[22]. As a novel contribution, we study unlicensed narrowband low-power and long-range communication. Unlicensed massive MIMO has been studied in other work in the context of spectrum sharing [23]. However, to the best of our knowledge, no studies have reported on massive MIMO to support LPWANs.

While the results are generally applicable, we here focus on communication tailored for IoT. This means that (i) a narrowband signal is used, (ii) the carrier frequency is sub-GHz, (iii) the number of gateway antennas are more limited than in cellular networks and (iv) the nodes can be considered static. As such,

we consider 32 antenna elements and no movement of the devices.

Whereas commonly the single-antenna device is denoted as the user equipment (UE) in a massive MIMO or Long-Term Evolution (LTE) context, in an Internet-of-Things setting the term *node* or *IoT node* is used. As we study the effects of massive MIMO in an Internet-of-Things setting, we use the term node to depict the end-device or single-antenna device.

In this paper, we assess the potential of deploying massive MIMO in the unlicensed sub-GHz band for upgraded IoT connectivity based on the measured channel responses. Thereto, we report on the experimental characterization of narrowband sub-GHz channels with different array configurations. The architecture and implementation of the experimental test set-up is further elaborated on in [24]. More specifically, the antenna design and holders, the limitations of operating in a license-exempt band and how it is implemented is discussed. Furthermore, the experimental campaign is elaborated on and the raw open-source data is referenced. Some first results are shown to evaluate the experiment.

To summarize, our contributions reported on here are (i) an analysis of channel propagation characteristics for large antenna array systems[7]. We demonstrate – based on the measurements – that the reliability and the number of simultaneous connections can be increased. Furthermore, the array gain can extend the coverage of the base station or allows to reduce the transmit power of the IoT devices. Despite the benefits, some challenges remain such as relatively large antennas and arrays and sporadic traffic that may result in a large overhead, requiring a new set of massive MIMO-specific protocols.

This paper is further organized as follows. In the next section, we introduce the system model and theoretic fundamentals. Section III introduces the measurement setup and scenarios. In Section IV, we present the exploration and assessment performed based on the experiments. Finally, in Section V the main conclusions of this paper are summarized and an outlook on future progress towards massive MIMO-upgraded networks for future IoT is given.

Throughout the paper, vectors are denoted by boldface lower case ($\mathbf{x}$) and matrices by boldface capital letters ($\mathbf{X}$). The superscripts $(\cdot)^{\mathsf{T}}$ and $(\cdot)^{H}$ are used to denote the transpose and the conjugate transpose operations, respectively. The absolute value is denoted by $|\cdot|$, $\|\cdot\|$ denotes the ℓ_2 norm and $\|\cdot\|_F$ is the Frobenius norm or Euclidian norm. The notations $\mathbb{E}\{\cdot\}$ and $\mathbb{V}\{\cdot\}$ denote the expectation and the variance of a random variable, respectively. An overline, e.g. $\bar{\mathbf{x}}$, indicates a normalized quantity. The eigenvalues of a matrix are obtained by the operator $\lambda(\cdot)$. The optional subscripts $(\cdot)_{\min}$ and $(\cdot)_{\max}$ are used to get the minimum and maximum value. The set of complex numbers is denoted by the symbol $\mathbb{C}$.

[7]The collected data is available at: `dramco.be/massive-mimo/measurement-selector/#Sub-GHz`. and (ii) an assessment of massive MIMO opportunities and challenges for IoT

Table 1: Measurement Setup

Parameter	Symbol	Value
Carrier frequency	f_c	869.525 MHz
Number of subcarriers (15 kHz)	F	2
Number of snapshots	N	1000[a]/6000[b]
Transmit power (coerced)	P_{tx}	22.6 dBm
Number of base station antennas	M	32
Number of IoT nodes	K	-
Base station array configuration		ULA/URA
Type of BS antenna		Patch
Type of UE antenna		Dipole
Sample interval		10 ms
Sample duration		66.67 µs
Modulation		OFDM
Subcarrier modulation		QPSK
UE height		1.5 m
BS height		7 m
Antenna polarization		vertical

[a] For static measurements.
[b] For continuous measurements.

II System Model and Theoretic Fundamentals

Channels. The channels are estimated for each base station (BS) antenna at different node positions and for different frequency points and time instances. An overview of the system parameters and used symbols can be found in Table 1. The total number of antennas is denoted by M. The subscript m specifies the antenna index. The total number of node positions is denoted by K and a given position index by k. As elaborated in [24], the channel is estimated over two frequency points F at different time instances N, with f and n denoting the frequency point and time instance index, respectively. Consequently, a channel matrix for a position k is expressed as $\mathbf{H}_k \in \mathbb{C}^{N\times F\times M}$. Note that the collected channel includes both small-scale and large-scale fading, as well as potential effects from the hardware and interfering devices. As a baseline to compare our results, we use the i.i.d. complex Gaussian channel, i.e., Rayleigh fading channel, as commonly used in theoretical studies. This is modeled as a complex random variable with zero mean and unit variance of power ($h \sim \mathcal{CN}(0,1)$).

Channel Estimation. The channel is estimated by sending a unique pilot signal from each single-antenna device to the base station. Each device sends a pilot signal at a dedicated frequency, i.e., during the pilot phase all devices

use distinct frequencies. The BS can estimate the channel response for each device at a specific location k based on the *a priori* known pilot sequence. The estimated channel is derived by correlating the complex conjugate of the pilot $\boldsymbol{\phi}$ with the received uplink signal $\mathbf{y}$:

$$\hat{\mathbf{h}}_k = \mathbf{y}\boldsymbol{\phi}^H \ . \tag{1}$$

The vector $\hat{\mathbf{h}}_k \sim \mathbb{C}^M$ denotes the estimated channel response between the M antennas and the single-antenna device at position k. For further analysis and readability, we will be using the vector $\mathbf{h}$ to denote the estimated noisy channel $\hat{\mathbf{h}}$.

Normalization. The channel $\mathbf{h}_k(n, f)$ at each position k is normalized such that the average channel gain over all antennas, frequencies and snapshots is equal to one, i.e., $\left\|\bar{\mathbf{h}}_k\right\| = 1$, i.e.

$$\bar{\mathbf{h}}_k(n, f) = \frac{\mathbf{h}_k(n, f)}{\sqrt{\frac{1}{NFM}\sum_{n=1}^{N}\sum_{f=1}^{F}\sum_{m=1}^{M}\left|h_{k,m}\left(n, f\right)\right|^2}}. \tag{2}$$

Channel hardening. We assess the channel hardening as a representative characteristics for the decrease of the fading with increasing number of antennas, by which the channel becomes more deterministic and the reliability of the link improves. According to [25], a channel $\bar{\mathbf{h}}_k$ experiences more channel hardening if

$$\frac{\mathbb{V}\left\{\|\bar{\mathbf{h}}_k\|^2\right\}}{\mathbb{E}\left\{\|\bar{\mathbf{h}}_k\|^2\right\}^2} \to 0, \quad \text{as } M \to \infty, \tag{3}$$

where the variance and expectation is taken over the frequency and time dimensions for a given position k. This means that as the number of antennas increases, the variation of channel gain decreases. Here, the standard deviation is considered, as is also done in [15]. This means that, for a subset of M base station antennas and each position k, the instantaneous channel gain, as dependent on time and frequency, is defined as

$$\overline{G}_k(n, f) = \frac{1}{M}\sum_{m=1}^{M}|\overline{h}_{k,m}(n, f)|^2, \tag{4}$$

resulting in an average channel gain for each position of

$$\mu_k = \frac{1}{NF}\sum_{n=1}^{N}\sum_{f=1}^{F}\overline{G}_k(n, f) = 1, \tag{5}$$

which no longer depends on the number of antennas at the base station as

we averaged with respect to all antennas M and will be equal to 1 due to the normalization. Note, a distinction is made between the channel gain and the array gain. The channel gain is the squared absolute value of the channel coefficient. In contrast, an array gain is here the sum of the channel gains of each antenna relative to the channel gain of a single antenna case. The array gain implies an additional gain of having multiple antennas, i.e., an array.

Finally, the standard deviation of the channel gain at a given position k can be computed as

$$\sigma_k = \sqrt{\frac{1}{NF}\sum_{n=1}^{N}\sum_{f=1}^{F}|\overline{G}_k(n,f) - \mu_k|^2}, \tag{6}$$

which is used to quantify the channel hardening by taking the difference between the complete set of base station antennas and one base station antenna.

Correlation coefficient. To compare the channel correlation between different channel pairs, the correlation coefficient[8] is studied. It is defined between two channel vectors $\mathbf{h}_i$ and $\mathbf{h}_j$ as

$$\delta_{i,j}(n,f) = \frac{\left|\bar{\mathbf{h}}_i(n,f)^H \cdot \bar{\mathbf{h}}_j(n,f)\right|}{\left\|\bar{\mathbf{h}}_i(n,f)\right\| \left\|\bar{\mathbf{h}}_j(n,f)\right\|}, \tag{7}$$

where the channels are normalized according to (2). The correlation coefficient is estimated by picking two random measurement locations (i and j). From these locations, we select one random snapshot (n) and frequency point (f) and use these channel vectors to compute the correlation coefficient. The correlation coefficient depicts the antenna-averaged channel correlation between two channel instances. In case of uncorrelated channels, the coefficient is zero, while the coefficient is one for channels which are parallel, i.e., equal up to a scaling factor.

Channel correlation. The channel correlation matrix per position is obtained as the mean over N snapshots of the user channel and its transposed channel conjugate for the same number of samples.

$$\mathbf{R} = \frac{1}{NF}\sum_{n=1}^{N}\sum_{f=1}^{F}\bar{\mathbf{h}}(n,f)\bar{\mathbf{h}}^H(n,f), \tag{8}$$

where $\mathbf{R} \in \mathbb{C}^{M\times M}$. It expresses the correlation between the channels observed by each antenna.

[8] To be complete, the correlation coefficient here defined is not the same as the correlation coefficient usually used in statistics.

The condition number. The joint orthogonality of multiple positions, or channels, is investigated by using the condition number [26], [27]. It is defined as

$$\kappa_{K,M}(n,f) = \frac{\lambda_{\max}(\bar{\mathbf{H}}(n,f)^H \bar{\mathbf{H}}(n,f))}{\lambda_{\min}(\bar{\mathbf{H}}(n,f)^H \bar{\mathbf{H}}(n,f))}, \tag{9}$$

with $\kappa_{K,M} \in [1,\infty)$, for M antennas and K users. The channel matrix $\bar{\mathbf{H}}(n,f)$ consists of the normalized channel instances of K positions $[\bar{\mathbf{h}}_1(n,f)\dots\bar{\mathbf{h}}_K(n,f)] \in \mathbb{C}^{M\times K}$. A high condition number means that at least one pair of channels is strongly correlated. When all channels are pairwise orthogonal, the condition number becomes one. The inverse condition number is chosen as a metric to be able to express the orthogonality in a finite range, i.e., $\kappa_{K,M}^{-1} \in [0,1]$.

Chordal distance. The chordal distance measures the orthogonality between two eigenspaces, represented as the p-dominant eigenvectors. By definition [28], the chordal distance between two matrices $\mathbf{U}_i$ and $\mathbf{U}_j$ is given by

$$d_c(\mathbf{U}_i,\mathbf{U}_j) = \left\| \mathbf{U}_i\mathbf{U}_i^H - \mathbf{U}_j\mathbf{U}_j^H \right\|_F^2, \tag{10}$$

where $\mathbf{U}_i \in \mathbb{C}^{M\times p}$ and $\mathbf{U}_j \in \mathbb{C}^{M\times p}$ are the unitary matrices that span over the number of antennas M and p-dominant eigendirections. The unitary matrices are obtained in the eigenvalue decomposition from the Hermitian matrix $\mathbf{R}$ as follows: $\mathbf{R} = \mathbf{U}\mathbf{D}\mathbf{U}^H$. Note that in order to estimate the chordal distance it is important to obtain the p-dominant eigendirections in advance.

III Measurement Setup and Scenario

The 5G massive MIMO testbed at KU Leuven[9] based on National Instruments equipment was used during these experiments. The testbed runs the LabVIEW Communications MIMO Application. This application was designed for LTE-TDD based transmission. Therefore, the LabView application had to be adapted to conform to the regulations of [29]. To be precise, the occupied bandwidth, the transmit power and duty cycle of the framework had to be altered. This is elaborated on in [24]. Table 1 summarizes the measurement setup.

The base station is, as mentioned before, equipped with 32 vertically polarized patch antennas. Two array configurations were used, a 4-by-8 URA (Fig. 1b) and a 32-element ULA (Fig. 1a). The patch antenna was designed to operate in the 868 MHz band. In theoretical massive MIMO papers a 32-element array may be considered relatively small, yet in absolute terms at

[9] `https://www.esat.kuleuven.be/telemic/research/NetworkedSystems/infrastructure/massive-mimo-5g`

Figure 2: Transmit node with a single dipole antenna.

this operation frequency the array is definitely quite large, i.e., 5.5 m for a 32-element ULA at 868 MHz or with a wavelength of 34.5 cm. The array consists of two-element holders. These holders facilitate the design of different array topologies. While in this measurement we use a rectangular and a linear uniformal array, cylindrical and distributed arrays can be easily constructed with this design. At the node side, a single dipole antenna is used (Fig. 2).

The measurements were conducted in front of the Department of Electrical Engineering (ESAT) building in Heverlee, Belgium. The measurement environment can be seen in Fig. 3. The base station was placed on the balcony at the first floor of the building at a height of 7 m.

During the experimental campaign, we collected the channels on all 32 antennas for static and continuous measurements. Between each static measurement position we moved the transmit antenna (node) 10 meters according to the paths shown in Fig. 3. The paths were chosen in order to have positions perpendicular and parallel to the base station, as well as having NLoS and LoS positions. As the measurements were done in summer, the presence of foliage on the trees has a non-negligible effect on the collected channels. Both the measurement data[10] and the processing scripts[11] are available in open-source.

When comparing LoS and NLoS scenarios, we use two static points per case. The locations of the measurement points are shown in Fig. 4 and further used in Section IV to study the effect of LoS and NLoS scenarios.

[10] `dramco.be/massive-mimo/measurement-selector/#Sub-GHz`
[11] `github.com/GillesC/MARRMOT`

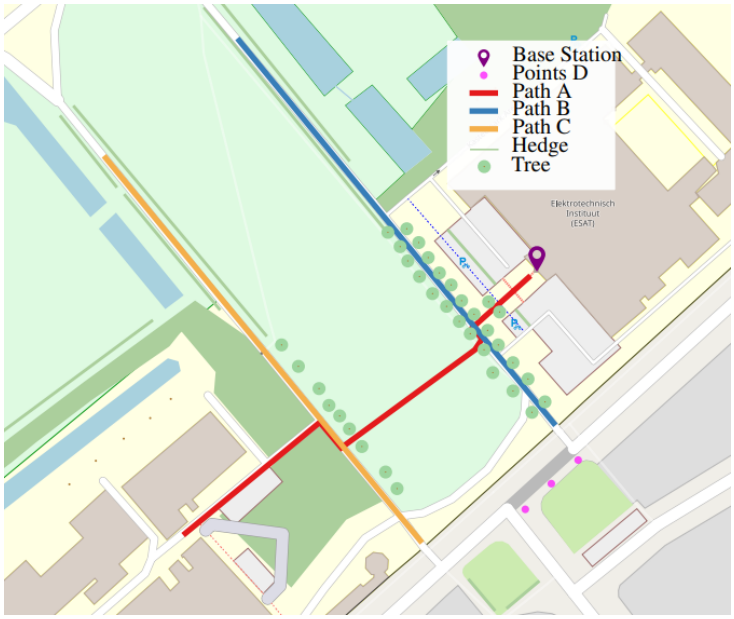

Figure 3: Overview of rural measurement area. All paths have a length of approximately 140 m.

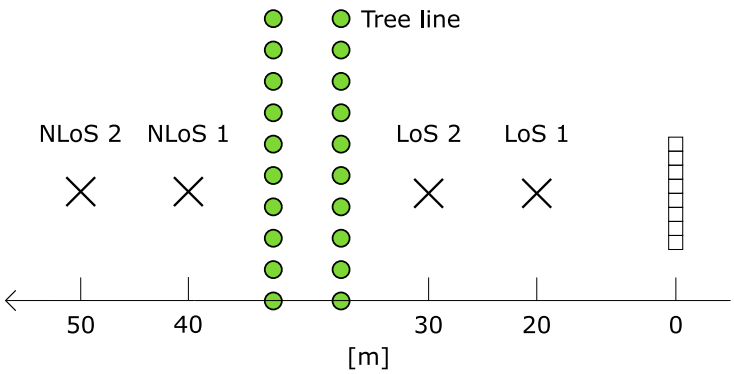

Figure 4: Points considered to be LoS and NLoS including distances (in m) with respect to the base station.

Figure 5: Antenna numbering with 8 randomly selected subsequent antenna elements (highlighted).

IV Evaluation

We here evaluate different performance metrics, grouped based on their impact on crucial aspects for IoT communication. Section A explores the benefits of massive MIMO regarding the reliability, coverage and energy efficiency of the IoT nodes. The ability to serve multiple nodes and a first look on how to schedule them is studied in Sections B and C.

When investigating the impact of the number of base station antennas, we selected M_s subsequent array elements according to their numbering. In the case of a ULA this always results in a ULA of M_s antenna elements, this in contrast to selecting random antenna elements. The same reasoning does not always hold for the URA configuration. An example where this does not hold is shown in Fig. 5. Consequently, the results of the URA configuration, with respect to the number of antennas, needs to be carefully interpreted. To be able to capture small-scale fading, while still have a negligible effect of the large-scale fading, we divided the continuous measurements in paths with a length of approximately $25\,\lambda$.

A Increased Energy Efficiency, Coverage and Reliability

The reliability, coverage and energy efficiency improvement are assessed by means of the channel gain diversity, combining gain and channel hardening effect. The combining gain allows reducing the transmit power of the nodes thanks to the increased gain when combining the many base station antennas. Equivalently, the coverage can be extended by the achieved combined gain. Furthermore, when a channel offers channel hardening, the variance of the channel gain decreases as the number of antennas increases, hence providing a more reliable channel. As a result, the fading margin at the IoT node can also be reduced. As the channel becomes more deterministic, the probability of packet losses decreases, and thereby the number of required retransmissions is reduced.

Channel Gain Diversity over the Array. In [16], it was observed that antenna arrays with a large aperture experience antenna-dependent large-scale fading. In this work, we have observed similar behavior even with a low number of antennas. Notably, the physical aperture of the array is larger for 868 MHz than 2.6 GHz as in [16]. The un-normalized average channel gain, summed over frequency and per base station antenna, is depicted in Fig. 6 for the two array configurations and a LoS and NLoS scenario respectively. By averaging the channel gain over time for each antenna element, we take away the small-scale fading present on each antenna. Fig. 6 shows that the large-scale fading can not be considered constant over the antennas as is frequently assumed in theoretical work [12]. Depending on the position of the antenna in the array, it can be shadowed or see different multi-path components; this naturally becomes

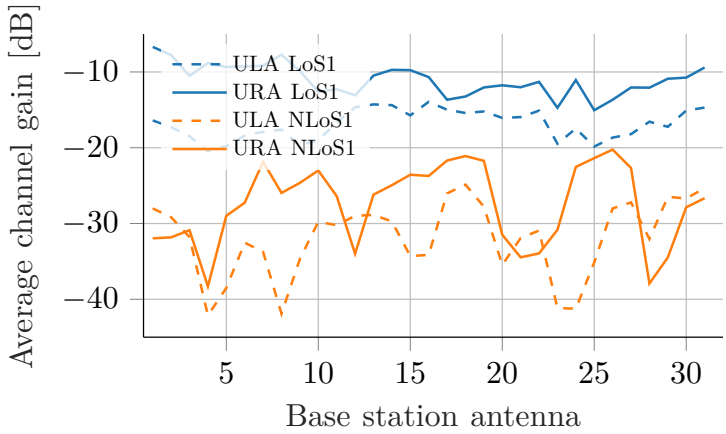

Figure 6: The average (over time) channel gain per antenna element demonstrates the presence of varying large-scale fading over the antennas. The antenna numbering is according to Fig. 5.

even more noticeable in the NLoS scenario for both array configurations. The average observed difference between the maximum and minimum channel coefficients between two antennas during one measurement is 15.4 dB and 13.2 dB for the ULA and URA, respectively. Depending on the location of the node and how the multi-path components travel in the environment, the antennas at the base station will hence not contribute equally to the overall received signal. Fig. 7 illustrates this by showing the average channel gain for all base station antennas and all measured points. The considerable differences demonstrate that spatial diversity can significantly improve the link reliability. It can also be noted that at some points, a specific antenna can be in a fading dip while being one of the strongest antennas at other points.

Channel Hardening. When increasing the number of antennas, the channel hardening effect appears. For a Rayleigh fading channel, the channel hardening becomes $10\log_{10}(\sqrt{M})$ when using the standard deviation for comparison as in (6). The channel hardening is here measured as the difference of the standard deviation of the channel gain when going from 1 to M antennas, i.e., 7.5 dB with 31 antennas. A comparison between i.i.d. Rayleigh fading and the measured channel with the ULA and the URA is shown in Fig. 8. Here, the average standard deviation of channel gain of a time window of size 600 for an increasing number of antennas is depicted, extracted from the continuous measurements along path B and C in Fig. 3. The antennas are chosen in the order that is outlined in Fig. 5.

In Fig. 8, a clear channel hardening effect can be seen as the standard deviation of channel gain decreases when the number of base station antennas

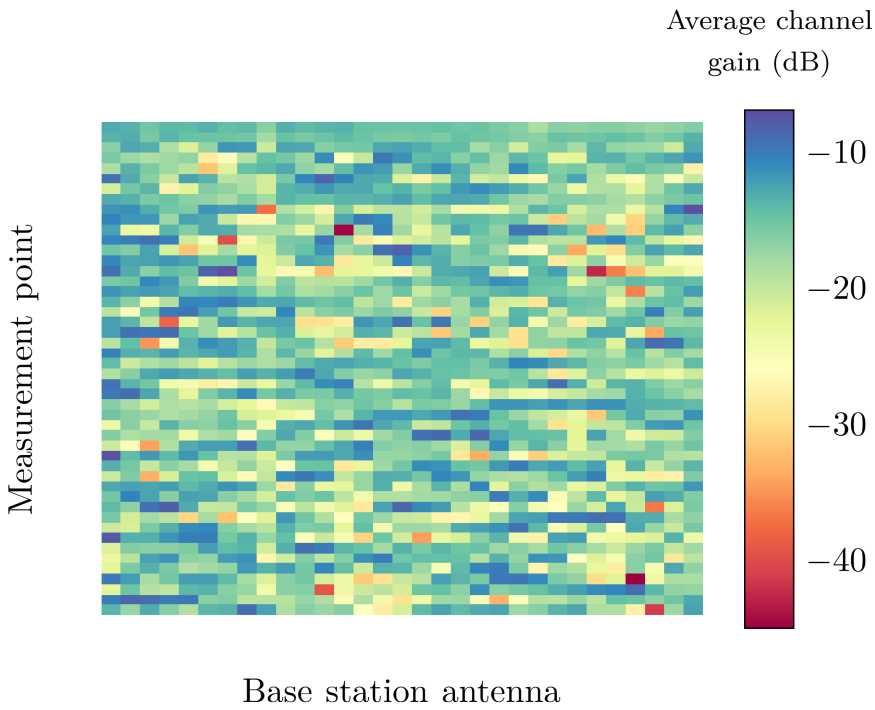

Figure 7: Average channel gain per base station antenna (ULA). Each row depicts the average channel gain per measurement point for each antenna element.

increases. In the beginning the URA has a lower standard deviation than the ULA until eight antennas where it saturates and is then bypassed by the ULA. For the ULA the average channel hardening is 3.2 dB and for the URA it is 2.3 dB. The reason for more channel hardening with the ULA is most likely due to better possibilities of exploiting the spatial diversity while adding more rows to the URA does not contribute as much. The channel hardening effect allows to reduce the fading margins and therefore the overall transmit power as well.

B Serving Multiple Nodes

The channel orthogonality is assessed by means of the correlation coefficient and the inverse condition number of channels captured at different measurement locations. The former describes the orthogonality of two nodes, while the latter shows the joint channel orthogonality of multiple nodes. Both metrics are evaluated with respect to the number of base station antennas. We consider on average 300 locations per antenna configuration. The actual static locations

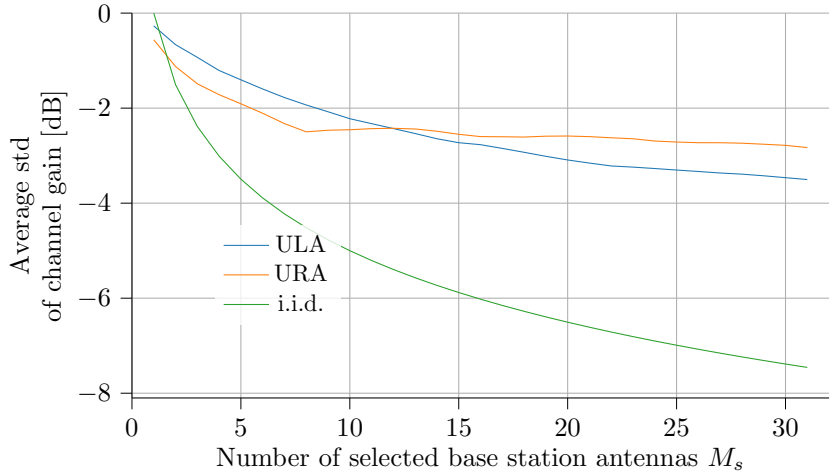

Figure 8: Average standard deviation of channel gain (6) when increasing the number of antennas for the ULA and URA.

were extended with virtual locations by splitting the continuous measurements in virtual locations, each with 100 channel instances, equivalent to capturing 1 second.

Correlation Coefficient. The correlation coefficient relates to the concept of favorable propagation, which also quantifies the ability to separate channels. When there is favorable propagation [30], the channel vectors are pair-wise orthogonal such that $\frac{1}{M}\mathbf{h}_i{}^H\mathbf{h}_j \to 0$ as $M \to \infty$ for two positions i and j.

Fig. 9 depicts the correlation between two channel instances from two random locations as a function of the number of base station antennas. The result was obtained by calculating the correlation coefficient – as defined in (7) – 100 000 times per antenna configuration and for different numbers of consecutive antennas. For i.i.d. Rayleigh fading the average correlation coefficient becomes $1/M$ [30]. Fig. 9 shows the same trend for the ULA, URA and i.i.d. Rayleigh fading for the first eight antennas. After eight antennas the decrease of the correlation flattens for the URA, demonstrating that adding a second row does not contribute as much to the decorrelation of the channels. This effect is much smaller in the ULA case, illustrating that increasing the size of the ULA increases the spatial diversity, as was also observed when studying the channel hardening.

The correlation between the channels for a LoS and NLoS case is shown in Fig. 10. The general trend shows that the ULA configuration captures channels which are less correlated than the URA configuration. Moreover, when deploying close to 32 antennas, the correlation coefficient for both NLoS

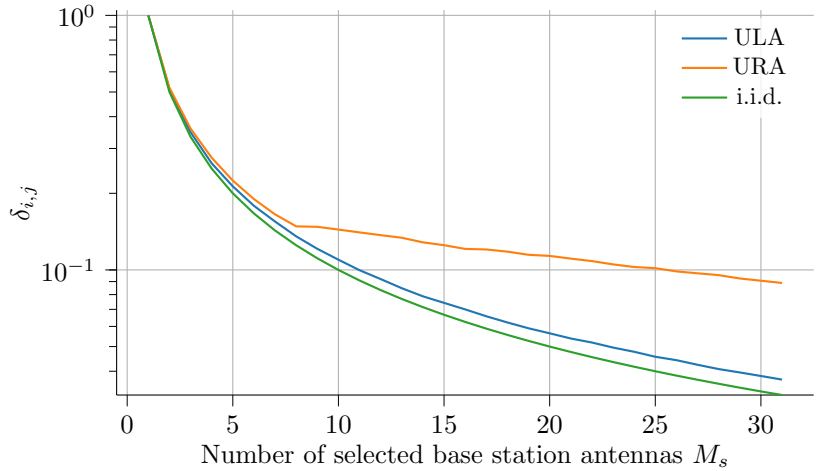

Figure 9: Average node correlation $\delta_{i,j}$ in (7) between the channel vectors of two random node positions, as a function of the number of BS antennas. Expressed in dB to better illustrate the difference between the graphs.

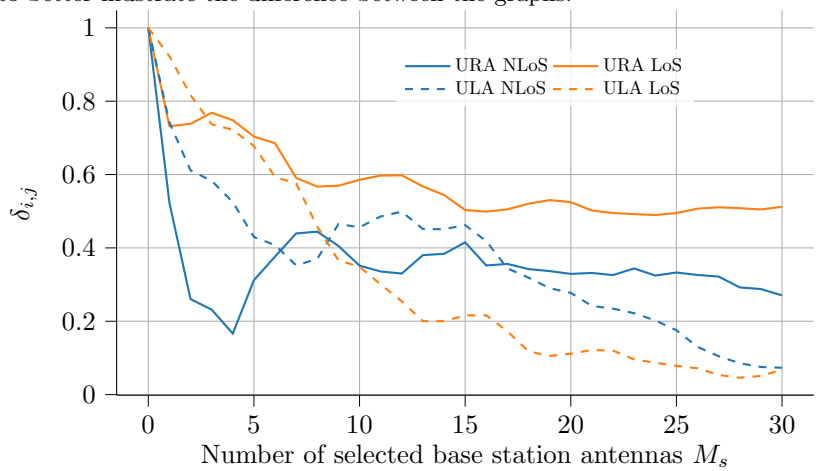

Figure 10: Correlation coefficient $\delta_{i,j}$ between the two LoS and NLoS users.

and LoS becomes equal. Hence, even in LoS, increasing the number of antenna elements in a ULA configuration contributes to the decorrelation of the channel coefficients such that nodes could be separated. However, for the URA, as expected this is trickier in LoS and the decorrelation of users is much more prominent in the NLoS scenario.

Orthogonality of Multiple Nodes. The orthogonality of multiple IoT nodes is assessed by examining the condition number [27] or the distance from

favorable propagation [13]. The normalization and the channel instance selection procedure are equivalent to that explained in Section B.

A large condition number implies strongly correlated channels, while a condition number of one indicates pair-wise orthogonal channels. The inverse condition number is chosen as a metric to be able to express the orthogonality in a finite range, i.e., $\kappa^{-1} \in [0, 1]$. The inverse condition number for two, five and ten users as a function of the number of base station antennas is shown in Fig. 11a. The users are randomly selected as discussed in Section B. Logically $\kappa_{K,M}^{-1}$ equals zero as long as K is larger than M.

We see that the $\kappa_{K,M}^{-1}$ of the ULA follows closely the ideal i.i.d. Rayleigh fading case and tends to move closer to this curve as the number of base station antennas increases; for the URA case, the distance from i.i.d Rayleigh fading is larger.

The empirical cumulative distribution function (CDF) is used to further elaborate on the impact of K and M in Fig 11b. There exist some strongly correlated channels, as is illustrated by the spread of $\kappa_{K,M}^{-1}$ over the entire range $[0, 1]$. This is also noticeable in the CDF of the correlation coefficient (Fig. 11b) as both ULA and URA show some correlation coefficients close to one. While there are not many strongly correlated signals, it still demonstrates the importance of adequate user grouping and scheduling.

C Scheduling IoT Nodes

Dominant Eigendirections. As demonstrated with previous metrics, we cannot assume i.i.d. Rayleigh fading channels but expect that signals, coming from the IoT nodes, have distinct directions. In other words, we expect that in this setting, nodes have dominant directions which do not change drastically over time. These dominant directions and their significance are studied by their eigendirections and could be used to schedule nodes.

The distribution of weak and strong eigendirections can be extracted from the channel correlation matrix $\mathbf{R}$ as defined in (8) [30]. The correlation matrix is obtained from the continuous channel collection along path B and C for a time window of size 600 samples, corresponding to approximately 25λ. A diagonal matrix $\mathbf{D}$ containing the eigenvalues is obtained through the eigenvalue decomposition of the correlation matrix. The eigenvalues are sorted in descending order. The higher the values of the first eigenvalues, the more energy is confined in a few eigendirections. Fig. 12 depicts the eigenvalues $\mathrm{tr}(\mathbf{D})$ of the channels for path C and B in Fig. 4. Most of the energy – between 68% and 85% – is carried by three eigendirections, regardless of the antenna array and node position. As we have a finite number of measured channel instances, the i.i.d. Rayleigh fading channel is also simulated with the same number of snapshots. Fig. 12 shows that the eigenvalues are distributed around 0 dB, whereas asymptotically all eigenvalues will be equal. Fig. 12 further reveals

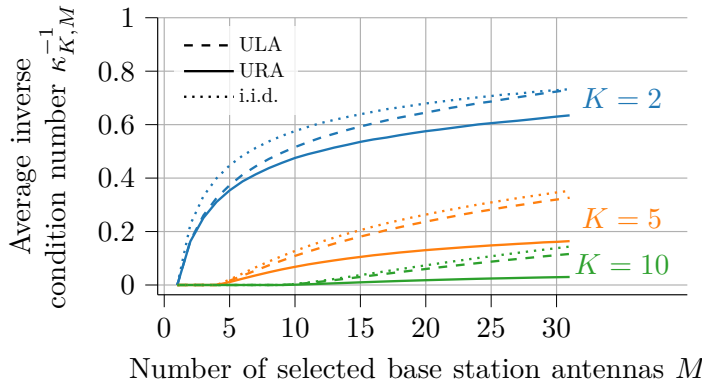

(a) The average inverse condition number $\kappa_{K,M}^{-1}$ for K IoT nodes and 32 antennas.

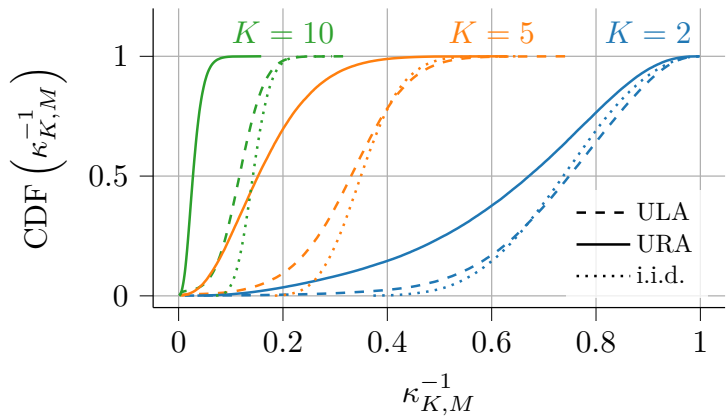

(b) CDF of the inverse condition number $\kappa_{K,M}^{-1}$ for K IoT nodes and 32 antennas.

Figure 11: The average and CDF of the inverse condition number $\kappa_{K,M}^{-1}$ for K IoT nodes and 32 antenna.

that the experimentally captured data are close to the asymptotic case. We can conclude that for both configurations and both paths, dominant directions are present. The latter is in contrast to the simulated i.i.d. case. The ULA and URA show similar trends on both paths.

The difference between the three dominant eigendirections is measured by computing the chordal distance, defined in (10). The chordal distance is used in [31], [32] to reduce the complexity when selecting users to be scheduled together, while still performing similar to full-CSI selection algorithms. Fig. 13

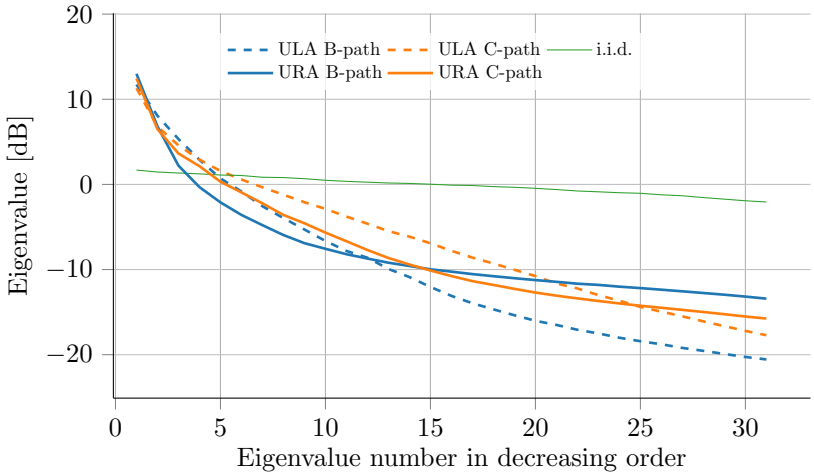

Figure 12: Eigenvalues ordered in descending order for different antenna topologies and different positions.

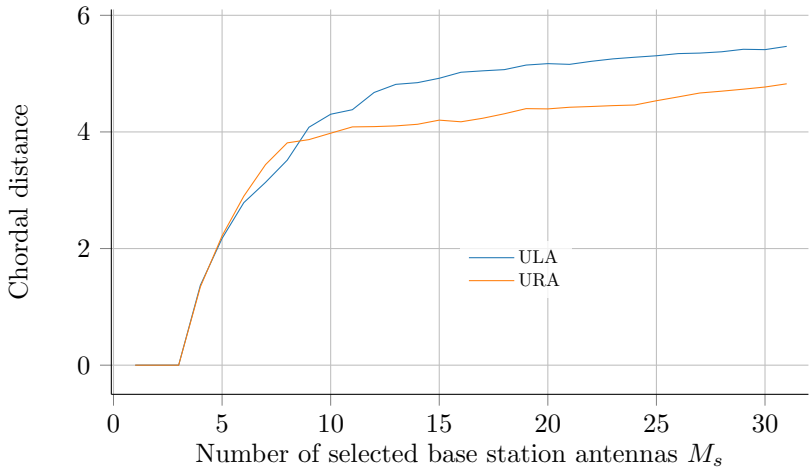

Figure 13: Chordal distance of 3-dominant eigenspaces between path B and C for the ULA and URA configuration.

presents the average chordal distance between the 3-dominant eigenspaces of paths B and C. This figure shows the degree of orthogonality of the eigenspaces between the aforementioned configurations. As expected, the difference between the eigenspaces increases when the number of antennas increases. The ULA increases the distance between the three eigenspace more rapidly by increasing the number of base station antennas, while with the URA it stagnates

after 8 antennas.

V Outlook and Conclusion

In this paper we have studied the opportunities of massive MIMO technology to upgrade LPWANs operating in the unlicensed sub-GHz band for future IoT applications. We have evaluated several relevant performance metrics, based on measurement data gathered through an experimental campaign; this data is now available open-source. The campaign covered both LoS and NLoS scenarios, and ULA and URA antenna array configurations were deployed. Our assessment confirms that both array gain and channel hardening are considerable. Hence, when combining the many antennas properly, the power consumption of the nodes can be reduced drastically and the link reliability can be increased. For example, for the case of a 32-antenna gateway this could specifically allow the battery-powered IoT devices to reduce their transmit power by M – or $10\log_{10}(M)$ dB. Or alternatively, use the additional combining gain to extend the coverage. Furthermore, the fading margins can be lowered due to the channel hardening effect. This effect also ensures that fewer retransmissions are required, which are shown in [33] to account for considerable energy consumption in current LPWAN technologies.

We performed an analysis of joint orthogonality of channels for different node positions. It shows that the relatively large array does receive quite different responses from these positions, opening the opportunity for spatial multiplexing of nodes. When comparing the URA and ULA, it is noticeable that while the received gains of both are similar, the channel correlation between different positions are quite different. This indicates that the average channel power per antenna is similar for both configurations, but the linear array also ensures a more diverse set of paths is received. The latter facilitates better decorrelation of nodes and is hence better suited for serving many nodes. Noteworthy is that even with users perpendicular to the array, the ULA still performs better than the URA. The ULA also outperforms the URA when users have the same azimuth angle with respect to the base station, as shown in Fig. 10.

The measured channels show the presence of a few dominant eigendirections that could used for scheduling users. It also demonstrates that i.i.d. Rayleigh fading does not hold in our scenarios. New models need to be designed to include sub-GHz massive MIMO propagation. These models can then be used to design new low-power IoT protocols.

Acknowledgment

This work was funded by the European Union's Horizon 2020 under grant agreement no. 732174 (ORCA project) and no. 731884 (IoF2020 program - IoTrailer use case). We would like to thank Vladimir Volski for designing the path antenna, Sofie Pollin for her help with the Massive MIMO testbed configuration, François Rottenberg for the fruitful discussions and our colleagues of Dramco for assisting us during the experiments.

References

[1] G. Callebaut and L. Van der Perre, "Characterization of LoRa Point-to-Point Path Loss: Measurement Campaigns and Modeling Considering Censored Data," *IEEE Internet of Things Journal*, vol. 7, no. 3, pp. 1910–1918, 2020.

[2] M. Xhonneux, J. Tapparel, O. Afisiadis, A. Balatsoukas-Stimming and A. Burg, "A Maximum-Likelihood-based Multi-User LoRa Receiver Implemented in GNU Radio," in *2020 54rd Asilomar Conference on Signals, Systems, and Computers*, Nov. 2020.

[3] M. N. Mahfoudi, G. Sivadoss, O. B. Korachi, T. Turletti and W. Dabbous, "Joint Range Extension and Localization for Low-Power Wide-Area Network," *Internet Technology Letters*, vol. 2, no. 5, e120, 2019. eprint: `https://onlinelibrary.wiley.com/doi/pdf/10.1002/itl2.120`.

[4] A. Dongare, R. Narayanan, A. Gadre *et al.*, "Charm: Exploiting Geographical Diversity through Coherent Combining in Low-Power Wide-Area Networks," in *2018 17th ACM/IEEE International Conference on Information Processing in Sensor Networks (IPSN)*, 2018, pp. 60–71.

[5] A. Hoeller, R. D. Souza, O. L. Alcaraz López, H. Alves, M. de Noronha Neto and G. Brante, "Analysis and Performance Optimization of LoRa Networks With Time and Antenna Diversity," *IEEE Access*, vol. 6, pp. 32 820–32 829, 2018.

[6] E. Björnson, E. de Carvalho, J. H. Sorensen, E. G. Larsson and P. Popovski, "A Random Access Protocol for Pilot Allocation in Crowded Massive MIMO Systems," *IEEE Transactions on Wireless Communications*, vol. 16, no. 4, pp. 2220–2234, 2017.

[7] A.-S. Bana, E. de Carvalho, B. Soret *et al.*, "Massive MIMO for Internet of Things (IoT) connectivity," *Physical Communication*, vol. 37, p. 100 859, 2019.

[8] B. M. Lee and H. Yang, "Massive MIMO for Industrial Internet of Things in Cyber-Physical Systems," *IEEE Transactions on Industrial Informatics*, vol. 14, no. 6, pp. 2641–2652, 2018.

[9] L. Liu and W. Yu, "Massive Connectivity With Massive MIMO—Part I: Device Activity Detection and Channel Estimation," *IEEE Transactions on Signal Processing*, vol. 66, no. 11, pp. 2933–2946, 2018.

[10] N. Saxena, A. Roy, B. J. R. Sahu and H. Kim, "Efficient IoT Gateway over 5G Wireless: A New Design with Prototype and Implementation Results," *IEEE Communications Magazine*, vol. 55, no. 2, pp. 97–105, 2017.

[11] B. M. Lee, "Improved Energy Efficiency of Massive MIMO-OFDM in Battery-Limited IoT Networks," *IEEE Access*, vol. 6, pp. 38 147–38 160, 2018.

[12] K. Senel and E. G. Larsson, "Grant-free massive MTC-enabled massive MIMO: A compressive sensing approach," *IEEE Transactions on Communications*, vol. 66, no. 12, pp. 6164–6175, 2018.

[13] H. Q. Ngo, E. G. Larsson and T. L. Marzetta, "Aspects of favorable propagation in Massive MIMO," in *2014 22nd European Signal Processing Conference (EUSIPCO)*, 2014, pp. 76–80.

[14] S. Gunnarsson, L. Van der Perre and F. Tufvesson, "Massive MIMO Channels," in *Wiley 5G Ref*. American Cancer Society, 2020, pp. 1–21. eprint: `https://onlinelibrary.wiley.com/doi/pdf/10.1002/9781119471509.w5GRef040`.

[15] S. Gunnarsson, J. Flordelis, L. Van der Perre and F. Tufvesson, "Channel Hardening in Massive MIMO: Model Parameters and Experimental Assessment," *IEEE Open Journal of the Communications Society*, vol. 1, pp. 501–512, 2020.

[16] X. Gao, O. Edfors, F. Rusek and F. Tufvesson, "Massive MIMO Performance Evaluation Based on Measured Propagation Data," *IEEE Transactions on Wireless Communications*, vol. 14, no. 7, pp. 3899–3911, 2015.

[17] X. Gao, O. Edfors, F. Tufvesson and E. G. Larsson, "Massive MIMO in Real Propagation Environments: Do All Antennas Contribute Equally?" *IEEE Transactions on Communications*, vol. 63, no. 11, pp. 3917–3928, 2015.

[18] M. Arnold and S. t. Brink, "Properties of Measured Massive MIMO Channels using Different Antenna Geometries," in *WSA 2019; 23rd International ITG Workshop on Smart Antennas*, 2019, pp. 1–5.

[19] M. Tran, O. Gustafsson, P. Källström, K. Senel and E. G. Larsson, "An Architecture for Grant-Free Massive MIMO MTC Based on Compressive Sensing," in *2019 53rd Asilomar Conference on Signals, Systems, and Computers*, 2019, pp. 901–905.

[20] Y. Beyene, C. Boyd, K. Ruttik, C. Bockelmann, O. Tirkkonen and R. Jäntti, "Compressive sensing for MTC in new LTE uplink multi-user random access channel," in *AFRICON 2015*, IEEE, 2015, pp. 1–5.

[21] F. A. Pereira de Figueiredo, F. A. Cardoso, J. P. Miranda, I. Moerman, C. F. Dias and G. Fraidenraich, "Large-Scale Antenna Systems and Massive Machine Type Communications," *International journal of wireless information networks*, vol. 2020, pp. 1–23, 2020.

[22] X. Cai, G. Zhang, C. Zhang, W. Fan, J. Li and G. F. Pedersen, "Dynamic Channel Modeling for Indoor Millimeter-Wave Propagation Channels Based on Measurements," *IEEE Transactions on Communications*, vol. 68, no. 9, pp. 5878–5891, 2020.

[23] A. Garcia-Rodriguez, G. Geraci, L. G. Giordano, A. Bonfante, M. Ding and D. López-Pérez, "Massive MIMO Unlicensed: A New Approach to Dynamic Spectrum Access," *IEEE Communications Magazine*, vol. 56, no. 6, pp. 186–192, 2017.

[24] G. Callebaut, S. Gunnarsson, A. P. Guevara *et al.*, "Massive MIMO goes Sub-GHz: Implementation and Experimental Exploration for LPWANs," in *2020 54th Asilomar Conference on Signals, Systems, and Computers*, 2020, pp. 1101–1105.

[25] H. Q. Ngo and E. G. Larsson, "No downlink pilots are needed in TDD massive MIMO," *IEEE Trans Wireless Commun*, vol. 16, no. 5, pp. 2921–2935, 2017.

[26] J. Maurer, G. Matz and D. Seethaler, "Low-Complexity and Full-Diversity MIMO Detection Based on Condition Number Thresholding," in *2007 IEEE International Conference on Acoustics, Speech and Signal Processing - ICASSP '07*, vol. 3, 2007, pp. Iii–61–iii–64.

[27] J. Hoydis, C. Hoek, T. Wild and S. ten Brink, "Channel measurements for large antenna arrays," in *2012 International Symposium on Wireless Communication Systems (ISWCS)*, 2012, pp. 811–815.

[28] E. Björnson, J. Hoydis and L. Sanguinetti, "Massive MIMO Networks: Spectral, Energy, and Hardware Efficiency," *Foundations and Trends® in Signal Processing*, vol. 11, no. 3-4, pp. 154–655, 2017.

[29] E. Cept, "ERC recommendation 70-03, Relating to the use of Short Range Devices (SRD)," *Electronic Communications Committee*, 2017.

[30] E. Björnson, J. Hoydis and L. Sanguinetti, "Massive MIMO Networks: Spectral, Energy, and Hardware Efficiency," *Found. Trends Signal Process.*, vol. 11, no. 3–4, 154–655, Nov. 2017.

[31] B. Zhou, B. Bai, Y. Li, D. Gu and Y. Luo, "Chordal Distance-Based User Selection Algorithm for the Multiuser MIMO Downlink with Perfect or Partial CSIT," in *2011 IEEE International Conference on Advanced Information Networking and Applications*, 2011, pp. 77–82.

[32] M. Taniguchi, H. Murata, S. Yoshida *et al.*, "Indoor Experiment of Multi-User MIMO User Selection Algorithm based on Chordal Distance," in *2013 IEEE Global Communications Conference (GLOBECOM)*, 2013, pp. 3959–3964.

[33] G. Callebaut, G. Ottoy and L. Van der Perre, "Cross-Layer Framework and Optimization for Efficient use of the Energy Budget of IoT Nodes," in *2019 IEEE Wireless Communications and Networking Conference (WCNC)*, IEEE, 2019, pp. 1–6.

Paper VI

mmWave massive MIMO in real propagation environment: Performance evaluation using LuMaMi28GHz

This paper presents measurement and analysis results for millimeter-wave (mmWave) massive multiple-input multiple-output (MIMO) performance in different real-life scenarios with moderate user equipment (UE) mobility. For the measurement campaign, the developed massive MIMO testbed operating at 28GHz called LuMaMi28GHz is employed. In this testbed, the base station has 16 transceiver chains with a fully digital beamforming architecture (with different pre-coding algorithms) and simultaneously supports multiple users with spatial multiplexing. The UEs are equipped with a beam-switchable antenna array for real-time antenna selection where the one with the highest channel magnitude, out of four pre-defined beams, is selected. We explore the potential benefit and features of mmWave massive MIMO systems with antenna selection based on both measured (and recorded) channel data and real-time system performance evaluation.

S. Gunnarsson, M. Chung, A. Johansson, L. Liu, F. Tufvesson, O. Edfors, O. Zander, Z. Ying, K. Samanta and C. Clifton,
"mmWave Massive MIMO in Real Propagation Environment: Performance Evaluation Using LuMaMi28GHz",
in *Proc. 55th Asilomar Conference on Signals, Systems, and Computers (ASILOMAR)*, Pacific Grove, California, U.S., Nov. 2021.

I Introduction

Massive MIMO is a technology [1], [2], which can enable reliable communication. Scaling up the number of antennas on the base station side and by exploiting spatial multiplexing, the system can simultaneously serve multiple users. The large antenna array results in an array gain and when scaling up the number of antennas, a second effect is that the variations of channel gain decreases, known as the channel hardening effect, and hence, the system can rely on a more stable channel, resulting in a more reliable system [3], [4].

Massive MIMO is quite well explored at sub-6 GHz but the trend is to also move the communication up in frequency [5], to be able to exploit a larger portion of the spectrum. A drawback is the larger pathloss; the shorter wavelength at higher frequencies results in a lower received power. To combat this larger pathloss in the higher part of the spectrum, one could deploy a massive MIMO system. With the array gain coming from the many antennas, the received power can increase and the system can benefit from the channel hardening effect.

At Lund University, there has previously been developed a massive MIMO testbed, LuMaMi [6]. The testbed can operate in real-time, simultaneously serving twelve users and is based on software-defined radio (SDR) technology. It has 100 coherent radio-frequency (RF) chains and a center frequency of 3.7 GHz and 20 MHz bandwidth. The system uses orthogonal frequency-division multiplexing (OFDM) and long term evolution (LTE)-like transmission parameters and operates in time division duplex (TDD) mode. This testbed has then been extended to operate at higher frequencies, i.e. LuMaMi28GHz [7], [8]. With 16 transciever chains and a fully digital beamforming architecture, the base station in this work serves two user equipments (UEs) that each are equipped with a beam-switchable array and can perform real-time antenna selection. With this approach, each UE only needs one transceiver chain, hence decreasing the hardware complexity and cost, but can still improve the performance by switching to a better beam when the current beam is e.g. shadowed.

In this work, we are exploring the potential benefit and features of using massive MIMO at mmWave frequencies with antenna selection. We demonstrate a real-time testbed with a fully digital beamforming architecture, which is able to serve multiple users. Based on measured channel data from Line-of-Sight (LOS) and Non Line-of-Sight (NLOS) scenarios, we assess the performance gain that can be achieved with channel-based antenna selection at the UE side for two different types of antennas.

The structure of the paper is as follows. First the measurement equipment, i.e. LuMaMi28GHz and the UEs, are presented with more details. This is followed by an outline of the measurements scenarios and the performed experiments. Then the results and related analysis is presented, before concluding the work.

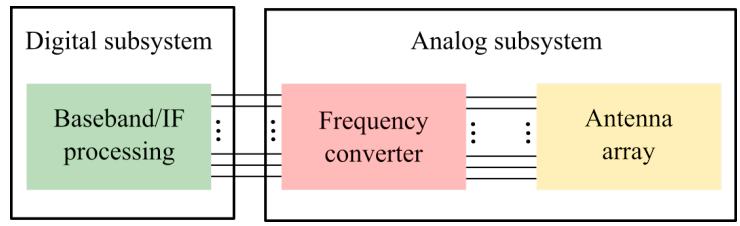

(a) Base station

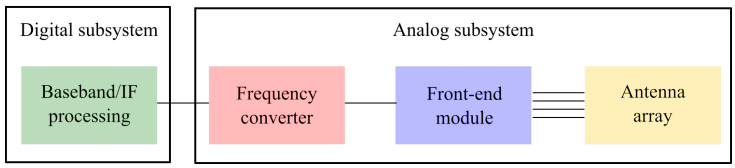

(b) UE

Figure 1: System overview including the digital and analog subsystems for the base station and the UEs.

II Measurement equipment

An overview of the system architecture for LuMaMi28GHz [7], [8] can be seen in Fig. 1a and includes the digital subsystem from the original testbed, which has been extended with an analog subsystem. This subsystem consists of frequency converters that converts between the 2.5 GHz intermediate frequency (IF) and the 28 GHz RF, which is then attached to the antenna array. In total, this fully-digital beamforming testbed is using 16 transceiver chains, with potential for further extensions. Each SDR in the digital subsystem has two transceiver chains, which is then connected to one frequency converter followed by four antennas. Two of these are used for transmitting and two for receiving.

As for the base station side, the UE side is also based on the original system and an overview of the system architecture can be seen in Fig. 1b. Each UE has then one transceiver chain leading to a frequency converter. Then there is a front-end module which includes a power amplifier, an RF switch and the module is used for the beam-switching. This module is then connected to four antennas, which are corresponding to the beams that you can switch through. The two antenna arrays can be seen in Fig. 2 with the yagi antenna array to the left and the patch antenna array to the right. The antenna switching can be controlled by the SDR with a certain strategy, e.g. selecting the beam with the highest channel gain. It is also possible to manually switch between the beams and this is what has been done in this work.

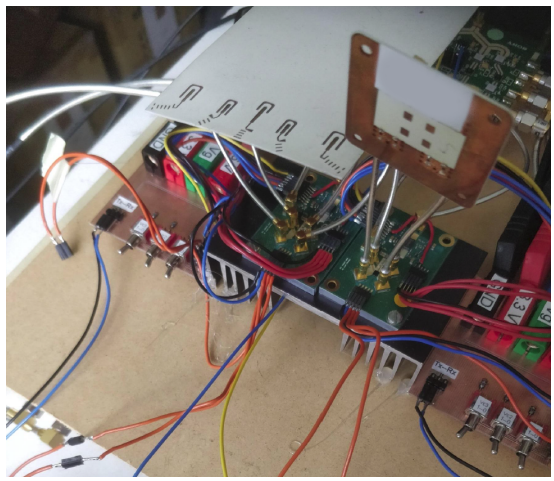

Figure 2: The UE antennas with the yagi antenna array (left) and the patch antenna array (right).

III Measurement scenario

The measurement location is an indoor lab at Lund University; the map where the experiments were performed can be seen in Fig. 3, including testbed and UE placements. The base station is placed in a corner, with the array pointing towards the starting position of the UE. In the LOS scenario in Fig. 3a, the UE started about 1 meter from the base station array and ended about 6.7 metres away. For the NLOS scenario, the UE started about 4.5 metres from the base station and approximately 1 meter from the wall to the right, moving in total approximately 1.3 metres.

The experiments were done both for a static case where the UE was moved about 10 centimetres between each measurement and also for a continuous case when UE was moving along the dashed lines. For the static experiments, each beam was measured at each point, collecting 100 samples during 1 second. One sample includes the channel between all base station antennas and active UE antennas and also 100 points over the bandwidth. For the continuous experiments, the experiment was repeated four times, one for each beam. Since the beams here were not measured simultaneously, these results will only give indications on what to expect, while the static experiments naturally are more precise. In the LOS experiment, 2000 samples were collected during 20 seconds and in the NLOS experiment, 1000 samples during in 10 seconds were stored.

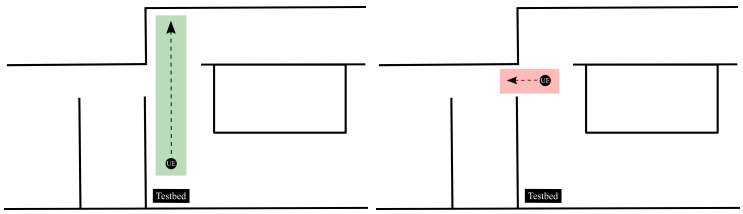

(a) LOS scenario **(b)** NLOS scenario

Figure 3: Map over the scenario where the experiments were performed in LOS and NLOS.

IV Results and analysis

Starting the analysis with exploring what a mmWave massive MIMO channel can look like, a static measurement was done at the initial position of the UE in Fig. 3b for 10 seconds, i.e. 1000 time samples. As initially stated, massive MIMO results in an array gain, which here can be seen as the difference between the lower surfaces and the upper surfaces, for both types of antennas in Fig. 4a and 4b, respectively. The surfaces on the top corresponds to when the channel from the UE's strongest beam to the 16 antennas at the base station side is combined, while the two lower ones in each figure are the channels from one of the strongest and one of the weakest UE beams, respectively, to one random base station antenna (the one to the upper left in the array in this case). Please note the different z-axes, which here are kept to better show the different surfaces for the patch antenna and since the weak beam from the yagi antenna is really week, potentially only noise, these would be less detailed if having the same z-axes.

In Fig. 4c and 4d, the channel gain for all four beams are shown over time and frequency when combining their respective channels to the 16 base station antennas. It can be seen that it results in a more stable channel in both time and frequency, for both the yagi and patch antenna, as compared to the one base station antenna cases, which can be seen in Fig 4a and 4b. In Fig. 4c and 4d, some of the beams are almost overlapping so the difference between the four different layers are not that clear but it gives an idea of what it can look like. What one also can see in the figures are that the patch antenna has a higher gain, moving the surfaces up, and the yagi antenna has a wider bandwidth, resulting in a finer resolution.

The results from the LOS scenario can be seen in Fig. 5 and Fig. 6, for the two different types of UE antennas. In Fig. 5a there are the static measurements for the yagi antennas and in Fig. 5b are the continuous measurements for the same antennas. What is seen is the channel gain for the four different beams over distance. Naturally the channel gain decreases as the UEs is moving away from the base station. Furthermore, as seen for the continuous measurement,

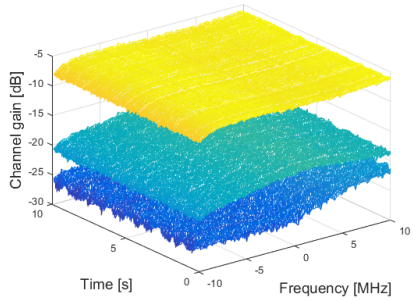

(a) Patch antenna array

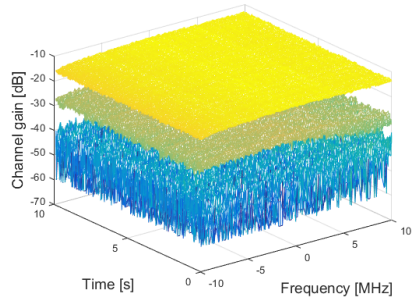

(b) Yagi antenna array

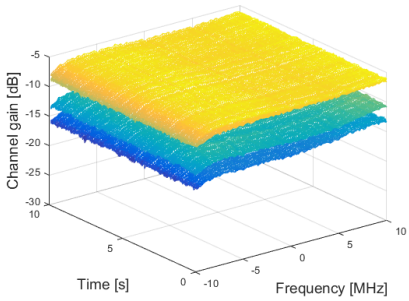

(c) Patch antenna array

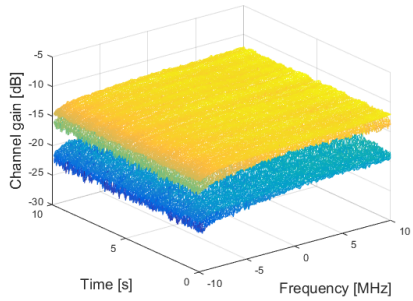

(d) Yagi antenna array

Figure 4: Channel gain over time and frequency for 1) 16 base station transceiver chains and the strongest UE beam (upper), 1 base station transceiver chain and one of the strongest UE beams (middle), 1 transceiver chain and one of the weakest beams (lower) in Fig. 4a and 4b and 2) 16 base station transceiver chains and the different beams in Fig. 4c and 4d .

there are also small-scale variations as the channel gain changes up and down between consecutive samples. In this experiment two beams are competing for being the strongest one, beam 2 and 4, and two which are weaker, beam 1 and 3. Remember that the comparisons between the graphs in this figure only are indicative and not exact, as well as the comparison between the figures, while the figure with the static measurements is more deterministic. The maximum gain difference observed here is a point where there is 11 dB between the strongest and weakest beam, as calculated from the static measurements.

In Fig. 6 the corresponding results can be seen for the patch antennas. In relation to Fig. 5, the curves are higher up due to the higher antenna gain. Similarly, there are two beams competing for being the strongest one and two which are weaker. The largest gain difference between two beams here can be found to be 13 dB. For the static measurement in Fig. 6a there are 55 meas-

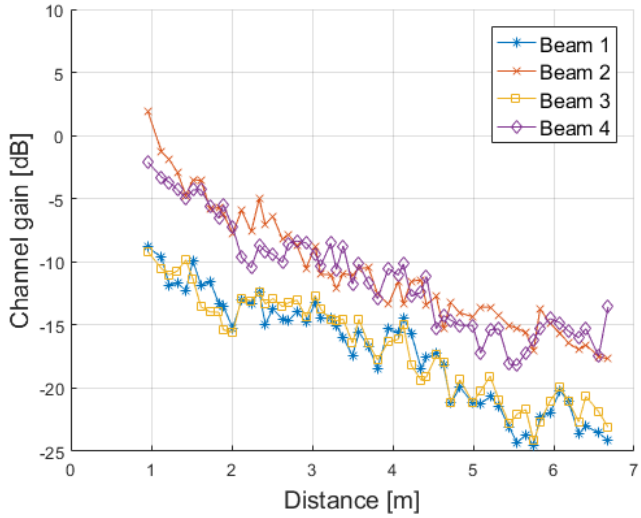

(a) Static

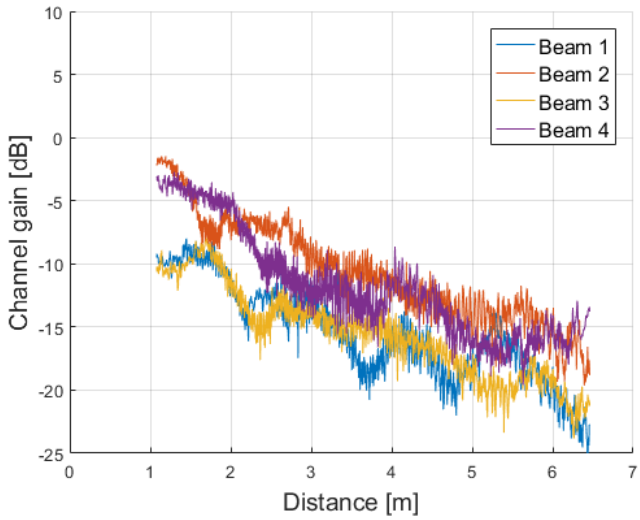

(b) Continuous

Figure 5: Channel gain versus distance for the experiment in Fig. 3a for all four beams in the yagi antenna array and both the static continuous experiment.

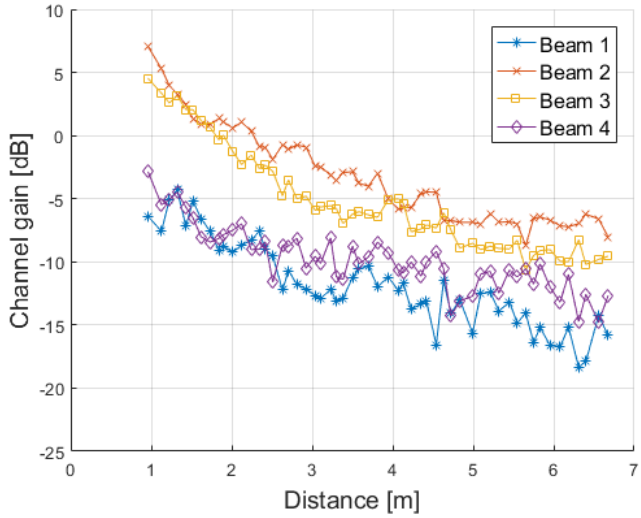

(a) Static

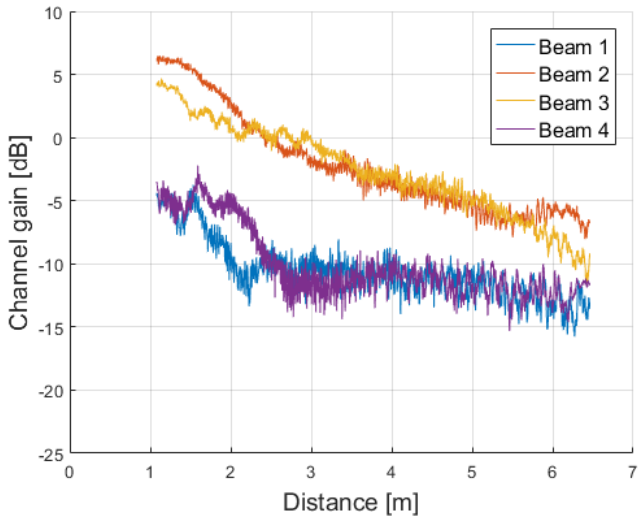

(b) Continuous

Figure 6: Channel gain versus distance for the experiment in Fig. 3a for all four beams in the patch antenna array and for both the static and the continuous experiment.

urement points along the line and for the continuous measurement there are 2000 measurement points. To be considered is that depending on the resolution of the measurement and how often an update of the choice of beam in the system is to be done, the gain from beam selection would differ. Hence there will be a trade-off between always using the strongest beam and how much resources, such as computing resources for implementing the selection algorithm or spectrum resources for sensing the channel at different beams, one would like to spend on updating the beam used.

For the NLOS scenario in Fig. 3b, the corresponding results are shown in Fig. 7 and 8. For the yagi antennas, the results are shown in Fig. 7a and 7b. In these figures, the first half is in LOS and then the channel gain drastically drops as the antennas become shadowed in the NLOS area. Similarly to the LOS scenario, as the channel changes, the strongest beam changes. Although not as much for the stronger beams in the static measurements. Also similar to the LOS experiments, there are two stronger and two weaker beams with the largest difference of 13 dB and also here the trade-off between the gain that is achievable if the strongest beam is chosen at all times versus what it costs to spend resources on updating too often can be considered. Marked in the figures are also approximate lines from where the antennas are shadowed.

The corresponding results for the patch antennas are shown in Fig. 8a and 8b. As for the LOS scenario, the curves for the patch antennas are higher up. Similar to the yagi antennas, one can see a fast drop in channel gain for all beams as the antennas become shadowed. With the resolution of 10 centimeters as for the static measurement here, one would not gain anything from switching as long as beam 2 is the one chosen. What the result would be with more frequent updates could be different. The largest difference between two beams is 14 dB for one point.

	Yagi antennas	Patch antennas
LOS	11 dB	13 dB
NLOS	13 dB	14 dB

Table 1: The measured gain differences between the weakest and strongest beam for the yagi and patch antennas in LOS and NLOS.

Summarizing the possible gains due to beam-switching, Table 1 shows the corresponding numbers for the yagi and patch antennas, respectively, in both LOS and NLOS. For these experiments, the maximum achievable gain between the weakest and strongest antenna is slightly higher for the patch antennas than the yagi antennas and the gain is also slightly higher in the NLOS scenario in comparison to the LOS scenario. Overall, there is a significant gain that can be achieved with channel-based antenna selection at the UE side.

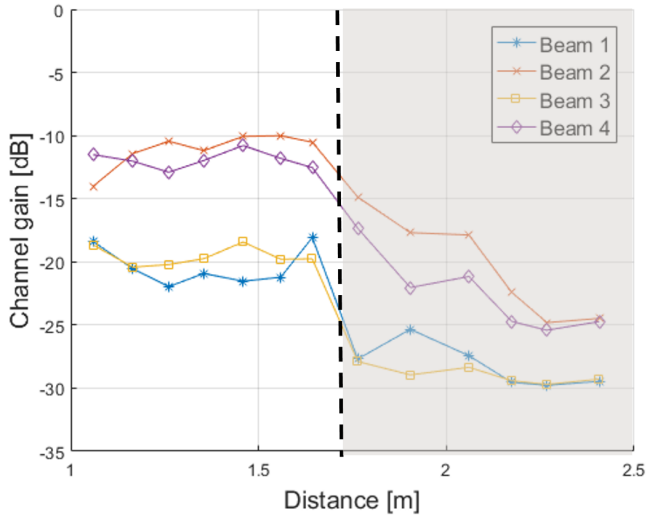

(a) Static

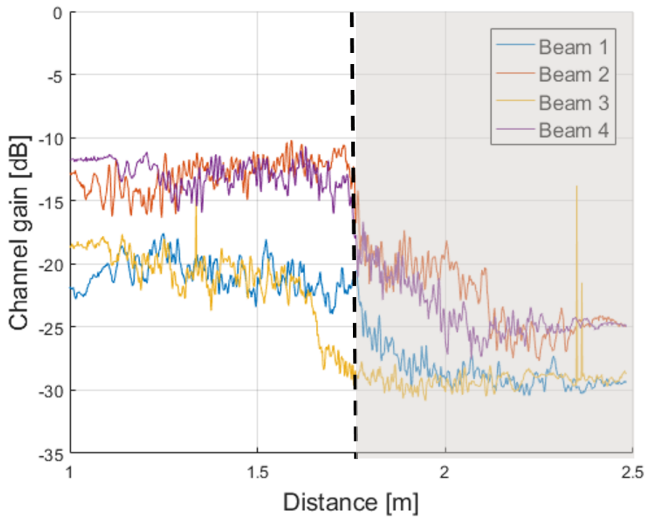

(b) Continuous

Figure 7: Channel gain versus distance for the experiment in Fig. 3b for all four beams in the yagi antenna array and for both the static and the continuous experiment.

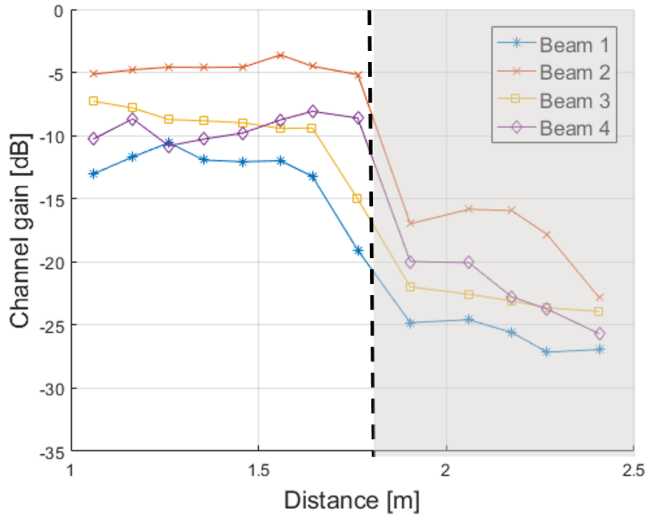

(a) Static

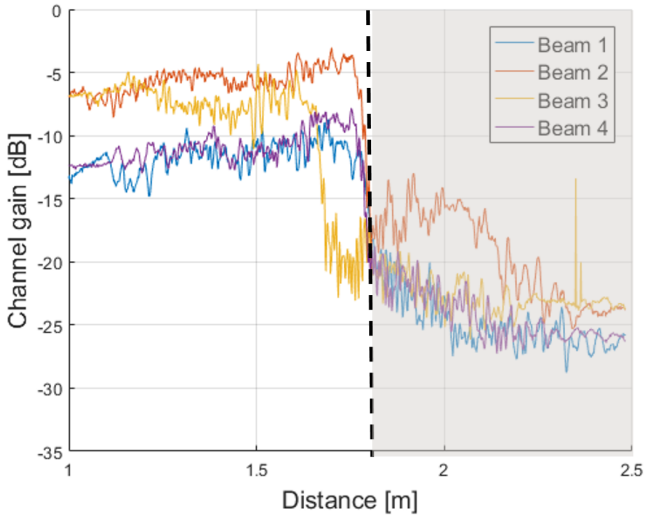

(b) Continuous

Figure 8: Channel gain versus distance for the experiment in Fig. 3b for all four beams in the patch antenna array and for both the static and the continuous experiment.

V Conclusions

First of all, this work demonstrates digital up conversion modules with inherent analog beamforming and beam selection as a complement to the already present digital beamforming at IF. The mmWave massive MIMO system can be used to increase the reliability due to both the demonstrated array gain and also the channel hardening effect. The performance evaluation of using antenna selection shows that the system can benefit from beam selection at the UE side; in these experiments gains up to 14 dB between two beams has been shown. Although the channel changes fast and the strongest beam changes often, there is a trade-off between the gain that can be achieved by switching beam and how often one actually is doing the update and this trade-off is to be further investigated.

Acknowledgment

We would like to thank Vinnova "Smartare Elektroniksystem" for the funding.

References

[1] T. L. Marzetta, "Noncooperative cellular wireless with unlimited numbers of base station antennas," *IEEE Transactions on Wireless Communications*, vol. 9, no. 11, pp. 3590–3600, 2010.

[2] E. G. Larsson, O. Edfors, F. Tufvesson and T. L. Marzetta, "Massive MIMO for next generation wireless systems," *IEEE Communications Magazine*, vol. 52, no. 2, pp. 186–195, 2014.

[3] H. Q. Ngo and E. G. Larsson, "No downlink pilots are needed in TDD massive MIMO," *IEEE Transactions on Wireless Communications*, vol. 16, no. 5, pp. 2921–2935, 2017.

[4] S. Gunnarsson, J. Flordelis, L. Van Der Perre and F. Tufvesson, "Channel hardening in massive MIMO: Model parameters and experimental assessment," *IEEE Open Journal of the Communications Society*, vol. 1, pp. 501–512, 2020.

[5] M. Shafi, J. Zhang, H. Tataria *et al.*, "Microwave vs. millimeter-wave propagation channels: Key differences and impact on 5G cellular systems," *IEEE Communications Magazine*, vol. 56, no. 12, pp. 14–20, 2018.

[6] S. Malkowsky, J. Vieira, L. Liu *et al.*, "The world's first real-time testbed for massive MIMO: Design, implementation, and validation," *IEEE Access*, vol. 5, pp. 9073–9088, 2017.

[7] M. Chung, L. Liu, A. Johansson *et al.*, "Millimeter-wave massive MIMO testbed with hybrid beamforming," in *2020 54th Asilomar Conference on Signals, Systems, and Computers*, 2020, pp. 309–313.

[8] M. Chung, L. Liu, A. Johansson *et al.*, "LuMaMi28: Real-time millimeter-wave massive MIMO systems with antenna selection," 2021. arXiv: 2109.03273 [eess.SP].